DISCLAIMER

This report was prepared as an account of work sponsored by an agency of the United States Government. Neither the United States Government nor any agency thereof, nor any of their employees, makes any warranty, express or implied, or assumes any legal liability or responsibility for the accuracy, completeness, or usefulness of any information, apparatus, product, or process disclosed, or represents that its use would not infringe privately owned rights. Reference herein to any specific commercial product, process, or service by trade name, trademark, manufacturer, or otherwise does not necessarily constitute or imply its endorsement, recommendation, or favoring by the United States Government or any agency thereof. The views and opinions of authors expressed herein do not necessarily state or reflect those of the United States Government or any agency thereof. Reference herein to any social initiative (including but not limited to Diversity, Equity, and Inclusion (DEI); Community Benefits Plans (CBP); Justice 40; etc.) is made by the Author independent of any current requirement by the United States Government and does not constitute or imply endorsement, recommendation, or support by the United States Government or any agency thereof.

SANDIA REPORT
SAND2025-13554R
Printed October 26, 2025

Sandia National Laboratories

Evaluating Variable-Impedance Magnetically-Insulated Transmission Lines as a Risk-Mitigation Measure for Next-Generation Pulsed Power

David Sirajuddin[1], Roman Shapovalov[2], Brian Hutsel[1], Evstati Evstatiev[1], Adam Darr[1], and Keith Cartwright[1]

[1]Sandia National Laboratories
P.O. Box 5800, MS-1195
Albuquerque, NM 87185

[2]University of Rochester
601 Elmwood Avenue
Rochester, NY 14642

Prepared by
Sandia National Laboratories
Albuquerque, New Mexico 87185
Livermore, California 94550

Issued by Sandia National Laboratories, operated for the United States Department of Energy by National Technology & Engineering Solutions of Sandia, LLC.

Available to DOE and DOE contractors from

U.S. Department of Energy
Office of Scientific and Technical Information
P.O. Box 62
Oak Ridge, TN 37831

Telephone: (865) 576-8401
Facsimile: (865) 576-5728
E-Mail: reports@osti.gov
Online ordering: http://www.osti.gov/scitech

Available to the public from

U.S. Department of Commerce
National Technical Information Service
5301 Shawnee Road
Alexandria, VA 22312

Telephone: (800) 553-6847
Facsimile: (703) 605-6900
E-Mail: orders@ntis.gov
Online order: https://classic.ntis.gov/help/order-methods

ABSTRACT

This project has produced the first detailed characterizations of power flow resulting from applying the "variable-impedance MITL" concept to real-life systems in Sandia's pulsed power program (Z and next-generation pulsed power (NGPP)). We present simulation results and analyses for constant-impedance versions of both Z and NGPP and survey the operational viability of several variable-impedance re-designs in the parameter space of linear tapers. Circuit modeling (SCREAMER/Bertha) was used to pinpoint promising candidate designs, and EM-PIC (Empire) simulations were used to evaluate these candidates more rigorously. This approach was particularly successful in the Z regime which resulted in the identification of several viable variable-impedance MITL designs for each level. The approach was more challenged in the operating space NGPP occupies, producing data points that speak to a more restrictive design space due to anode plasma turn-on. In the end, we were able to converge on one viable variable-impedance design for the highest inductance line (level "F") and one for the highest current line (level "A").

Altogether, the body of simulation evidence presented in this report suggest there does exist flexibility in operating space for magnetically-insulated transmission lines (MITLs) having variable geometric impedance to be a potential enabling technology for safely increasing current delivery (and potentially lowering stack voltage) in pulsed-power drivers by manipulating electron losses; however, operating points for a particular design must be carefully screened. Circuit and EM-PIC modeling provided consistent verdicts in safe operating regimes for operational viablity, but additional physics such as anode plasma turn-on which is included in Empire but not in SCREAMER/Bertha was found to be a critical factor affecting power flow that lead to different assessments between the codes. It is not always the case that the occurence of anode plasma caused a design to fail (some designs turned on anode plasma yet still delivered load currents meeting design targets); the details matter such as how early in the pulse anode surfaces break down (and how large a region). However, in every case that it did fail it was found that the feedback from anode plasma was the cause (i.e., turning off the anode plasma model in Empire restored agreement with the circuit model prediction). As circuit simulations represent an efficient and practical means of surveying design space compared to more computationally-expensive approaches such as EM-PIC, it could be prudent to invest in the research and development of models to include the effects of anode plasma such as ion emission in circuit codes.

The variable-impedance MITL design is a new concept that enables controlled manipulation of the initial electron losses in the outer MITL and can be tested on Z today. We encourage follow-on work to explore further optimization (including alternative variable-impedance profiles, e.g., having constant dZ/dR), and to confirm the major findings presented in this report by fielding test hardware on actual Z shots.

ACKNOWLEDGMENTS

This work was funded by the LDRD #233055 “Evaluating variable-impedance magnetically-insulated transmission lines as a risk-mitigation measure for NGPP” at Sandia National Laboratories. Sandia National Laboratories is a multimission laboratory managed and operated by National Technology & Engineering Solutions of Sandia, LLC, a wholly owned subsidiary of Honeywell International Inc., for the U.S. Department of Energy’s National Nuclear Security Administration under contract DE-NA0003525.

This paper describes objective technical results and analysis. Any subjective views or opinions that might be expressed in the paper do not necessarily represent the views of the U.S. Department of Energy or the United States Government.

The team would like to thank Dr. Rick Spielman for his collaboration on this research. Dr. Spielman’s publication series on variable-impedance magnetically-insulated transmission lines [39, 36] established the foundation from which this research builds on.

NOMENCLATURE

AK: Anode-Cathode.

ASAP: Assured Survivability and Agility in Pulsed Power mission campaign.

Bertha: A circuit simulation code developed by the Naval Research Laboratory [11]

BDL: (short for "**B** dot dℓ") A simulation diagnostic for $\oint_{a,k} \mathbf{B} \cdot d\boldsymbol{\ell}$, used as a proxy for calculating surface currents at the anode (a) or cathode (k) via the integral form of Ampere's circuital law, $\oint_{a,k} \mathbf{B} \cdot d\boldsymbol{\ell} = \int \mu_0 \mathbf{J}_a \cdot d\mathbf{A} = \mu_0 I_{a,k}$.

CAD: Computer-Aided Design.

Diagnostic: (short for "simulation diagnostic") A diagnostic queries an ongoing simulation for information at discrete time(s) and records this data to a file and/or prints to screen (when applicable). More formally, a diagnostic is a functional $\mathscr{D}$ over a field F whose evaluation at each $t^k_{stride} = k\Delta t_{stride}$ ($k \in \mathbb{N}$) yields a datum $F \mapsto \mathscr{D}[F] : \mathbb{R}^m \to \mathbb{R}^n$ where m is the dimension of the domain and $n \in \{0,1,2,3\}$.

EDL: (short for "**E** dot dℓ") A simulation diagnostic for $V = \int_a^k \mathbf{E} \cdot d\boldsymbol{\ell}$, where V is the line voltage.

EM-PIC: Electromagnetic Particle-in-Cell.

Empire: A performance portable, massively parallel, fully 3D unstructured electromagnetic plasma simulation code developed at Sandia National Laboratories [2]. This code was used to produce all particle-in-cell simulations in this project work.

HPC: (e.g., HPC cluster) High Performance Computing.

LDRD: Laboratory Directed Research and Development.

MITL: Magnetically-Insulated Transmission Line.

NGPP: (e.g., NGPP facility) Next-Generation Pulsed Power. A future pulsed power concept intended to achieve operating regimes beyond a "ZX" facility (see definition below)

SCREAMER: A circuit simulation code originally developed at Sandia National Laboratories [37]

TL: Transmission line.

ZX: (e.g., ZX facility) Z eXtended. Tentative name for a planned upgrade to the existing ZR (Z refurbished) facility to reach even higher load currents (e.g., two times higher).

CONTENTS

LIST OF FIGURES

1. INTRODUCTION

To date, all updates to the Z accelerator have adhered to a pulsed-power engineering design principle to maintain constant geometric impedance in the vacuum section for as long a region as engineering constraints allow[1]. To fulfill the expanding needs in the national laboratory mision space, a second major upgrade to the Z accelerator (Z eXtended, or "ZX") and a next-generation pulsed-power (NGPP) facility capable of delivering $\sim$ 40 MA and $\sim$ 60 MA to a load, respectively, have been proposed. These needs include both the national security demands for enhanced radiation effects testing and the category of fundamental science which includes dynamic materials research, extending opacity datasets, and the continued assessment of fusion concept performance such as the magnetized liner inertial fusion (MagLIF) and large-scale holhraums in different (perhaps more opportune) parameter spaces [35]. While the design requirements for such next-generation facilities have been agreed upon, the means of achieving these operating parameters is not finalized and has been the subject of active research for at least the past 15 years [36, 41, 42, 18, 35, 40, 32, 31, 30, 25]

As concerns NGPP, this would be a new facility so the (as-yet finalized) design is not currently restricted to a given size. However, as it stands, it is not clear if NGPP will be cost-effective. Using current pulsed-power understanding, scaling up to NGPP will require a vacuum section with larger radius (R) than Z today. This is due to the simultaneous desire to maintain a known operational design point for the driver impedance ($Z \sim h/R$) while contending with the requirement that increases to the gap height (h) become necessary in the connecting insulator regions to safeguard against flashover as we extrapolate to the next-generation regimes (e.g., $\sim$ 2x needed to reach 60 mega-amperes of current using conventional accelerator designs). For constant-impedance MITLs, this larger radius (equivalently, longer wave transit time τ) results in increased driver inductance $L = Z\tau$. This increased reactance more aggressively throttles the current rise $dI/dt = V/L$ over the pulse length, limiting what peak current can be achieved. The gains in current are not completely undercut (and experts have assessed that a 60 MA class pulsed-power driver can probably be achieved using such design principles [36]), but the implication of this tradeoff is that there exists an increased pulsed-power risk for scaling up to NGPP and this represents a major increase in cost and accelerator size. Revising the MITL profiles to reduce inductance, if viable, could help meet design targets (increasing dI/dt), decrease pulsed-power risk, and increase cost-effeciveness of such an accelerator. On the other hand, ZX will be an upgrade in place. Modifications to existing components that fit within the

[1]For the azimuthally-periodic Z machine, this design approach results in a "constant impedance region" made up of conical transmission lines, which have constant (cone) angle yet *narrowing* gaps in the direction approaching the load. The constant impedance region ends at the location where gaps narrow to the empirically-informed minimum tolerance of 1 cm whereafter this gap size is strictly enforced by by hardware design ("constant gap region"). The constant gap region, which has constant gap but variable geometric impedance, extends a few centimeters on Z the rest of the MITL to meet the convolute entrance.

same machine footprint will be required. Revising the magnetically-insulated transmission lines (MITLs) designs for this sytem also appears to represent a potentially viable solution consistent with these constraints. The constant-geometric impedance regions of Z in the vacuum sections can be tailored to produce MITLs with lower overall inductance. This has potential benefits including anticipated current gains (i.e., higher $dI/dt = V/L$ for the same pulse width τ), and lowering stack voltage. In both cases, this would come at the cost of overstepping the empirical design guidelines of maintaining constant impedance. However, this notional "cost" should be clarified and specifically quantified to allow future pulsed power designers have all the information they need to meet their design goals. If successful, this concept could be a significant enabling technology that could be employed not only ZX and NGPP, but more broadly to refurbishments or next-generations versions of other facilities in Sandia's pulsed power apparatus including HERMES-III [29] and Saturn [4].

To be clear, the major reason constant geometric impedance MITLs are employed is because they are known (from the seminal Magnetically Insulated Transmission Experiment[2] (MITE [47])" and theory [6, 7, 23, 21, 22, 26, 27, 17]) to cooperate with the conditions required to establish and maintain high quality magnetic insulation[3]. In our previous experience with simulating Z [16] the electron flow layers in the outer MITLs are seen in EM-PIC are *extremely* well-insulated (occupying at most 250 μm of the narrowest AK gaps which are $\sim$ 1 cm, or 2.5% of the AK gap). This appears to be overly conservative, and that there should be room in operating space to pursue further gains if the magnetic insulation is managed adequately.

Initial investigations [39] in modeling have suggested that magnetically-insulated transmission lines (MITLs) having variable-geometric impedance maintain robust magnetic insulation comparable with constant-geometric-impedance MITLs. However, unanswered questions such as the actual level of current lost during the setup of magnetic insulation and the extent of re-trapping (or loss) of vacuum-electron-current flow during equilibrium had yet to be addressed. Furthermore, related concerns such as the actual energy deposited from electrons on the anode during these stages and how this impacts the onset of anode plasmas presents additional questions whose answers are critical for determining the viability of using variable-impedance transmission lines in a Z upgrade or NGPP. Finally, the overall inductance changes could impact the voltage on the stack, which could be another reason this impact NGPP designs resulted in lower voltages. The gains would be even higher if NGPP designs lean towards using six levels, which discussions have touched on previously.

In this research, we further investigate this idea using modeling and simulation to vet the concept on both Z and NGPP. A tandem simulation approach as employed to survey candidate designs using low-computational-cost circuit simulations while pursuing optimizations under the parameter space of linear tapers for variable-impedance designs. Our circuit simulation approach allows rapid simulation turnaround and enables the consideration of many design candidates. The results will provide predictions for current loss, but not be able to provide answers to more detailed questions such as the actual electrode heating from the distribution of electrons impacting the anode. Therefore, we leverage circuit simulations to broadly survey and identify design

[2] "The magnetically insulated transmission experiment (MITE) culminated in the first efficient self-limited MITL [48]

[3] "maintain" means not challenge; impedance transitions will produce perturbations to this flow layer. The question is if a MITL flow layer can tolerate these perturbations.

candidates that meet or exceed target requirements (e.g, load current). For these down-selected candidates, we pursue answers to the more detailed questions related to safe operation (e.g., anode heating distributions) using 3D electromagnetic particle-in-cell (EM-PIC) Empire simulations. This secondary evaluation using EM-PIC can answer not only these questions about distributions but includes additional physics for which there are not curently models for in circuit simulations (e.g., postive ion emission from anode plasmas). Altogether, this two-stage assessment allowed us to provide a rigorous grade for MITL design viablity insofar as modeling and simulation.

By project end, we have produced a large body of simulation-based evidence and contribute data points for the first time to the operating space of variable-impedance MITL systems on real-life exemplars of interest (Z and NGPP). In particular, this project has delivered the following main contributions:

1. **Z redesign**:

    a) A strictly constant-impedance version of Z has been designed; this constitutes our "baseline" from which variable-impedance versions are generated[4]

    b) This baseline system was characterized in simulation one level at a time ("single-level models"), circuit (SCREAMER) and EM-PIC (Empire) results are presented for all 4 levels (levels "A", "B", "C", "D")

    c) 20 variable-impedance designs (linear tapers) have been comprehensively characterized by SCREAMER circuit simulations (5 candidate designs for each of the 4 levels)

    d) 10 design candidates (down-selected from the circuit simulation survey) have been comprehensively characterized by electromagnetic particle-in-cell (EM-PIC) Empire simulations; 3 designs each for levels A, B, C and 1 design for level D

    e) Based on the above results, a set of viable design recommendations for a "variable-impedance Z" system was proposed (in this report referred to as the `VAR3-VAR3-VAR3-VAR1` system); this final design recommends reductions to MITL inductance for each level at 40%, 40%, 40%, 20% on levels A, B, C, and D, respectively.

        i. the combined `VAR3-VAR3-VAR3-VAR1` Z circuit model has been set up in SCREAMER with simulation and analysis completed

        ii. the combined `VAR3-VAR3-VAR3-VAR1` Z EM-PIC model has been set up in Empire, simulation results are forthcoming (not presented in this report)

    f) Extended studies using circuit simulations have been completed:

[4]Upon interrogating the Z MITL geometries in CAD files, we discovered that signficant fractions of all levels of Z (except level "D") are not strictly constant impedance as is commonly claimed. Levels C and D have regions where this is true (the "outer plate" for level C while level D is constant impedance for a longer extent spanning both its "outer plate" and "middle plate"). Meanwhile, levels A and B have *no* regions that are constant impedance.

i. Alternative options for combined variable-impedance Z (20% reductoin for all levels, 30% reduction for all levels, 40% reduction for all levels) have been set up in SCREAMER with simulations and analysis completed; altogether these results form a portfolio of operating characteristics for vairous design options according to circuit modeling.

ii. The combined variable-impedance Z models have been extended to include an optimized imploading load; this load has been optimized to clarify how each combined variable-impedance design scores on a real-life load

2. **Next-Generation Pulsed Power (6-level)**:

a) Operating characteristics (Bertha circuit modeling and Empire electromagnetic particle-in-cell simulations) for all levels (level "A" through "F") have ben completed for an NGPP point design[5]

b) Circuit modeling (Bertha) predictions for the operating characteristics of ≥ 5 variable-impedance MITL designs for each level have been completed (≥ 30 designs in total)) are provided

c) EM-PIC simulation (Empire) results for the operating characteristics for a selection of the above variable-impedance MITLs are documented here are presented

d) viable variable-impedance designs according to both Bertha and Empire were converged on for levels A and F

Ultimately, the viabilty of these results must be confirmed by fielding the proposed hardware on real Z shots. This is required to comment on the technology's viability for Z and future pulsed power (e.g., ZX and NGPP). The final design set of design recommendations presented here for Z have been fully optimized according to both circuit and EM-PIC for levels A, B, and C, but not for level D. If follow-on work is to be invested in, depending on the objectives (e.g., "proof-of-concept" vs. optimized power flow) it could be prudent to revisit level D to optimize the gains to the fullest extent. Circuit results for level D have been explored in a combined-level model, but not as-yet in EM-PIC.

These designs (or a finalized version resulting from further optimization) could be completed to the engineering level-of-detail by working with computer-aided design drafting technologists. For reasons of cost, fabrication of just one of the levels could be pursued (e.g., level D which is the highest inductance line). Simulations indicate there are side effects associated with tailoring the impedance of just one level while keeping the others unchanged, as we will show[6]; however, these happen at early stages (say, $< 10\%$ of maximum current) and is redirected as the main pulse takes off in level D so should not interfere with confirming trends including: (1) the lower of stack voltage and (2) increase in load currents. Finally, the quality of magnetic insulation should be

[5]NGPP point design 12297; this point design strictly follows the aforementioned pulsed-power design principles: MITLs consist of a constant impedance region down to gaps narrow to minimum 1 cm whereafter a constant gap region continues until to the convolute entrance

[6]bottom line up front: this exercise alters an approximate inductive balance that currently exists among the levels of Z today which lead to "back currents" into the line whose inductance was lowered.

characterized in detail using a host of diagnostics including Faraday cups positioned throughout the MITL to quantify losses as we have found in our studies that loss currents are a critical safety factor due to the threat of turning on anode plasma which drastically changes the operating landscape.

Due to the comprehensive nature of this work, only a fraction of results are included in this final report. The models (geometries, meshes, input decks, spreadsheets, material data files), raw simulation output, tables, plots, Paraview visualizations of mesh data, rendered snapshots in time and animations, and slides produced from this project work are available upon both reasonable, and appropriate[7], request.

[7]Due to materials containing U.S. Atomic Energy Act (AEA) Tier 3 information (e.g., detailed machine specifications of Z), release will generally be restricted to members of the tri-lab National Nuclear Security Administation (NNSA) workforce with a need to know.

2. TECHNICAL APPROACH

For both Z and Next-Generation Pulsed-Power (NGPP) systems, we employ a tandem simulation approach. First, we employ low-cost circuit modeling (either Bertha or the SCREAMER simulation code) to survey a broad survey of candidate MITL designs for operational viablity[1]. Secondly, we follow-up on promising designs identified from circuit simulation results with detailed evaluation using high fidelity electromagnetic particle-in-cell (Empire) simulations. Any designs that both circuit and EM-PIC simulations agree a design is viable we recommend for next steps.

2.1. Circuit Modeling

Two circuit codes were employed for this research[2]. For Z simulations, the SCREAMER code (originally developed at Sandia National Laboratories [37]) was employed. For the NGPP-6 simulation work, the Bertha code (developed by the Naval Research Laboratory [11]). Both codes incorporate pulsed-power-relevant physics models including dynamic loads and magnetically-insulated transmission line (MITL) circuit elements. Code-specific implementation details are outlined in their respective application sections (Section 4.1 for Bertha and Section 3.1.2 for Screamer).

2.2. Electromagnetic Particle-in-Cell Modeling

It is widely accepted that first principles particle-in-cell (PIC) [3, 13] simulations are the most trusted design tool for power flow devices. Electromagnetic Particle-in-Cell simulations are performed for both Z and NGPP systems using the relativistic particle-in-cell capability in Empire: a performance-portable finite element electromagnetic plasma simulation code for unstructured meshes [2] developed at Sandia National Laboratories. The code has been developed with pulsed power as one of main use-cases, having well-tested models for various physics models (Figure 2-1) required to simulate Z and NGPP, including the following list of highlights which cover the major capabilities and diagnostics we use in this project work:

1. **Boundary Conditions**

[1] We define operational viability as a design that meets design targets (e.g., load current delivered) while meeting safety standards (e.g., peak stack voltage guidelines).

[2] Note: the code employed for each system was solely determined by team member (circuit modeler) expertise. The code is not a reflection of one code being considered a better "fit" for a given regime or problem.

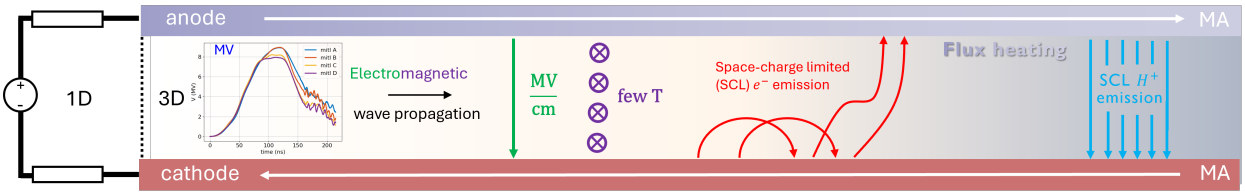

Figure 2-1. The germane processes in the outer MITLs of Z are illustrated. Our electromagnetic particle-in-cell simulations capture all of these including H^+ emission which is an effect of anode plasma formtion. There is as-yet no corresponding model in circuit codes (SCREAMER or Bertha) which highlights another utility for interrogating design safety with more than just circuit simulations.

- *Fields*[3]: perfect electrical conductors (PECs), perfect magnetic conductors (PMCs), periodic (PBCs)
- *Particle handling*: absorbing, reflecting[4], periodic (PBCs)
- *Particle injection*: Space-charge-limited emission from surfaces, thresholded by electric field strength (e.g., cathode electrons) or self-consistent surface temperature (e.g., anode ions)
- *Circuit-coupling*: self-consistent 1D transmission lines [20] coupling (currents I and voltages V) to 2D/3D electromagnetic domains (B and E, respectively). This enables machine-scale simulations through heterogeneous (1D-3D) modeling where most of the accelerator ($\sim$ meters) is accurately represented as 1D transmission lines (TEM wave propagation) and only in the high energy density regions developing approaching the convolute ($\sim$ 10s cm) is 3D EM-PIC required. This results in feasible problem sizes with judicious use of resources (e.g., focusing on a smaller region allows higher resolution meshes).

2. **Surface heating**: a boundary value problem defined by each face on a surface mesh is set up on a 1D grid ("thermal grid") where the heat equation is solved. Various volumetric source terms Q options are available including:
   - *Joule (Ohmic) heating*: $Q = j^2/\sigma(\sigma < \infty)$ is calculated based on the B field penetrating each cell of the 1D thermal grid as determined from solving the magnetic diffusion equation.
   - *Particle flux heating*: $Q = Q_{BBB}$ energy deposition per unit volume is determined from the (relativistic) Bohr-Bethe-Bloch stopping power model for a given material (we model Z MITLs as SS304)
3. **Diagnostics**

[3]PECs: $\mathbf{n} \times \mathbf{E} = 0$, PMCs: $\mathbf{n} \times \mathbf{H} = 0$

[4]reflecting boundary conditions for particles are employed with PMC field conditions to model a "mirror" boundary (i.e., mirror symmetry). In this work, we start with the 360° Z convolute domain. We take this down to the minimum periodic-unit of the post-hole convolute hardware (30°) where PBCs could be employed. Instead, we are able ot further reduce the domain size by exploit mirror symmetry in the hardware geometry to reach a final angular domain of 15° (PMC fields, reflecting particles)

- *Field Line Integrals*: $\int_a^k \mathbf{E}\cdot d\boldsymbol{\ell}$ (`EDLs`) and $\oint_{a,k} \mathbf{B}\cdot d\boldsymbol{\ell}$ (`BDLs`) as proxies for line voltage V (by definition) and the anode (a) or cathode (k) currents $I_{a,k} = \texttt{BDL}/\mu_0$ (from Ampere's law). Note that $I_e = I_a - I_k$ can be used to determine the vacuum current carried by electrons in MITLs.
- *Convection Current Tallies*: used to record anode loss currents over a sideset (a group of mesh surfaces)
- *Temperature at Point*: used to record anode temperature histories at chosen locations
- *Temperature Mesh Data*: used to store anode temperature on a per cell basis for visualization
- *Moment Mesh Data*: used to record electron and ion moments (e.g., number density) one per cell basis for visualization

3. Z REDESIGN

This thrust aims to assess variable-impedance versions of the "outer MITLs" of the Z accelerator and provide final recommendations demonstrating benefits that these potentially provide to Z and future facilities.

3.1. System Overview: the Z accelerator

The 33-meter diameter Z machine (Figure 3-1) drives mega-joules of combined electrical energy stored in 36 pulsed power modules (Marx generators) at its outer perimeter through a set of radially convergent parallel transmission [41] towards a load at the machine center. In the first stage, the individual pulses from each module charge intermediate storage capacitors (ISCs). The ISCs are triggred by controlled laser-triggering switches which can be programmed according to pulse shaping demands of the experiment. Subsequently, the pulses enter the water-insulated pulse-forming lines (PFLs) where a sequence of output transmission lines are mediated by self-breaking water switches to achieve additional pulse sharpening. The pulses combine in a water convolute where the fields are rotated 90 degrees, and output into the vacuum region of the accelerator through four *magnetically-insulated* transmission lines (the "outer MITLs"). The four pulses combine in a current adder topology known as a *post-hole convolute* which feed a single transmission line (the "inner MITL"), that delivers a combined 20-25 MA (load dependent) pulse to a load over $\approx$ 100 ns.

MITLs in pulsed-power accelerators are generally designed to have constant impedance insofar as engineering and safety constraints allow[1]. In particular, the outer MITLs of Z are often said to be one example of this pulsed-power engineering guidance). In this design thrust, we revisit this guiding principle and assess in detail the operating characteristics resulting from MITLs whose impedance profiles are actively tailored ("variable-impedance MITLs" [36, 39]). In ideal (lossless) operation, inductive current gains are expected. But, in the extreme conditions encountered on Z we can anticipate these gains will compete with losses. Our simulation-based study will survey design space in order to understand where the point of diminishing returns in this exercise lies, and to clarify how much flexiblity exists in parameter space.

[1] e.g., for radially convergent pulsed power drivers, conical MITLs is one example of a transmission line geometry having constant impedance. These are geometries with constant angle but a progressively narrower gap in the downstream direction. A common safety criterion is to maintain AK gaps in the outer MITLs $\geq$ 1 cm. On Z, this is strictly enforced at the point where narowing gaps achieve this critical value, creating a region owith constant gap but varying impedance for the remainder of its length.

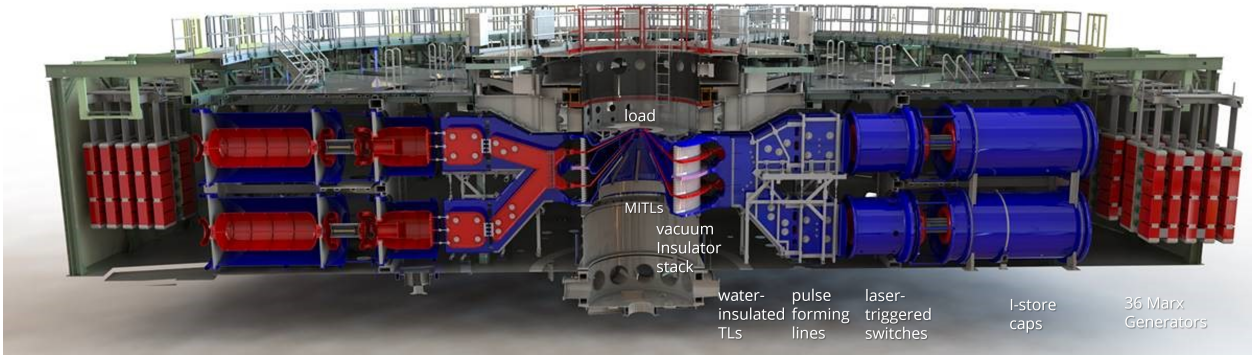

Figure 3-1. (Hardware rendering) cross-section of the Z accelerator

3.1.1. Technical Approach

Our initial plan for the Z thrust was to generate results for the reference case (Z as it exists today, or "Z today") and compare operating performance assessments of variable-impedance versions of these outer MITLs in order to assess improvements. However, upon interrogation of the outer MITL geometries (CAD files), we discovered that every level of Z has significant stretches of its total length having non-constant impedance (even outside the "constant gap" regions). If we proceeded with this exercise to revise impedance profies based on the outer MITLs as they exist on Z today, our results would provide a comparison of our variable-impedance designs versus the original set of (what are ultimtely also) variable-impedance MITLs. The outcome of such an exercise would have been an *optimization*. More seriously, the value of these results would be restricted to this one specific system. In order to broaden the impact of our findings, we pivoted our approach to a simulation-based investigation that could inform understanding of variable-impedance MITLs *as a concept* compared to the conventional pulsed-power choice of constant-impedance MITLs. In pursuit of this goal, we redefined the initial step in our project plan to first design a constant-impedance version of Z. Once that *baseline* has been established, we consider perturbations from this baseline for each level and assess operational viability (whether a design meets design targets while adhering to accepted safety metrics). Specifically, we survey the parameter space of linear tapers. We approach this design task using a tandem simulation strategy: (1) circuit simulations are used to interrogate the design space more efficiently. From these results, (2) promising candidates are identified for further scrutiny and simulated in Empire (EM-PIC) to confirm safe operation and design targets are met. We do this for all levels which are named A (highest current line), B, C, and D (highest inductance line). After we have examined the portfolio of results and have identified a viable combination of designs (for each leve), we combine them for an all-in-one simulation to see how the overall design grades.

3.1.2. SCREAMER Circuit Modeling

A SCREAMER [15, 37] input deck modeling Z consists of a single text file that can easily exceed 8,000 lines. In order to meet our design-oriented objectives, an extensible workflow for creating variations to a "large convolute" Z circuit model was developed. Specificaly, a MATLAB program

was developed to generate the deck from input parameters, ensuring consistency and minimizing errors across multiple configurations (e.g., lossless vs. lossy MITL, static vs. imploding load).

Developing the baseline circuit model itself was the very first step in this work (Figure 3-2).

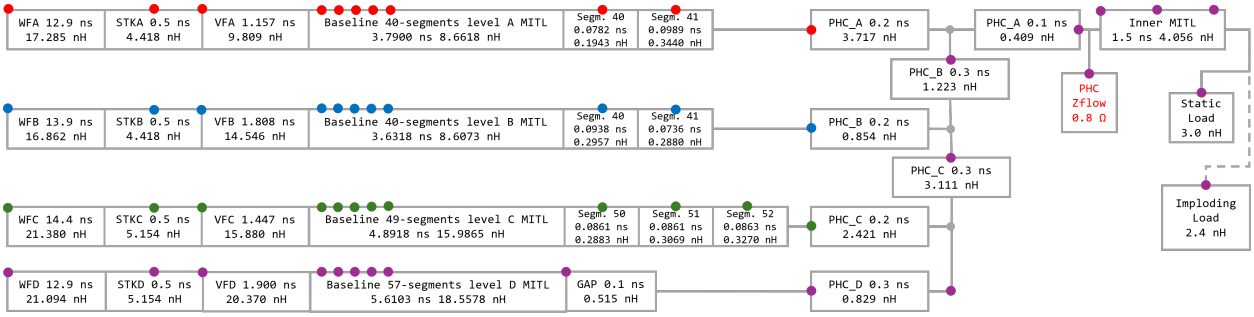

Figure 3-2. (Baseline SCREAMER Z model) The transition time and inductance in each box represents the total values of all circuit elements (not shown) included in that box.

A-level vacuum serial inductance	22.726 nH
B-level vacuum serial inductance	24.59 nH
C-level vacuum serial inductance	5.209 nH
D-level vacuum serial inductance	40.272 nH
All levels vacuum parallel	8.6 nH
Inner MITL	4.056 nH
Total vacuum excluding load	12.655 nH

Table 3-1. Inductance breakdown for the baseline Z model.

In this section we step through the above diagram at a high-level to explain how it was built and to clarify the various models used in Z circuit simulations. The "top" branch in the SCREAMER model is Level D, with the remaining levels attached at distributed convolute locations. This is followed by the inner MITL and the load. The water flares on each level are driven by an open-circuit voltage waveform generated by a legacy Bertha full-Z model [14]; the same waveforms are used in Empire. The inductance breakdown is shown in Table 3-1. The combined inductance of all MITL levels in parallel, including the convolute, is 8.6000 nH, and the total vacuum inductance is 12.655 nH

Water flares WF, insulator stack, and vacuum flares VF are modeled as lossless transmission line blocks TRLs [38]. WF and stack elements were directly ported from the full Bertha model while those for the vacuum flares (except for Level D which was also adopted from Bertha) were built from the Empire 3D geometry. Empire provided the total inductance L and transition time τ (Appendix B.3) and the impedance of the SCREAMER TRL element was calculated as $Z = L/\tau$. Example circuit elements that were implemented for WF stack and VF for baseline level A Z model are given in Figure 3-3 (compare with B-4).

This project work focuses on modification made to the outer MITLs. In order to facilitate tailoring the impedance profiles of the outer MITLs, each MITL was divided into equally spaced segments (≈ 0.1 ns) along its boundary on the MITL AK midline. This decomposition allows us to model

```
! Level A
! Total WF inductance (Z x t) is 17.2854 nH
! Total WF length is 12.9000 ns
!
!TRL LIN  time (s)   impedance (Ω)
TRL  LIN  4.000E-09  1.667
TRL  LIN  5.700E-09  1.078
TRL  LIN  2.200E-09  1.424
TRL  LIN  1.000E-09  1.340
```

(a)

```
! Level A
! Total stack inductance (Z * t) is 4.4181 nH
! Total stack length is 0.5000 ns
!
!TRL LIN  time (s)   impedance (Ω)
TRL  LIN  2.000E-10  8.850
TRL  LIN  3.000E-10  8.827
```

(b)

```
! Level A
! Total VF inductance (Z * t) is 9.8087 nH
! Total VF length is 1.1571 ns
!
!TRL LIN  time (s)    impedance (Ω)
TRL  LIN  2.6240E-10  15.0475
TRL  LIN  3.8690E-10  9.9419
TRL  LIN  3.3260E-10  4.7379
TRL  LIN  1.7520E-10  2.4993
```

(c)

Figure 3-3. (SCREAMER input file stubs) Level A definitions for the segmented water flare, stack, and vacuum flare circuit elements.

to arbitrary MITL geometries via stairtep approximation by making circuit-level changes equivalent to adjusting segment dimensions. The segments were modeled using MITL [38] circuit elements to account for pre-insulation electron losses, with a resolution time set to be ten times smaller than the segment transition time. The total inductance was calculated as $L = Z\tau$ where Z is the segment impedance (Ω) and τ is the segment length (ns). This total inductance value was independently verified using the exact formula and was in excellent agreement.

The convolute region was followed by a variable-resistance SCREAMER [38] Plasma Opening Switch (POS) model, which allows modeling of total losses upstream of the outer MITL. The POS Zflow value of 0.8 Ω was determined by comparison with Empire data for the reduced Z model, which showed excellent agreement with the SCREAMER simulations in our baseline comparisons.

The load used in SCREAMER simulations was either a 3 nH stati load (modeled as a single series inductance) or a 2.4 nH imploding load, modeled using the SCREAMER [38] Cylindrical Foil Model (CYLFOIL block), which provides diagnostics of the imploding load's velocity, position, kinetic energy, and other electrical parameters.

3.1.2.1. Anode Heating Due to Initial Electron Losses

Anode temperature was calculated as a post-processing step using SCREAMER output. Specifically, the increase in anode temperature resulting from the initial, uninsulated electron losses at each MITL segment was calculated as:

$$\Delta T_{anode} = \frac{1.4}{C} \int_{t_{start}}^{t_{end}} \frac{J_{loss} V_{anode}(t)}{R[V_{anode}(t)]} dt \tag{3.1}$$

Here, J_{loss} is the electron-loss current density ($\mathrm{A/cm^2}$), V_{anode} is the anode voltage (V), R is the electron range in the anode ($\mathrm{g/cm^2}$), and C is the anode specific heat capacity [$\mathrm{J/(g \cdot ^\circ C)}$]. The integration is performed over the time duration of the electron losses. The constant 1.4 is an electron multiple-impact factor, suggested by Dr. R. Spielman, accounting for reemission and reabsorption at small incident angles.

The integral was evaluated using custom MATLAB code, with J_{loss} and V_{anode} obtained from SCREAMER simulations, and R interpolated as function of anode voltage based on the NIST

database [1]. Further details on the anode heat calculations implemented in our model can be found in [34].

3.1.3. Empire Modeling

Our starting point for this simulation work is the Empire model for the "18a" (large) convolute hardware completed under the plasma grand challenge LDRD [16]. A high fidelity geometry was created from the engineering CAD file using an in-house geometry/meshing software, Cubit (Figure 3-4).

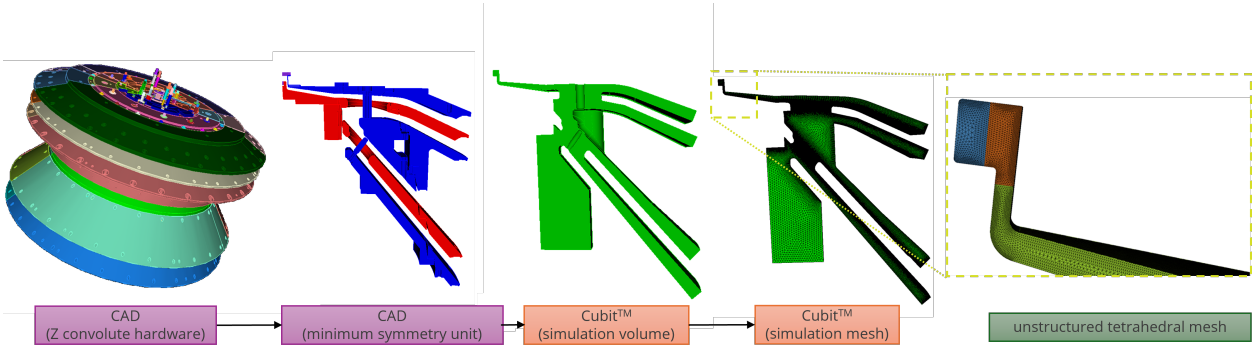

Figure 3-4. Creation of the legacy convolute simulation geometry and mesh in steps. Going from left-to-right: we import the CAD file for the convolute hardware into Cubit, a minimum symmetry unit is cut out, the simulation domain is extracted (the space between anode and cathode hardware) and defeatured, finally a refined mesh is generated that faithfully resolves the high order geometry curves. Notes: (1) the power flow direction is inward for the first 360° picture, then right-to-left in the cut-out views; (2) we take full advantage of the mesh being unstructured simplices, using more resolution (more cells) only where needed (e.g., near surfaces that emit particles); (3) the lower-left boundary on the simulation volume is not a physical boundary, but rather represents a modeling *decision* for how to close the domain to form a single volume for meshing (and simulation). As can be seen from the hardware pictures to the left, the lower region is empty space. Only as much space is included in our simulation model as as necessary to not miss any significant details, e.g., particle flows.

This original model consists of a 3D EM-PIC domain representing the load, inner MITL, convolute, and a portion of each outer MITL. In this research, we are interested in characterizing power flow in the entire outer MITL region. To fulfill this modeling need, we extend the original 3D domain out to the vacuum insulator stack (Figure 3-5(a)-(b)). As this extension lies within a purely axisymmetric region, we were able to extend the domain more simply than working directly with the CAD files, opting to draw its 2D profile from (R,Z) coordinates exported from the CAD file instead. A 3D volume is generated by sweeping the 2D profile about the vertical axis (Figure 3-5(c).

To complete the model, the outer boundaries of the 3D EM-PIC domain (one for each level) are continued several meters upstream into the water flare region using 1D transmission line domains derived from the Z Bertha circuit model [14]. The resulting 1D-3D Empire model resulting from this pursuit is shown in Figure 3-6.

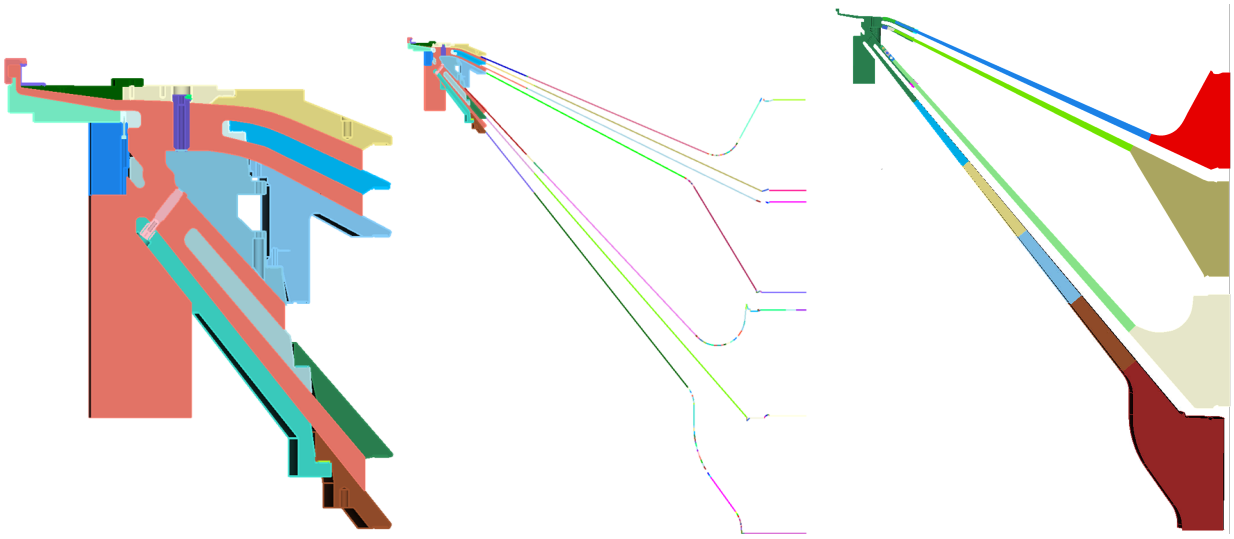

(a) (b) (c)

Figure 3-5. Our project objectives required modeling the entire vacuum region of Z. Panel (a) shows our starting point which is a legacy model from prior work. Note that both the hardware and simulation volume (salmon-colored) are shown for context. Panel (b) shows the domain extended out to the vacuum-insulator stack from (R,Z) coordinates exported directly from the engineering CAD drawing for the outer MITLs. Panel (c) shows the resulting simulation domain.

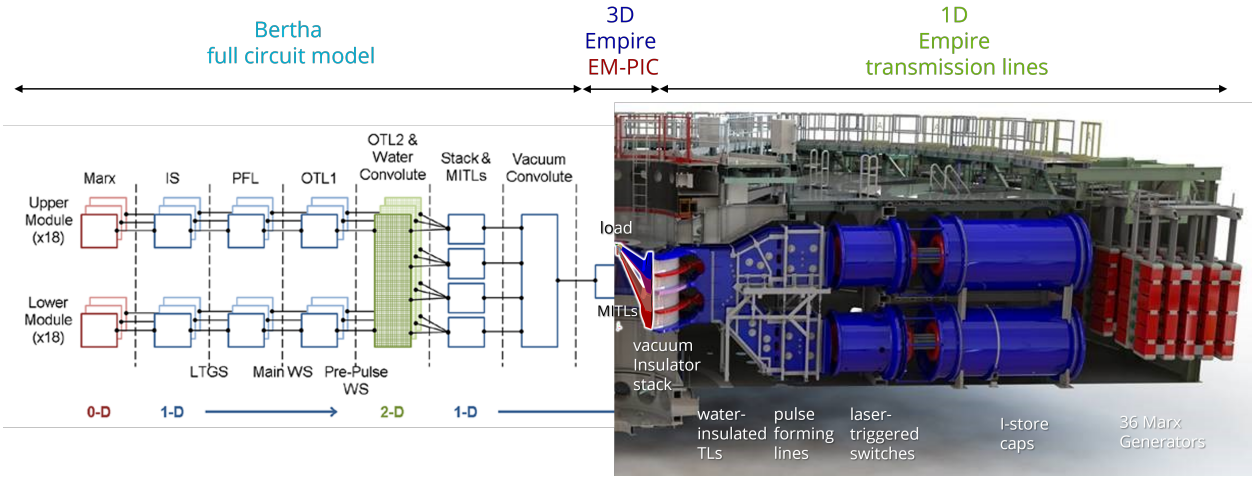

Figure 3-6. A hardware rendering of the Z-machine cross-section is shown. The left half has been peeled away to show the region the full Bertha circuit models (full machine). On the right half, we have the labeled regions the heterogeneous Empire model consisting of 1D transmission line domains (translated from the Bertha circuit parameters) coupled to a 3D EM-PIC domain covering the full vacuum region. Note that the overlayed 3D EM-PIC domain in the center is true to size. Some

Even with this heterogeneous modeling approach to make machine-scale simulations more feasible, the extended domain we are now considering (up to $R \approx 1.5$ m, see Figure 3-5) results in an $\approx$ 500M element mesh even with the most judicious meshing decisions. For our objectives, we anticipate needing to turn around *many* simulations to vet promising design concepts. A problem size this large is too computationally expensive to fit into that schedule and workflow. Therefore, to facilitate our objectives we further decomposed the domain. For level D studies, we replaced the 3D extensions of levels A, B, and C (Figure 3-5(c)) with 1D transmission lines leaving what we refer to as the "extended level D domain" (Figure 3-7(d)). This resulted in a 147M element mesh which is a more feasible problem size; however, it is still big enough to almost precludes opportunities for performing the due diligence necessary to establish confidence in our simulation answers[2]. That being said, since our scope for the Z thrust at this time in the project consisted solely of redesigning level D (the highest inductance line on Z), this stretch problem was seen as worth the trouble since it provided fuller power flow characterization, extending into the convolute and including the machine load. A typical simulation used 147M elements, peaking at just under 1B particles prior to magnetic insulation then averaging 0.25B particles for the remainder of the simulation which used 179,191 time steps (1e-12 sec steps) to reach 201 ns into a pulse that peaks around 150 ns. A typical HPC job used 10,224 cpu-cores (214 compute-nodes) for 29 wall-hours.

Approaching the end of year 2, discussions with leadership lead to a redirection of priorities and our project scope expanded to cover all levels of Z. An even more tractable problem design would be required to make the rapid progress required to address all levels. The strategy decided was to employ the approach used in the NGPP design thrust (Section 3) which is described in more detail in Appendix C. This procedure consistently removes the need to model more than one level at a time in 3D by lumping the downstream combination region for each level as an equivalent inductance calculated by the legacy Z Bertha circuit model. These inductances were used to define 1D Empire transmission lines that could be coupled to the downstream side this time. The main advantage from doing this was not in the cost-savings from excluding the (small) convolute volume, but in producing a domain that now lies completely in the axisymmetric region of the accelerator. This allows us to freely choose the angle of our wedge domain rather than be restricted by the post-hole convolute periodicity (30 degrees). By reducing our wedge angle to as low as 2.5 degrees, meshes were no larger than 7M elements (maximum resolution: 200 microns), particle counts averaged at 20M, and simulation turnover was 12 wall-hours (typically using 900 cpu-cores (25 compute-nodes)) to complete the 190k time steps (10^{-12} sec steps) required to simulate an entire load pulse duration to the very end (214.6 ns). This problem size is very reasonable and enabled significant throughput on Sandia's HPCs throughout this project work. The individual level domains are shown in Figures 3-7(a,b,c) for levels A, B, and C, respectively.

[2] i.e., refinement studies to ensure the simulations have reached converged answers. We were able to do such a calculation once during the winter holiday when HPC traffic was minimum. This simulation used 2x mesh resolution, had 2x particle count and 2x time resolution (341M element mesh, peaking at just under 3B particles before magnetic insulation then averaging 0.5B for the remainder of the simulation which used 230,960 time steps (5e-13 sec steps) to reach 173 ns into a pulse that peaks around 150 ns). The simulation was run on 24k cpu-cores (500 compute-nodes) for 47 wall-hours. The refined simulation showed no significant differences beyond diminished PIC noise in the operating metrics tracked such as anode loss hisotories. Time-averaged data between the base case and the 2x refinement were almost indistinguishable which suggests our base simulation had adequate resolution.

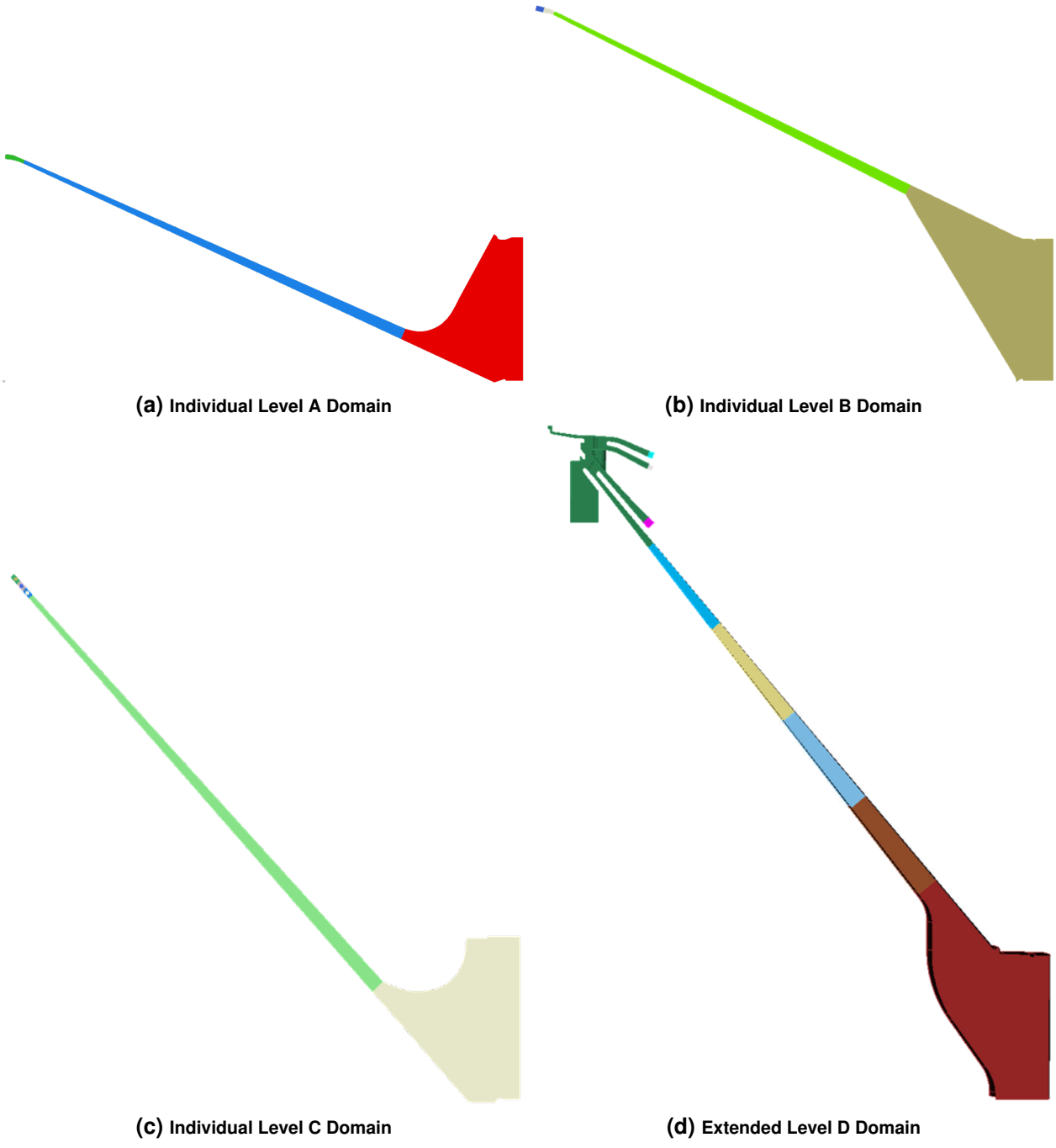

(a) Individual Level A Domain

(b) Individual Level B Domain

(c) Individual Level C Domain

(d) Extended Level D Domain

Figure 3-7. The simulations domains used to study individual levels of Z in EM-PIC are shown (compare with Figure 3-5).The solid colors in the middle region on levels A, B, and C show the "main MITL" region which is the constant impedance region of the MITL. In subsequent sections, we tailor the profile of only the main MITL sections and assess differences to operating performance. Note that the main MITL region on level D is shown, but is not a single color in this figure (its downstream endpoint is the convolute entrance).

In all cases, Empire (EM-PIC) and SCREAMER (circuit) modeled the same domain, whether that be the Extended Level D domain or the individual level domains for levels A, B, and C.

3.2. Individual Level Design & Analysis

3.2.1. Constant-Impedance Z

Constant-impedance version of Z were designed with the following two main guidelines in mind: (1) we define the constant-impedance MITL design in each level for as long in the downstream direction as possible[3], and (2) we ensure the same endpoint gap is maintained on the downstream side. In the following Section 3.2.2, we tailor the impedance profile in *only* the constant-impedance regions (which we refer to as the "main MITL" section, Figure 3-7) in order to assess benefits from reducing the overall inductance. Thus, the motivation behind guideline (1) is to maximize the impact of our designs by varying the impedance over as large a region as possible. The motivation behind the second consideration is to ensure that our designs mate with the existing post-hole convolute entrance. While this is a practical concern, it also convenient in that it allows us to use the same load circuits for every design since no changes are made downstream. In practice, the combination of guidelines (1) and (2) result in a two regions: a constant-impedance region (main MITL) and a transition region.

Starting with the extended 2D profiles which defines Z today (Figure 3-5), we follow the same procedure for each level. First, the cathode profile line (which we confirmed has constant slope on every level) is extended back to the machine centerline. It is then straightforward to redraw the anode profile[4] to exactly intersect the cathode line at $R = 0$ (Figure 3-8). This results in a conical MITL for this level which has constant impedance. Repeating these steps for every level, we create a constant-impedance Z described by $2.28\,\Omega$, $2.37\,\Omega$, $3.26\,\Omega$, and $3.30\,\Omega$ for levels A, B, C, and D, respectively. The full set of parameters describing all constant-impedance levels is summarized in Table 3-2 which were measured in the Empire 3D model along the AK midline using the geometry/meshing software, Cubit. This information was translated and incorporated into an equivalent SCREAMER circuit model. The resulting impedances for constant-impedance Z are slightly smaller than Z today. Therefore, we expect slightly (but not significantly) higher load currents than the nominal 25 MA we would get for Z today.

[3] this results in a minimum gaps slightly under the 10 mm pulsed-power engineering guideline. However, we deliberately proceeded with these designs as we were interested in assessing how hard a line this *empirical* (not rigorously determine) guideline really is. In the NGPP design thrust, we do mind this guideline which presents an intersting complimentary set of results that strictly follow conventional guiding wisdom. Generally, we found in our Z design studies that going under this gap size (insofar as our designs did) was not a clearly deal breaker on its own. In individual (decoupled) level simulations of the level having the smallest gap (MITL D which reached a minimum gap of 0.8602 cm), SCREAMER simulations predicted this region heated up beyond anode plasma breakdown thresholds while Empire showed it was safely under this limit. However, in combined level simulations, SCREAMER predicts level D drops below thresholds when variable designs are included; this is what we mean by this gap size is not a deal breaker "on its own", there is both an upstream effect and an inter-level effect that factors in. On the other hand, If the Empire results are to be trusted then it was not an issue even for an individual level (decoupled) system.

[4] We point out that it is possible to pursue the opposite approach where the cathode is revised to to form a cone with the existing anode. Making changes to the cathode side is generally not recommended since small changes to the cathode geometry can lead to field enhancements. This can affect electron emission onset during the pulse and have feedback on the resulting MITL flow dynamics.

Level	Outer R (cm)	Outer gap (cm)	Outer Zvac (Ω)	Inner R (cm)	Inner gap (cm)	Inner Zvac Ω)	Angle (deg)
A	128.7487	4.8958	2.28	24.6048	0.9356	2.28	23.8784
B	120.9057	4.7791	2.37	23.9216	0.9456	2.37	27.0303
C	122.2593	6.6637	3.268	23.9073	1.3031	3.268	47.8832
D	122.1612	6.7337	3.305	15.5387	0.8602	3.3192	50.6591

Table 3-2. Design parameters for the "Constant-Impedance Z" (baseline) MITLs

As an example, we show the finalized constant-impedance level A domain in Figure 3-9. This figure also shows the segmentation used in both the circuit model and in the EM-PIC domain. This faciliates making as one-to-one comparisons as possible between simulation predictions from Empire (EM-PIC) and SCREAMER (circuit) simulations. We developed the models together to ensure both circuit and EM-PIC agree on the same segment boundaries and segment centroids so that point-to-point comparisons can be made for voltages, currents, temperatures and segment-to-segment comparisons can be made for anode losses. An example of a SCREAMER model summary for the main MITL section is given as Table 3-3 where the segments are contextualized in Figure 3-9). More complete summaries of the SCREAMER main MITL models is provided in Appendix D.

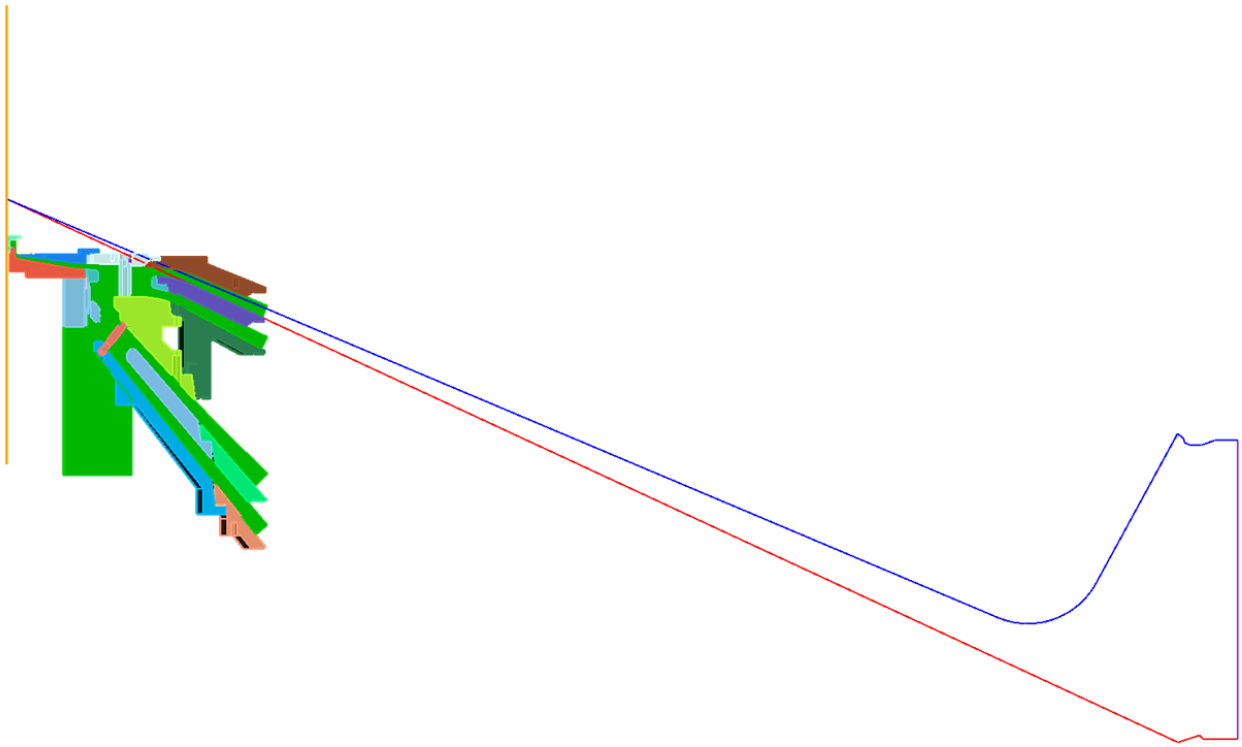

Figure 3-8. (Constant-Impedance Z, Level A) A new anode line (top; blue) is drawn to intersect the existing cathode line (bottom; red) when extended back to the machine centerline. A surface body (gold) at $R = 0$ was created for the purposes of seeking a common intersection point which forms the cone apex.

The models for every level were first checked for consistency by comparing results from lossless

Segm	midpoint-cm	gap-cm	length-cm	Zvac-Ohms	Eon-kV/cm
1	127.447	4.846	2.847	2.2800	20000
2	124.843	4.747	2.847	2.2800	20000
3	122.240	4.648	2.847	2.2800	20000
4	119.636	4.549	2.847	2.2800	20000
5	117.033	4.450	2.847	2.2800	20000
6	114.429	4.351	2.847	2.2800	20000
7	111.825	4.252	2.847	2.2800	20000
8	109.222	4.153	2.847	2.2800	20000
9	106.618	4.054	2.847	2.2800	20000
10	104.015	3.955	2.847	2.2800	20000
11	101.411	3.856	2.847	2.2800	20000
12	98.807	3.757	2.847	2.2800	20000
13	96.204	3.658	2.847	2.2800	20000
14	93.600	3.559	2.847	2.2800	20000
15	90.997	3.460	2.847	2.2800	20000
16	88.393	3.361	2.847	2.2800	20000
17	85.789	3.262	2.847	2.2800	20000
18	83.186	3.163	2.847	2.2800	20000
19	80.582	3.064	2.847	2.2800	20000
20	77.979	2.965	2.847	2.2800	20000
21	75.375	2.866	2.847	2.2800	20000
22	72.771	2.767	2.847	2.2800	20000
23	70.168	2.668	2.847	2.2800	20000
24	67.564	2.569	2.847	2.2800	20000
25	64.961	2.470	2.847	2.2800	20000
26	62.357	2.371	2.847	2.2800	20000
27	59.753	2.272	2.847	2.2800	20000
28	57.150	2.173	2.847	2.2800	20000
29	54.546	2.074	2.847	2.2800	20000
30	51.943	1.975	2.847	2.2800	20000
31	49.339	1.876	2.847	2.2800	20000
32	46.735	1.777	2.847	2.2800	20000
33	44.132	1.678	2.847	2.2800	20000
34	41.528	1.579	2.847	2.2800	20000
35	38.925	1.480	2.847	2.2800	20000
36	36.321	1.381	2.847	2.2800	20000
37	33.717	1.282	2.847	2.2800	20000
38	31.114	1.183	2.847	2.2800	20000
39	28.510	1.084	2.847	2.2800	20000
40	25.907	0.985	2.847	2.2800	20000

Table 3-3. (Example: Level A Constant-Impedance Baseline) SCREAMER Circuit model for the main MITL region of constant-impedance level A. The columns `Zvac` and `Eon` list the segment vacuum impedance and the electric field threshold to turn on (space-charge-limited) electron emission (the same value is used in the Empire model for consistency), respectively. All segments are modeled as `MITL` elements in SCREAMER .)

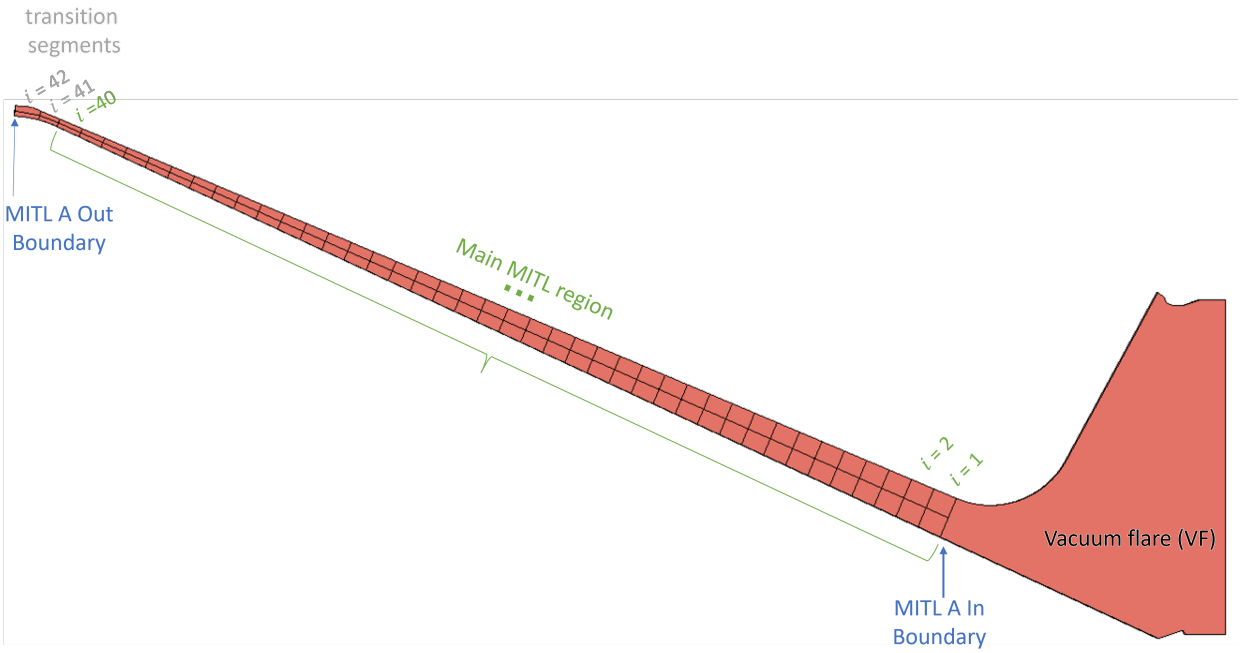

Figure 3-9. the segmentation used in the circuit is shown.

simulations. In SCREAMER, this means losses are turned off for any MITL elements. In Empire, this means we do not emit particles and do a field-only simulation. After consistency was confirmed for a level, comparisons were made with "losses" (i.e., each code turns on models for as many of the main processes in MITLs (Figure 2-1) as it can and in its own way. For example, in SCREAMER we turn on the MITL subroutine for these elements which has a model implemented to smoothly turn off losses based on local voltage and current. This is a model for magnetic insulation. In Empire, we do not turn on a model but turn on particles. Since EM-PIC codes integrate macroparticle orbits, magnetic insulation is realized self-consistently by interacting with the EM fields. One notable capability gap between the two modeling approaches is that there is as-yet no means in circuit codes to model H+ emission; this underscores the necessity of using a higher fidelity approach such as an EM-PIC code to circle back on any promising MITL designs in order to more comprehensively evaluate candidate performance. In this work, we have found anode plasma to be one of the most importnat factors in assessing the operational viablity and safety of a given MITL design. Unless otherwise mentioned, every lossy simulation shown in this work using Empire has every process turned on in Figure 2-1, which includes H+ emission.

We have developed a number of point-to-point comparisons between circuit and EM-PIC simulations to check consistency, confirm outcomes, and overall to facilitate characterization of MITL power flow. We present a selection of these results below to clarify the operating characteristics of our baseline system which is a constant-impedance version of Z.

Figure 3-10 measures voltages at selected locations locations in the downstream direction, starting with the water flare (WF). As the driving pulse ramps up, electron emission is able to occur even as far upstream as the insulator stack ($\approx$ 45 cm AK gap). Electron emission (and flow electrons) change the local operating impedance and have the the effect of sharpening the voltage

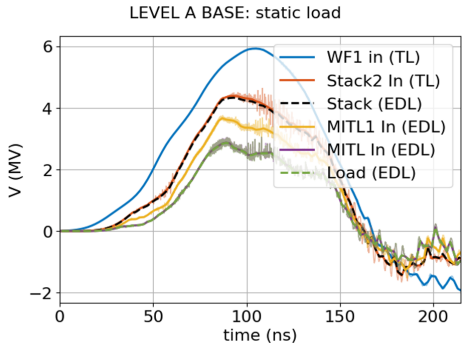

(a) Empire: Individual Level A Domain

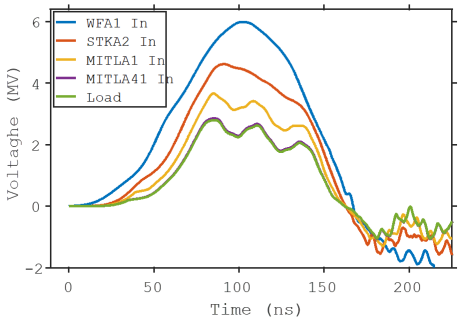

(b) SCREAMER: Individual Level A Domain

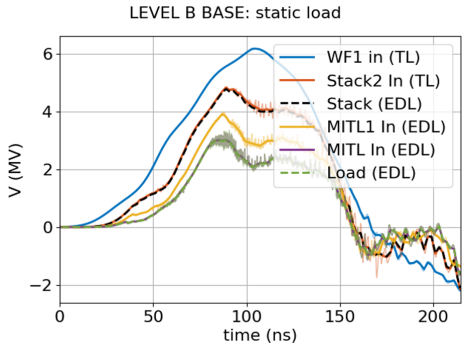

(c) Empire: Individual Level B Domain

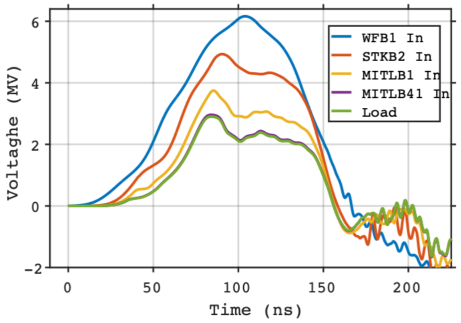

(d) SCREAMER: Individual Level B Domain

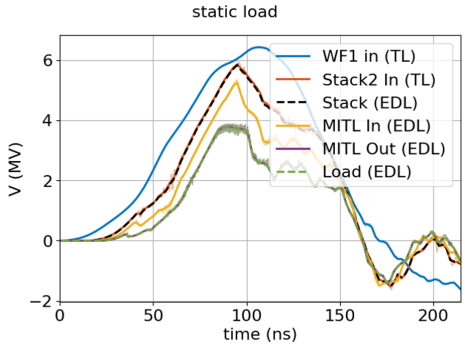

(e) Empire: Individual Level C Domain

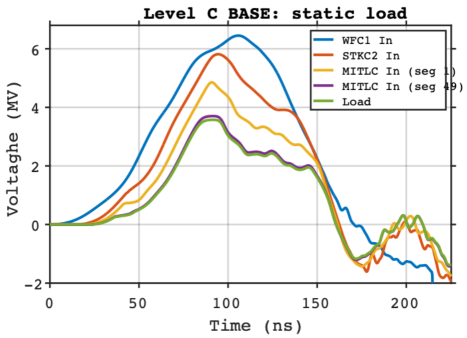

(f) SCREAMER: Individual Level C Domain

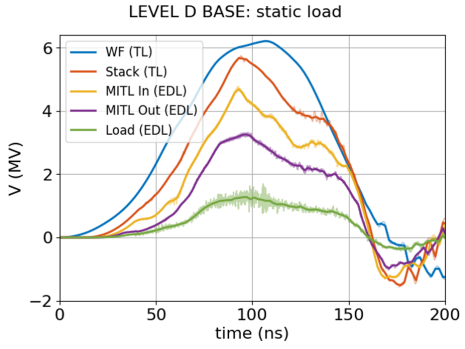

(g) Empire: Extended Level D Domain

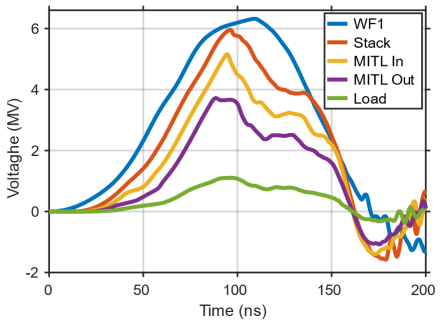

(h) SCREAMER: Extended Level D Domain

Figure 3-10. (Constant-impedance Z) Simulated voltages for each level are shown at select locations. Note that "WF" labels the water flare and that "load" is the downstream output of a given domain meaning the Extended level D is the actual load on Z whereas the load for individual levels A, B, and C is the output of the MITL domain. In the Empire plots, raw output is plotted semi-transparently while the darker line of the same color plots the 2-ns time-averaged data to help clarify trends.

at a given location as well as increasing the peak voltage compared to lossless simulations (not shown). This effect can be seen on every level of Z. Figure 3-11 and 3-11 are shown further clarify operating characteristics by studying voltages and currents at common locations. Compared to lossless simulations, including losses leads to slightly lower currents at early times due to electron loss fronts but after the onset of magnetic insulation there is apparently no visible changes to the MITL currents which is a testament of how well magnetic insulation works in constant-impedance systems.

An interesting feature appears in the level D currents just prior to the main ramp where the current becomes negative. This highlights the importance when considering re-designs to preserve the approximate inductive balance that exists between the levels of Z. In this exercise, we created a constant-impedance geometry for level D but left the remaining levels alone. Current driven into convolute (current adder) region from other levels see a lower inductance path in level D which is already a relatively late line compared to the other levels. This results in current momentarily being pushed into level D before the main pulse arrives. Note that the reason this does not occure in the other level simulations is because level D models an "extended" domain which includes not only the convolute but a few 10s of centimeters of the other levels. This also gives a datapoint that speaks to the extent our approach for modeling the other levels A, B, and C with a lumped inductance for the convolute is truly equivalent. Our tests of these decoupled level domains (Section C) showed this approach produces strong agreement agrees for the load current and stack voltages compared to the full model. But, the fact that it does not show the same negative current feature seen in level D which models the extended domain shows one example of how it is not quite equivalent. This is expected because modeling a combination region as a single number just effects transit time on propagating waves (i.e., reactance), the feedback from this reduced model is not more detailed and those lack of details explain the differences observed here. This example also highlights the need to do a combined calculations ("all levels simulations") at least in the end of our design task in order to proprerly assess the operating characteristics.

The load current is shown in Figure 3-13 for each level. In particular, we point out that the extended level D simulation whose load is the same as the machine load on Z shows a similar current delivery as Z today for a short load ($\approx$ MA). The other levels also show similar currents to Z today for the measurement shown here ("load" refers to the output of a given domain so for levels A, B, and C this is the current delivered to the convolute entrance). This is an important conclusion as it confirms "do no harm" principles were upheld in our design task of creating a constant-impedance version of Z. It performs very similar to Z today. This gives us a starting point from where variable-impedance designs can be explored (See next section 3.2.2).

Finally, we report two related metrics: loss currents (Figure 3-14) and anode temperature (Figure 3-15) versus machine radius. The anode temperature plots show lower temperatures are predicted by Empire almost everywhere. The non-monotonic trends in the Empire data is a first example of the kind of detail EM-PIC can clarify compared to circuit models. The irregular heating is due to breaches from insulated laminar flow and scrape-off from vortices flowing through gaps that narrow in the downstream direction, as well as the stochastics of PIC simulations. The reason for the lower anode temperatures in Empire compared to SCREAMER is seen in the loss plots. Empire, which self-consistently realizes magnetic insulation from first principles on a particle-by-particle basis, simulates a significant reduction of electron losses

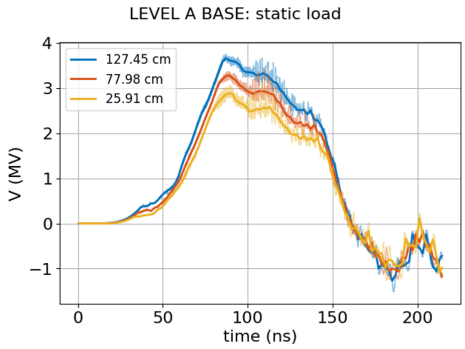

(a) Empire: Individual Level A Domain

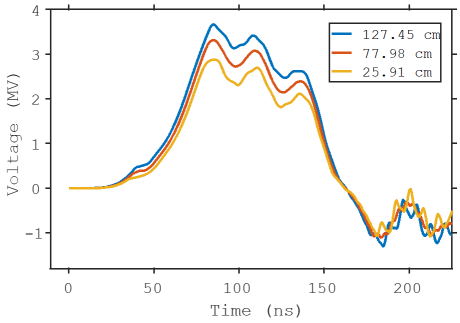

(b) SCREAMER: Individual Level A Domain

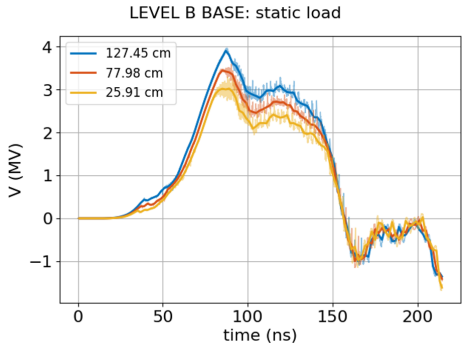

(c) Empire: Individual Level B Domain

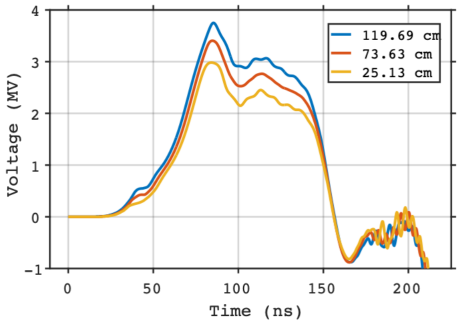

(d) SCREAMER: Individual Level B Domain

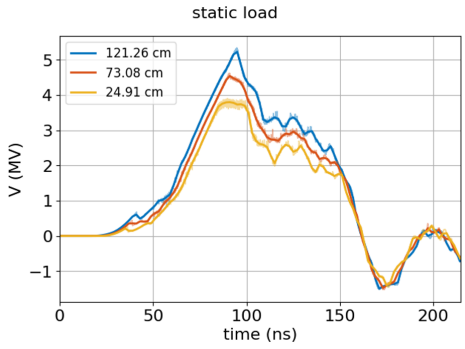

(e) Empire: Individual Level C Domain

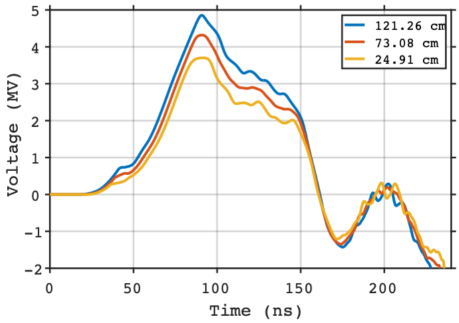

(f) SCREAMER: Individual Level C Domain

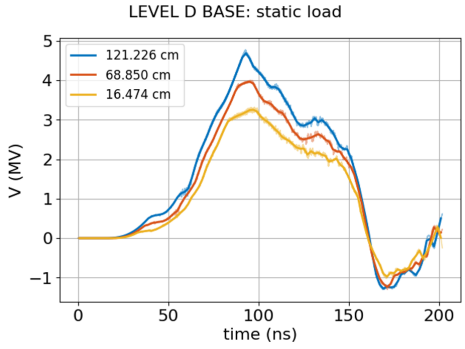

(g) Empire: Extended Level D Domain

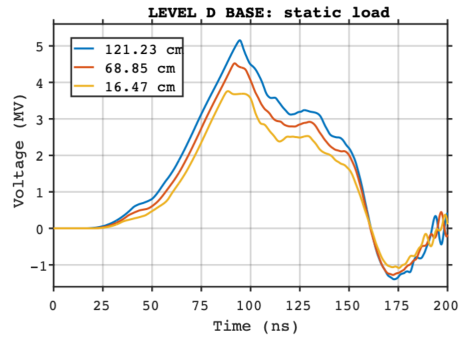

(h) SCREAMER: Extended Level D Domain

Figure 3-11. (Constant-impedance Z) Simulated voltages at the start, middle, and end of each main MITL region

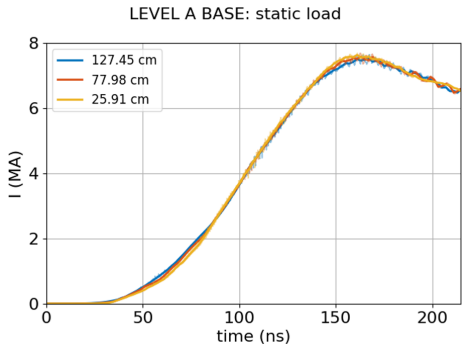

(a) Empire: Individual Level A Domain

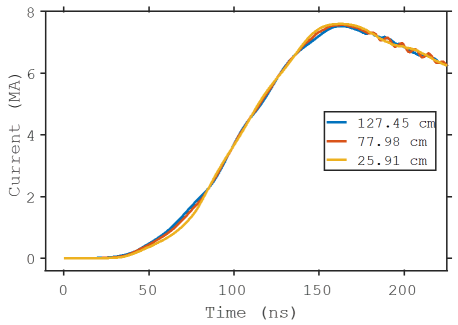

(b) SCREAMER: Individual Level A Domain

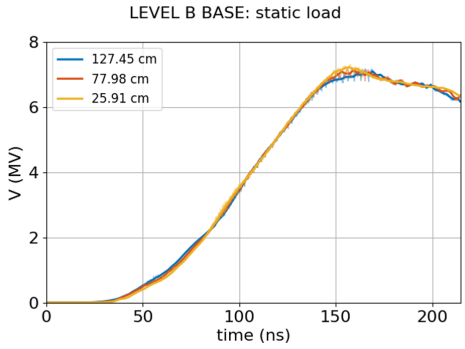

(c) Empire: Individual Level B Domain

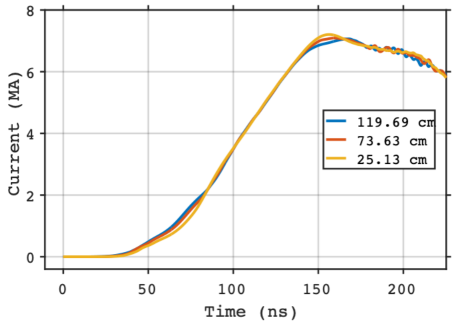

(d) SCREAMER: Individual Level B Domain

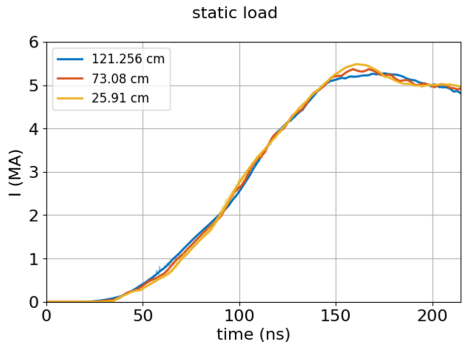

(e) Empire: Individual Level C Domain

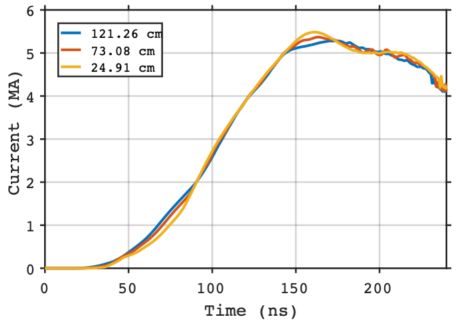

(f) SCREAMER: Individual Level C Domain

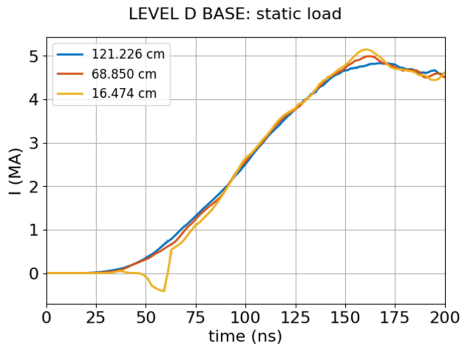

(g) Empire: Extended Level D Domain

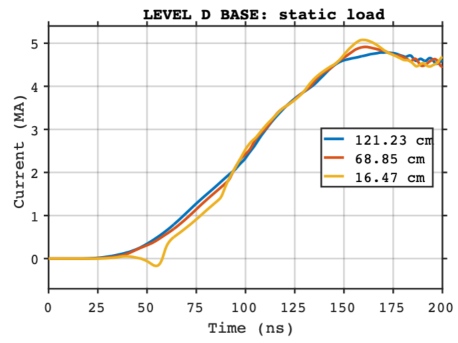

(h) SCREAMER: Extended Level D Domain

Figure 3-12. (Constant-impedance Z) Simulated anode currents at the start, middle, and end of each main MITL region

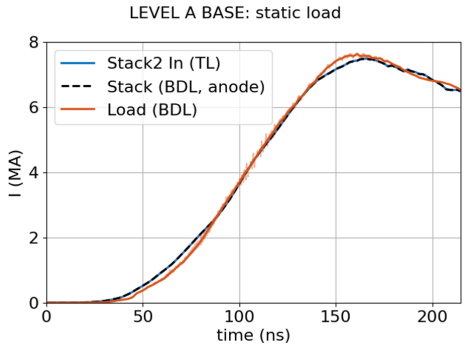

(a) Empire: Individual Level A Domain

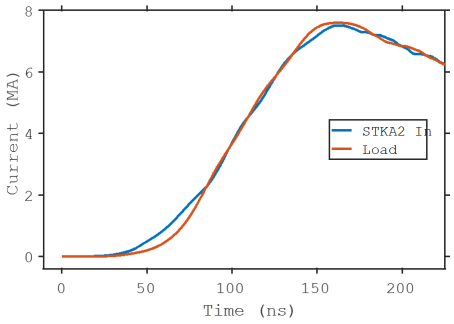

(b) SCREAMER: Individual Level A Domain

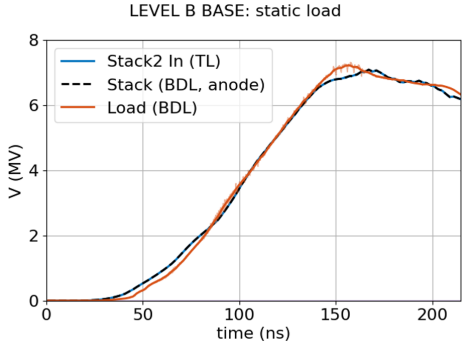

(c) Empire: Individual Level B Domain

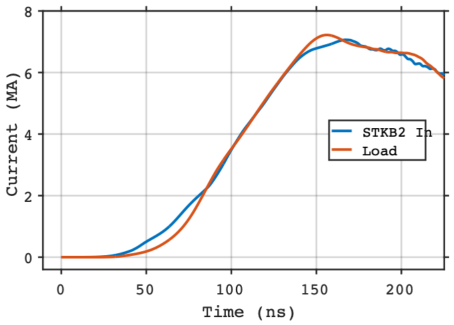

(d) SCREAMER: Individual Level B Domain

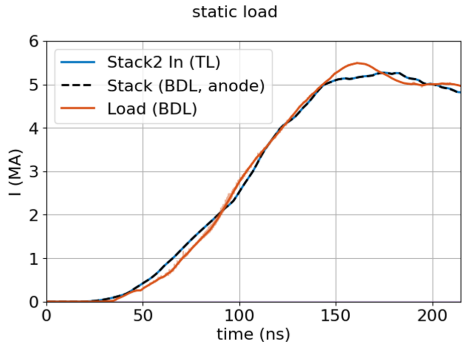

(e) Empire: Individual Level C Domain

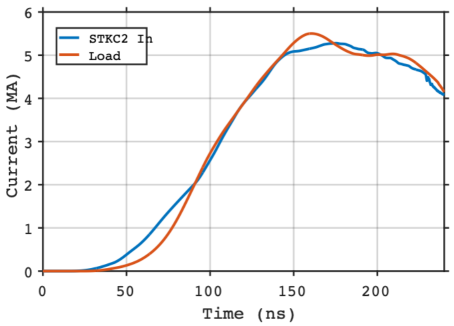

(f) SCREAMER: Individual Level C Domain

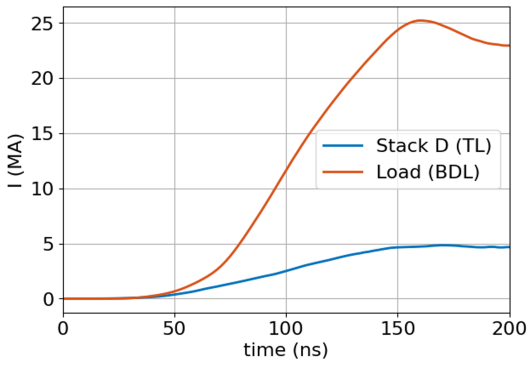

(g) Empire: Extended Level D Domain

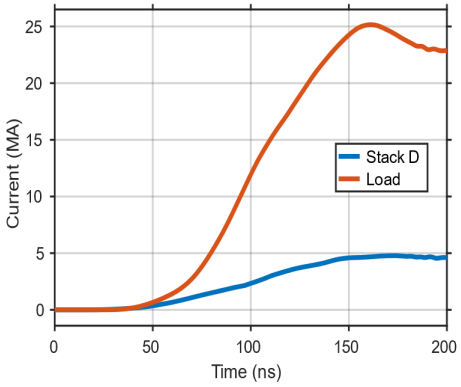

(h) SCREAMER: Extended Level D Domain

Figure 3-13. (Constant-impedance Z) Simulated anode stack vs. load currents. Note that "load" is the downstream output of each domain; the Extended level D is the actual load on Z whereas the load for individual levels A, B, and C is the output of the MITL domain.

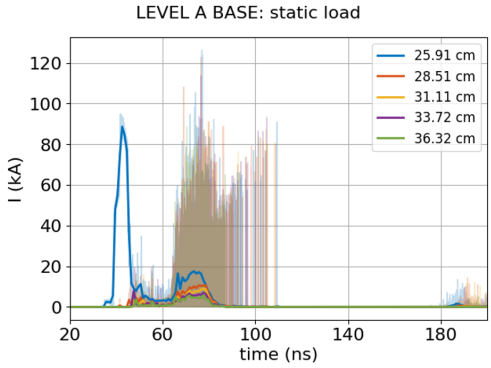

(a) Empire: Individual Level A Domain

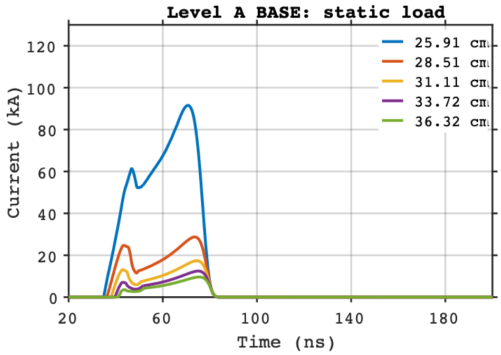

(b) SCREAMER: Individual Level A Domain

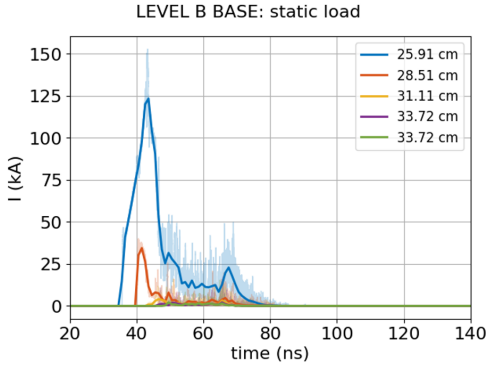

(c) Empire: Individual Level B Domain

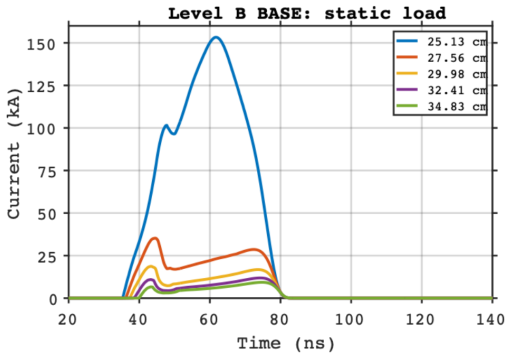

(d) SCREAMER: Individual Level B Domain

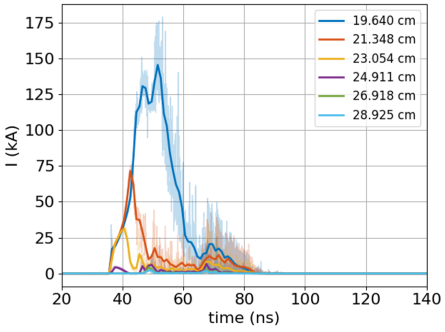

(e) Empire: Individual Level C Domain

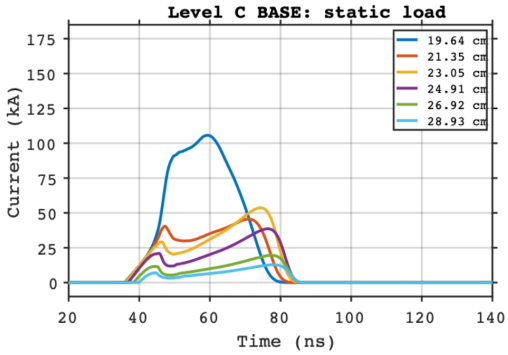

(f) SCREAMER: Individual Level C Domain

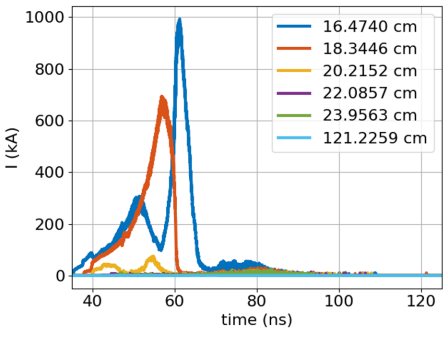

(g) Empire: Extended Level D Domain

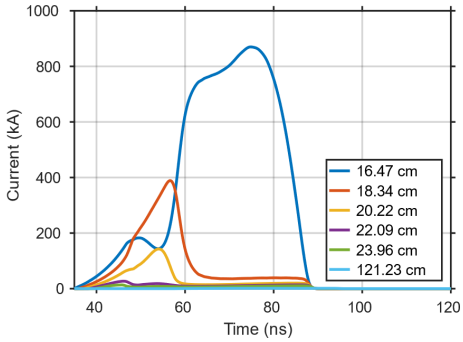

(h) SCREAMER: Extended Level D Domain

Figure 3-14. (Constant-impedance Z) Simulated anode losses in the main MITL region

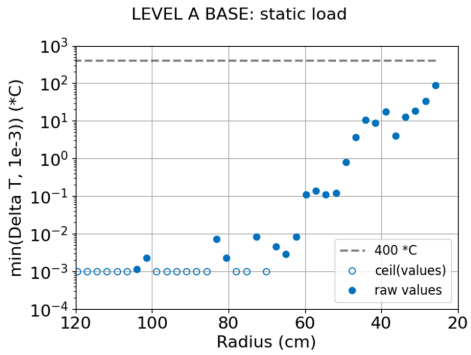

(a) Empire: Individual Level A Domain

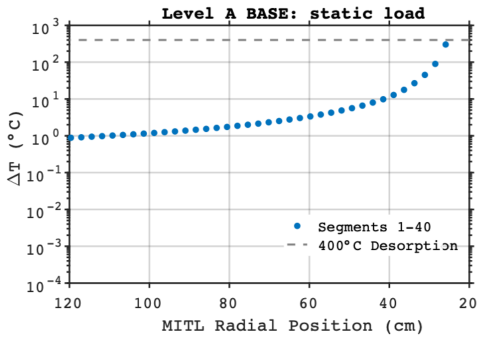

(b) SCREAMER: Individual Level A Domain

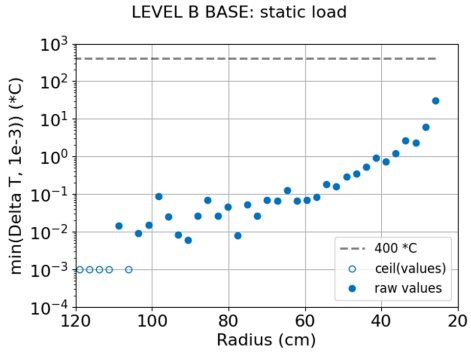

(c) Empire: Individual Level B Domain

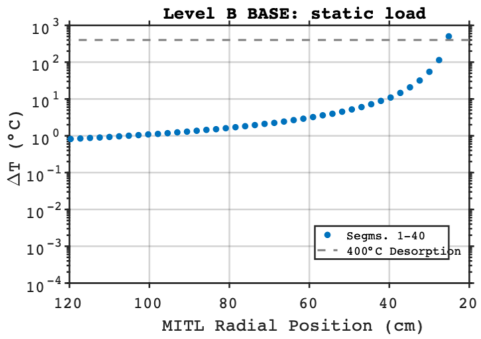

(d) SCREAMER: Individual Level B Domain

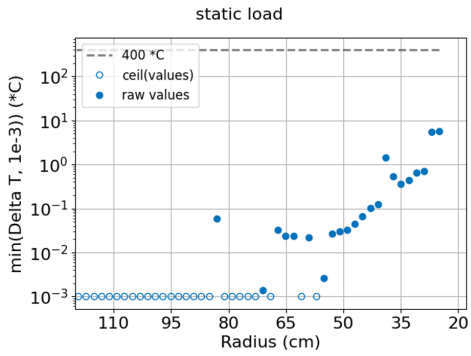

(e) Empire: Individual Level C Domain

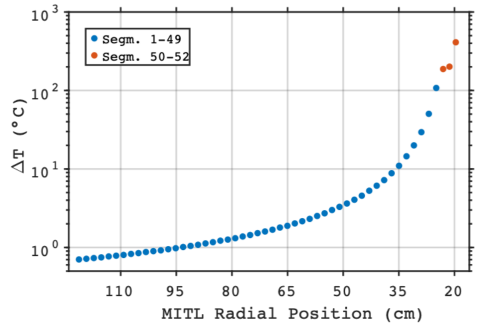

(f) SCREAMER: Individual Level C Domain

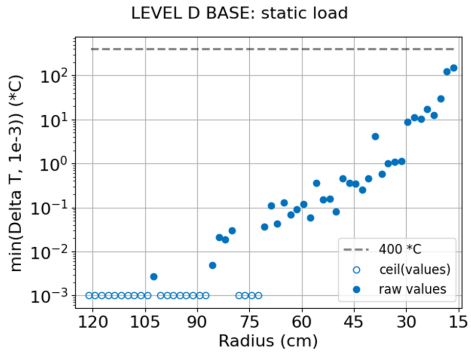

(g) Empire: Extended Level D Domain

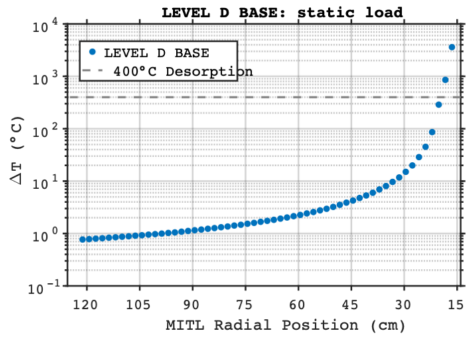

(h) SCREAMER: Extended Level D Domain

Figure 3-15. (Constant-impedance Z) Simulated anode temperature vs radius. On the Empire plots, open circles mark data whose values $\Delta T \approx 0$ deg, but which have been plotted at exactly $\Delta T = 10^{-3}$ to allow trends to be seen more clearly. Otherwise, the y-axis would need to span orders of magnitude to include negligible values (e.g., $\Delta T = 10^{-12}$).

sooner than SCREAMER which gradually turns off losses according to its model. Empire continues to show losses after magnetic insulation turns on (e.g., level A); again, this is due to scrape-off electrons from the vortex components of the flow layer which is not captured in circuit modeling. That being pointed out, these losses are seen to represent only brief contributions (spikes) to the total heating with average losses < 20 kA. For a MITL carrying mega-amperes of current, this is insignficant and definitely a safe design.

Finally, the features of current loss at early times can be commented on. Empire's loss curve rises more sharply than in SCREAMER, meaning electron emission turns on more rapidly in Empire compared to SCREAMER model. Resolving this discrepancy is less obvious since Empire and SCREAMER both use emission model settings whose values are chosen for different reasons[5] Therefore, it is not clear if Empire or SCREAMER is closer to the "ground truth". However, given the excellent level of agreement between the codes in the operating metrics we are interested in (e.g., load current) it is clear that these emission turn-on settings are not a sensitive parameter on the results.

[5]In EM-PIC codes, one of the main considerations is to choose a slow enough ramp time to prevent "checkerboarding" in the emission pattern. This happens when the injected charge from a given mesh face is large enough to turn off cells nearby (halo effect) and is an effect of both macroparticle discreteness and finite-size emission surfaces (cells). In our simulations, we use a 2-ns ramp time to smoothly throttle emission from zero to the Child-Langmuir (space-charge) limit over this amount of time. In our experience in simulating pulsed power accelerators (and the regimes therein), for a 50-ns rise time pulse this amount of steering of the injecton physics in time is gentle enough to prevent checkerboarding while not influencing the dynamics later in time. This is just one of several user-defined parameters in a standard PIC injection model that is made to enable modeling emission in a variety of circumstances and regimes.

3.2.2. Variable-Impedance Z

From the constant-impedance baseline designs for each level (Section 3.2.1), we considered a series of variable-impedance versions in the parameter space of linear tapers. Each design was produced by choosing a desired decrease in inductance (e.g., 20% compared to baseline) and then determining the corresponding (smaller) AK gap at the "MITL In" boundary (equivalently, the vacuum flare downstream exit) required to meet this design constriant. A circuit model for each design was created (similar to Section 3.1.2) and simulated using SCREAMER. The results were collected to allow assessment of operating performance across the designs, and to identify design candidate recommendations for further scrutiny using electromagnetic particle-in-cell (EM-PIC) simulations in Empire. Employing EM-PIC provides more detailed characterizations of operating performance and safety (e.g., *distributions*, rather than segment tallies, of anode losses and corresponding surface temperatures), is more trusted due to its high fidelity (e.g., magnetic insulation is not turned on with a model, but realized from first principles due to particles interacting self-consistently with the fields), MITL flow physics is resolved in full detail (i.e., resolves deviations from equilibirum flow such as instablities and vortex flow), and it can include additional physics for which no circuit models currently exist (e.g., anode plasma emission of H+ ions).

In our design thrust, we considered inductance reductions of 20%, 30%, 40%, 50%, and 60% for levels A, B, and C which are summarized in Figues 3-16 to 3-18. The individual level domains (Section 3.1.3) were used for rapid turnaround both in SCREAMER and Empire simulations. Level D was studied using the "Extended Level D" domain which included the convolute and regions downstream. This larger problem only permitted study of one candidate design (Table 3-18) to be simulated in Empire which was in year 1 of the project. To meet our deliverables on our tight timeline, project priotization required us to move on to the remaining levels. We had planned to return to level D to do an Empire/SCREAMER design optimization exercise as we show here for levels A, B, and C but time did not permit us to come full circle on this. Therefore, the cross-code evaluation of level D presented in this section consists of just the one variable-impedance design (`Variable1`)[6]. Both SCREAMER and Empire results agree this design is viable.

MITL	Desired $\Delta L/L$	MITL L (nH)	Outer R (cm)	Outer gap (cm)	Outer Z (Ω)	Inner R (cm)	Inner gap (cm)	Inner Z (Ω)	Screamer $\sum(Z\tau)$	Vacuum L (nH)	Vacuum $\Delta L/L$
Baseline MITL		8.6618	128.7487	4.8958	2.2800	24.6048	0.9356	2.2800	8.6618	45.709	
Variable 1	20%	6.9295	128.7487	3.5946	1.6740	24.6048	0.9356	2.2800	6.9282	43.975	3.79%
Variable 2	30%	6.0633	128.7487	2.9461	1.3720	24.6048	0.9356	2.2800	6.0642	43.111	5.68%
Variable 3	40%	5.1971	128.7487	2.2955	1.0690	24.6048	0.9356	2.2800	5.1974	42.245	7.58%
Variable 4	50%	4.3309	128.7487	1.6448	0.7660	24.6048	0.9356	2.2800	4.3306	41.378	9.48%
Variable 5	60%	3.4647	128.7487	0.9942	0.4630	24.6048	0.9356	2.2800	3.4638	40.511	11.37%

Figure 3-16. (Z Level A) Variable-impedance design candidates

[6]N.B. several additional level D `Variable*` designs are contained within the larger study of the combined levels simulation section. Please note those results are from circuit modeling alone and have not as-yet been evaluated in EM-PIC.

MITL	Desired $\Delta L/L$	MITL L (nH)	Outer R (cm)	Outer gap (cm)	Outer Z (Ω)	Inner R (cm)	Inner gap (cm)	Inner Z (Ω)	Screamer $\sum(Z\tau)$	Vacuum L (nH)	Vacuum $\Delta L/L$
Baseline MITL		8.6073	120.9057	4.7791	2.370	23.9216	0.9456	2.370	8.6073	52.117	
Variable 1	20%	6.8858	120.9057	3.5026	1.737	23.9216	0.9456	2.370	6.8864	50.396	3.30
Variable 2	30%	6.0251	120.9057	2.8634	1.420	23.9216	0.9456	2.370	6.0246	49.534	4.96
Variable 3	40%	5.1644	120.9057	2.2262	1.104	23.9216	0.9456	2.370	5.1655	48.675	6.60
Variable 4	50%	4.3037	120.9057	1.5870	0.787	23.9216	0.9456	2.370	4.3037	47.813	8.26
Variable 5	60%	3.4429	120.9057	0.9478	0.470	23.9216	0.9456	2.370	3.4419	46.951	9.91

Figure 3-17. (Z Level B) Variable-impedance design candidates

MITL	Desired $\Delta L/L$	MITL L (nH)	Outer R (cm)	Outer gap (cm)	Outer Z (Ω)	Inner R (cm)	Inner gap (cm)	Inner Z (Ω)	Screamer $\sum(Z\tau)$	Vacuum L (nH)	Vacuum $\Delta L/L$
Baseline MITL		15.9865	122.2593	6.6637	3.268	23.9073	1.3031	3.268	15.9865	77.373	
Variable 1	20%	12.7892	122.2593	4.8856	2.396	23.9073	1.3031	3.268	12.7871	74.173	4.14%
Variable 2	30%	11.1906	122.2593	3.9986	1.961	23.9073	1.3031	3.268	11.1910	72.577	6.20%
Variable 3	40%	9.5919	122.2593	3.1096	1.525	23.9073	1.3031	3.268	9.5913	70.978	8.27%
Variable 4	50%	7.9933	122.2593	2.2205	1.089	23.9073	1.3031	3.268	7.9916	69.378	10.33%
Variable 5	60%	6.3946	122.2593	1.3335	0.654	23.9073	1.3031	3.268	3.4419	64.828	16.21%

Figure 3-18. (Z Level C) Variable-impedance design candidates

MITL	Baseline 3.3-Ω	Variable 2.5-Ω	ΔL	$\Delta L/L$
D-level MITL	18.558 nH	14.938 nH	3.620 nH	19.51%
D-level total	40.272 nH	36.652 nH	3.620 nH	8.99%
All level in parallel	8.399 nH	8.307 nH	0.092 nH	1.10%
Total vacuum excluding load	12.455 nH	12.363 nH	0.092 nH	0.74%

Figure 3-19. (Z Level D) Variable-impedance design candidate

SCREAMER simulations were performed for all designs summarized in tables 3-16 to 3-19. In this section, we showcase only the designs identified as main candidates in our design pursuits. These designs ({`Variable2`, `Variable3`, `Variable4`}) for level A, B, and C were the down-selected candidates chosen to be scrutnized in more detail using EM-PIC simulations based on encouraging predictions from circuit modeling. Only select plots found to be most important for identifying a winning design for each level are presented here. We also present results for the single variable-impedance design we studied for level D (`Variable1`).

A major design target is load current (Figure 3-27). Noting that our naming convention (`Variable1`, `Variable2`, ...) is chosen so that so that higher index values correspond to greater reductions to inductance (20%, 30%, ...), the circuit simulation results for each level A, B, and C show increasing (yet modest) gains as we go from `Variable2` to `Variable3` to `Variable4` due to increasing inductive savings. Both Empire and SCREAMER also predict in every case (level D included) the important result that *increasingly variable impedance profiles sharpen the pulse rise*.

Our first design exercise using the individual level domains was the highest current line which is level A. The SCREAMER results for load current show `Variable5` has gone beyond the point of diminishing returns (Figure 3-20(b)). The trend is further clarified in Figure 3-26(b), which shows not only increased losses but increased duration of losses the more aggressive the design is. By the time we reach `Variable5`, losses continue for 105 ns which is as long as a typical pulse width. The losses exceed 2 MA and stay above 1 MA for $\approx$ 75 ns of that time. Compare this to the baseline case which incurs total losses < 260 kA and for 50 ns. When using circuit modeling as a design tool, *duration of total losses appears to be a useful design metric*.

Therefore, we reject `Variable5` based on the results of circuit simulations and identify among the remaining candidates `Variable4` as a design of interest for Empire to evaluate in full detail using electromagnetic particle-in-cell. It turned out that the Empire simulation for level A (Figure 3-20(a)) diverged from circuit predictions (Figure 3-20(b)), instead predicting that `Variable4` delivers signficantly *less* current (6.9 MA) compared to the baseline (7.6 MA peak). Thus, based on the results of EM-PIC simulations, `Variable4` was deemed not viable as a MITL design.

We show a clue in Figure 3-20(a) as to what went wrong with this design. This plot adds a `Variable4 (e-only)` Empire simulation (dotted black line) that is identical every way to full `Variable4` simulation (gold line) except H+ emission (a consequence of anode plasma turn-on) has been turned off. This "e-only" Empire simulation agrees with SCREAMER that the design delivers the highest load current. Therefore, it is the H+ emission (which circuit codes do not have models for) that changed the operating characteristics of this MITL design. Including H+ emission results in lower load current and is responsible for Empire reversing the verdict of viable to non-viable. The bigger picture of power flow is further clarified by examining electron losses summed over the entire anode (Figure 3-26). Empire simulates less electron losses compared to SCREAMER both in peak value and in duration, yet Empire also predicts the lower load current. This is because power flow is carried by electromagnetic wave propagation; load current is not solely determined by "electrons lost" between a reference starting point (e.g., stack current) and measured end point (i.e., load current). The space charge and currents from H+ and electrons filling the gaps in the regions approaching the load have direct consequences on the

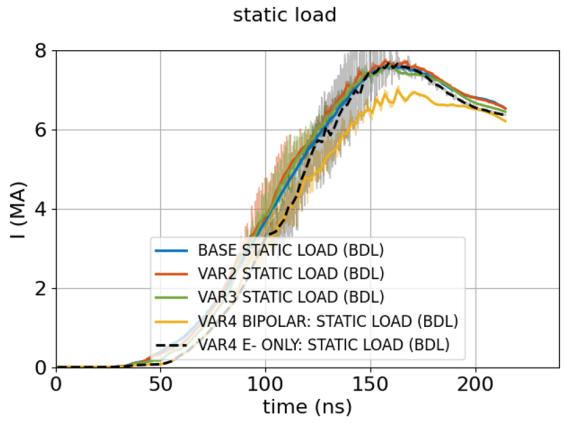

(a) Empire: Individual Level A Domain

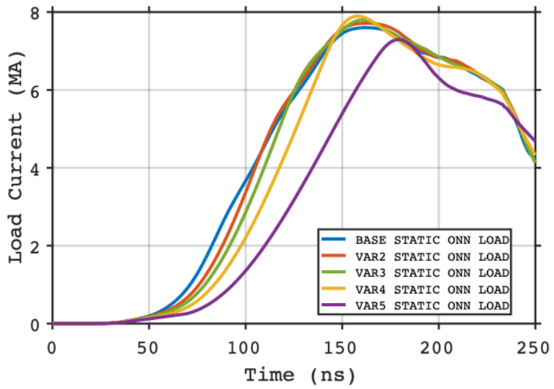

(b) SCREAMER: Individual Level A Domain

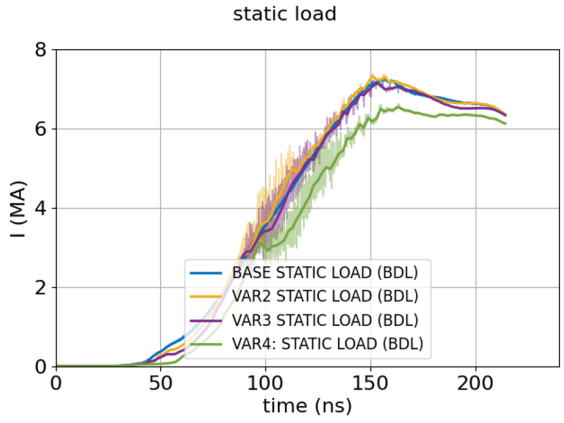

(c) Empire: Individual Level B Domain

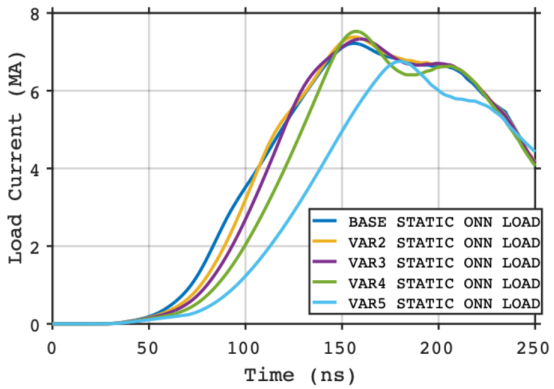

(d) SCREAMER: Individual Level B Domain

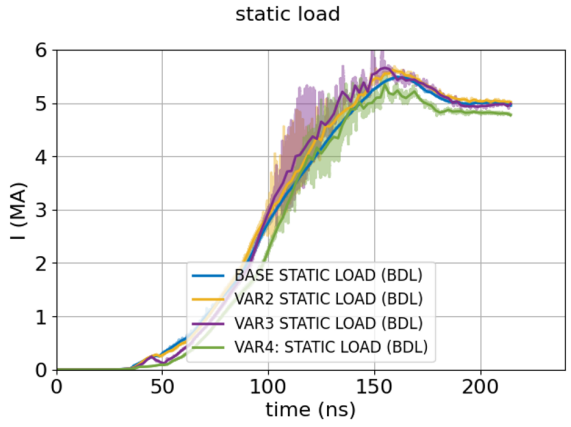

(e) Empire: Individual Level C Domain

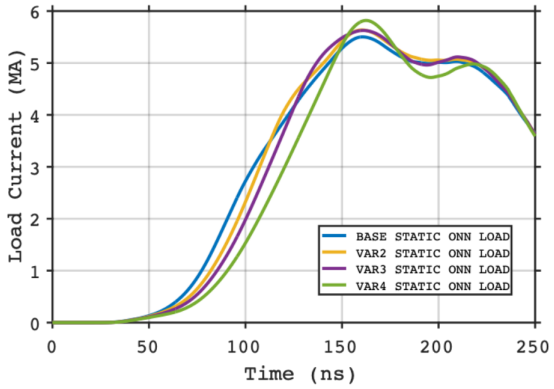

(f) SCREAMER: Individual Level C Domain

Figure 3-20. (Variable-impedance Level A, B, C Designs) Simulated load currents. Note that "load" is the downstream output of each domain; Individual levels A, B, and C is the output of the MITL domain.

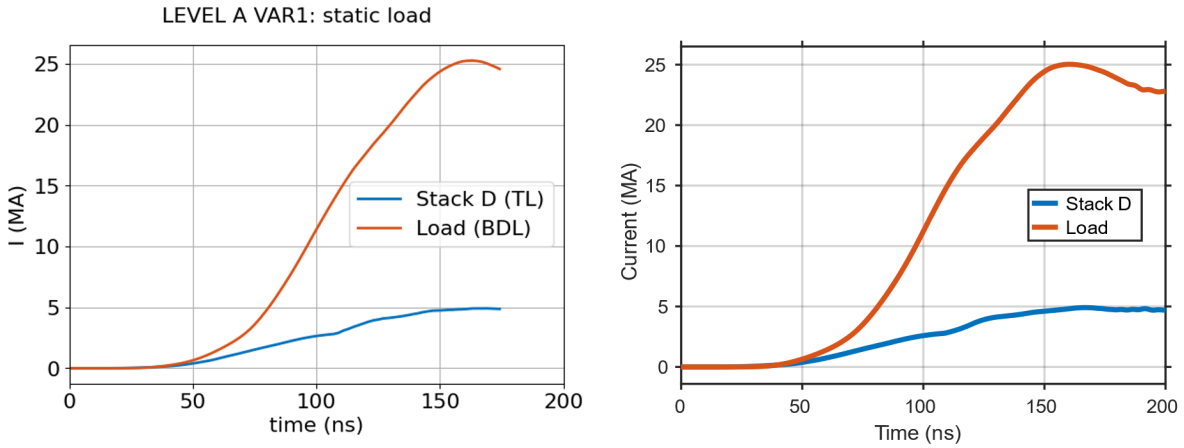

(a) Empire **(b) SCREAMER**

Figure 3-21. (Variable-impedance Level D Design) Simulated load currents. Note that "load" is the downstream output of each domain; the Extended Level D domain includes the convolute domain so its load is the same as the Z machine load.

propagation of the driving pulse transmitted through this region. This results in reduced power flow ($|\mathbf{E} \times \mathbf{H}|$) and a lower current delivered to the load.

The event of anode plasma turn-on affects the anode heating history, and is the reason Empire predicts higher anode temperatures for significant regions of the MITL (Figure 3-28(a,b)). This is because the creation of anode plasma can result in a powerful feedback that significantly changes the electron loss dynamics whose region of effect grows with time. The reason is straightforward: magnetic insulation appears to be relatively easy to defeat and the presence of positive ions in the gap can be a strong enough outside influence to sabotage marginally stable flow features such as vortices (a feature of the flow that is also not captured in circuit models). In Figure 3-22, we visualize e^- number density, H+ number density, and anode surface temperature at various snapshots in time and compare this case (`Variable4`) with a safe design (constant impedance baseline) to clarify the consequences of this effect.

When viewed as an animation, this reveals a dramatic scene where electron vortices $\mathbf{E} \times \mathbf{B}$ drifting downstream at roughly constant velocity ("leftward" in these pictures) suddenly detach from the bulk insulated-electron layer at the cathode (bottom) surface and are accelerated towards the anode (top) side. Figure 3-23 highlights this feature by providing a surface rendering of only the electrons (H+ hidden), while Figure 3-24 shows a full view of the MITL flow to illustrate how outsized an effect this really is.

The electron vortices are not completed absorbed at the anode, however, remaining largely intact and continue to $\mathbf{E} \times \mathbf{H}$-drift towards the load but on the anode side (rather than the cathode side). Electrons subsequently scrape off from the outer layers of these rotating vortices leading to

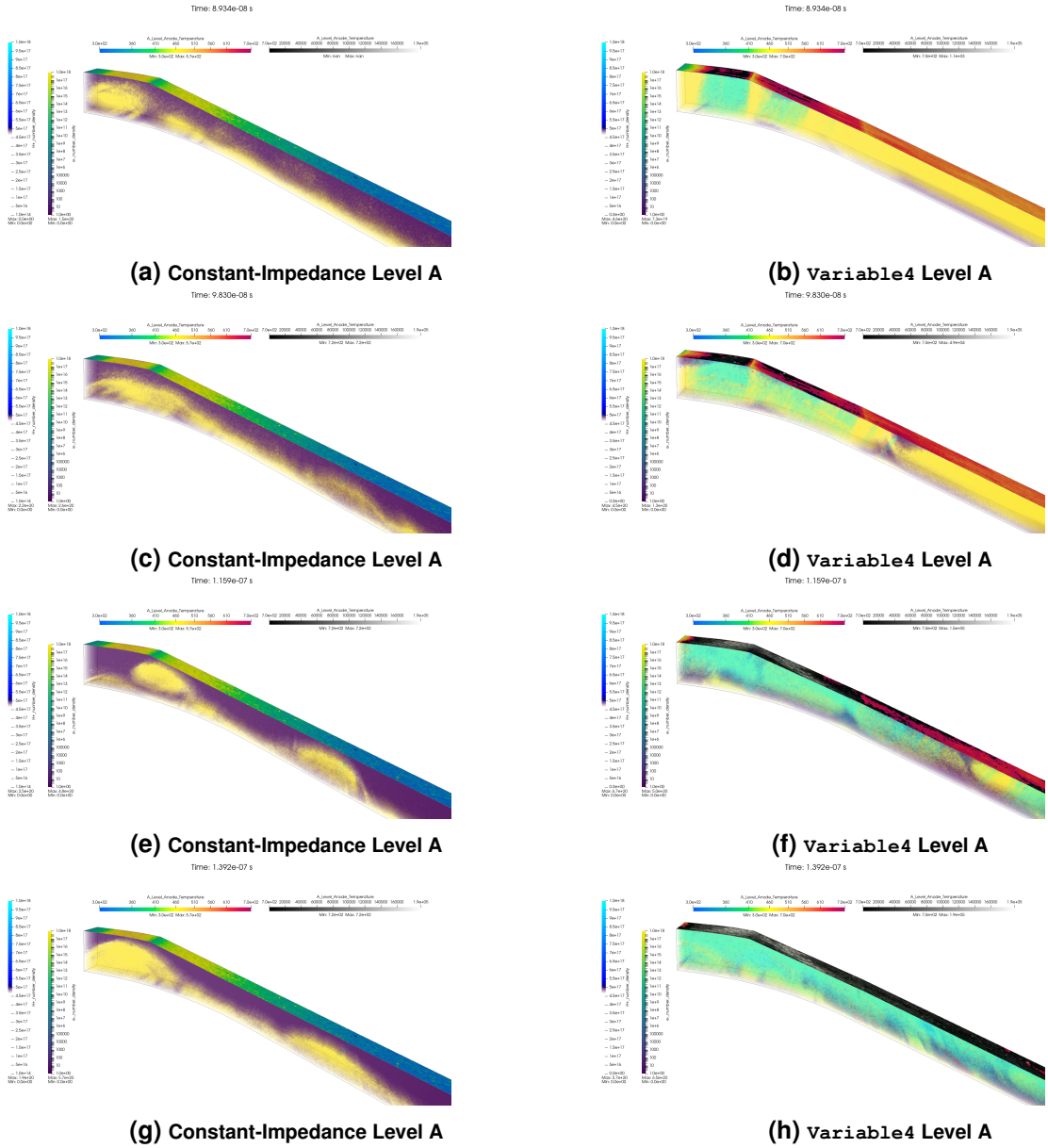

(a) Constant-Impedance Level A

(b) `Variable4` Level A

(c) Constant-Impedance Level A

(d) `Variable4` Level A

(e) Constant-Impedance Level A

(f) `Variable4` Level A

(g) Constant-Impedance Level A

(h) `Variable4` Level A

Figure 3-22. (Level A: Constant Impedance vs. `Variable4`) A volume rendering of the e^- (yellow), H^+ (cyan) number densities are shown at various snapshots in time alongside anode (top surface) temperatures. The colors for anode temperature are chosen so that it a rainbow color map shows increased heating from $300K \leq T_{anode} < 700K$ and switches to a black-white scheme for $T_{anode} \geq 700$ K with white corresponding to the hotter temperatures. This choice enables detailed gradation to be shown while allowing the binary interpreation of where anode plasma has turned on ($T_{anode} \geq 700$) compared to where it has not. The region where anode plasma turns on draws in electrons throughout the pulse leading to ongoing losses in a growing region. Note that in the later `Variable4` frames, electrons are obscured from view due to the rendering of H^+ populations which occupy the same space. This is a consequence of visualization settings (i.e., transparency); this region is filled with both species populations. In contrast, once magnetic insulation sets up in the constant-impedance level A, it is maintained throughout the rest of the pulse resulting in minimal losses.

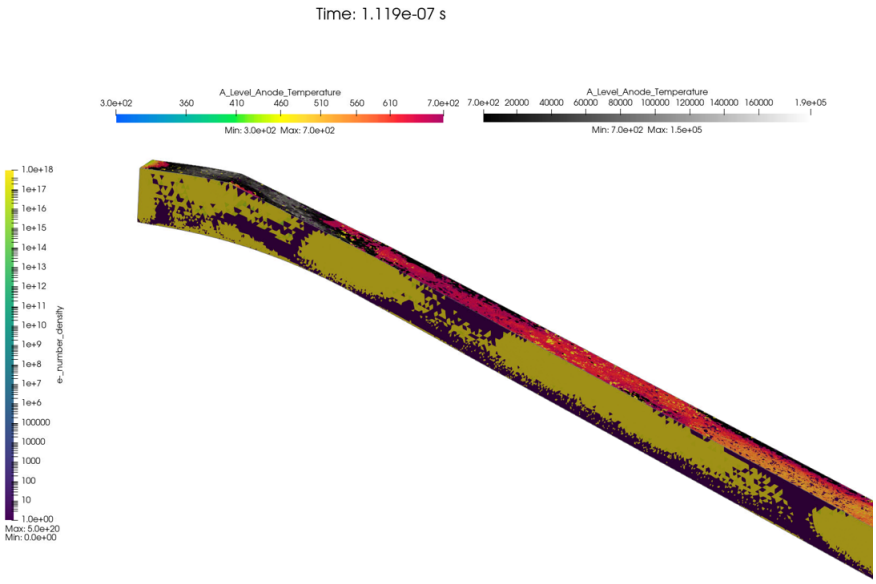

Figure 3-23. (Level A `Variable4`) Simulated e^- number density (yellow) and anode temperature are shown as *surface renders* to allow clear discernment of the actual spatial extent of the electron vortices within the AK gap (H+ number density hidden). Anode plasma has turned on wherever the top surface follows the black-white colormap. Notice that electron vortices lift off the cathode (bottom) side showing a clear void region underneath. As seen in Figure 3-24, this effect picks up further upstream compared to what might be expected. This is typical picture of electron flow throughout the pulse for `Variable4` and highlights what is an outsized influence of the H+ region on upstream insulated flow.

ongoing losses (Figure 3-25) and heating throughout the pulse in a neighborhood[7][8]. This neighborhood, in turn, breaks down into anode plasma over time which extends the range of effect just described even further upstream. A positive feedback loop is set up which causes the anode plasma region to grow over the course of the pulse, leading to an extended loss duration that is on the order of the pulse width itself.

As `Variable4` was found to be too aggressive, we walked back our selection to consider `Variable2` and `Variable3`. As can be seen by the load currents and losses, Empire agrees with SCREAMER that these two are viable designs. This highlights that in the safe regimes (without H+ emission), SCREAMER and Empire are both reliable design tools.

In the same set of figures, we present the results from our SCREAMER/Empire studies for levels B and C. The plots for these levels tell a similar story as level A: SCREAMER predicts `Variable4` as the best candidate while Empire determines it went too far, resulting in power flow being compromised due to anode plasma turn-on. `Variable2` and `Variable3` were determined as viable by both SCREAMER and Empire.

[7] note that the minimum gap in all A-level designs is 0.986 cm. While this value is under conventional pulsed-power guidelines to maintain outer MITL gaps $\geq$ 1 cm, we point out this gap also exists in the constant-impedance version of level A. Therefore, on it's own it is not the cause of these consequences to power flow. It should also be said that 0.986 cm is only marginally under 1 cm and the guideline is empirical, not rigorously converged on.

[8] It is interesting to point out that electron vortex flow on the anode side is also what happens in the inner MITL of Z (not shown here)

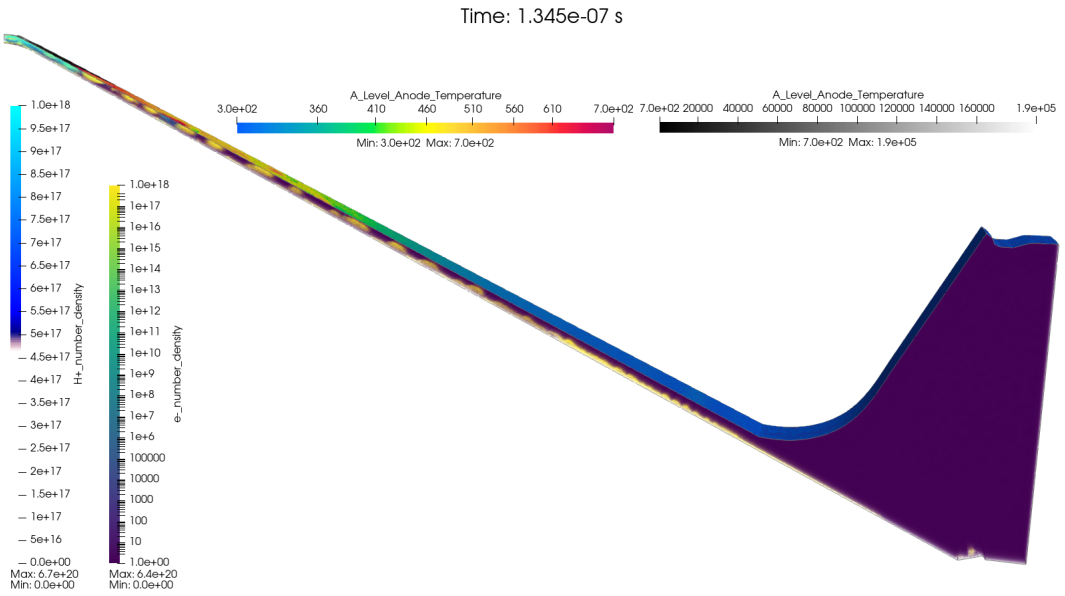

Figure 3-24. (Level A `Variable4`) A full view of electron and H+ number densities (volume render) in an overly aggressive variable-impedance MITL A design. Simulated e^- (yellow), H^+ (cyan), and anode (top surface) temperatures are shown. Electron vortices being to be pulled into the anode plasma quite far upstream. Notice that this produces a patterning of hot spots on the anode side that appears to be a signature of the same spacing between each vortex component of the insulated flow upstream.

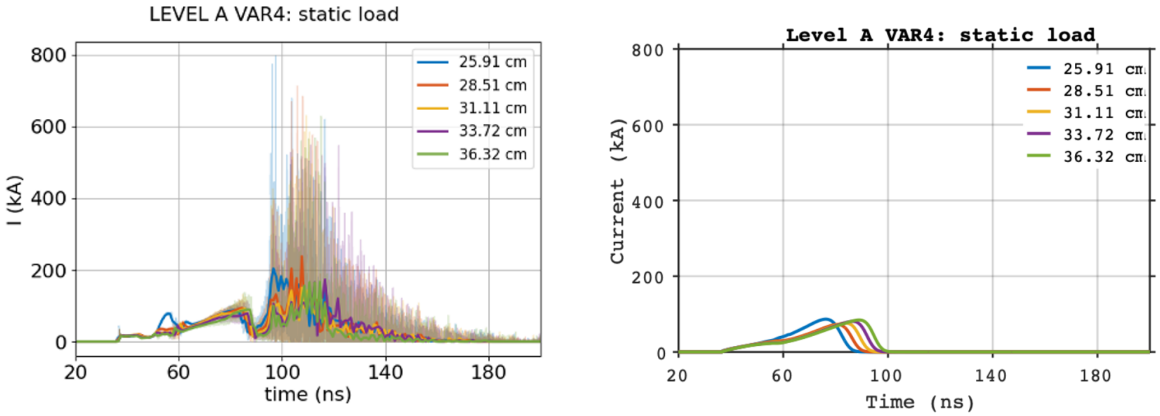

(a) Empire **(b) SCREAMER**

Figure 3-25. (Level A `Variable4`: Empire vs. SCREAMER) Anode current loss is plotted for the downstream-most segments. SCREAMER registers zero losses at late time due to loss model only considering magnetic insulation. Empire continues to record losses throughout the pulse due to anode plasma which cannot be captured by circuit models.

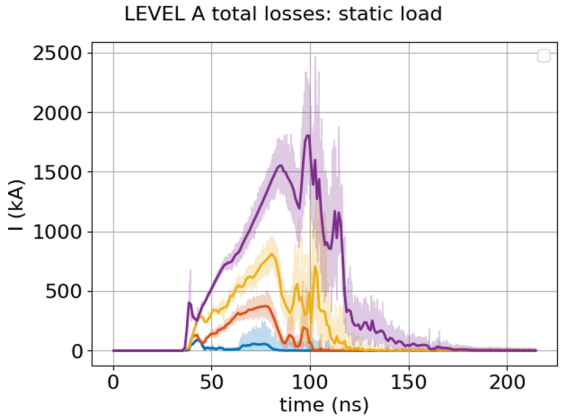

(a) Empire: Individual Level A Domain

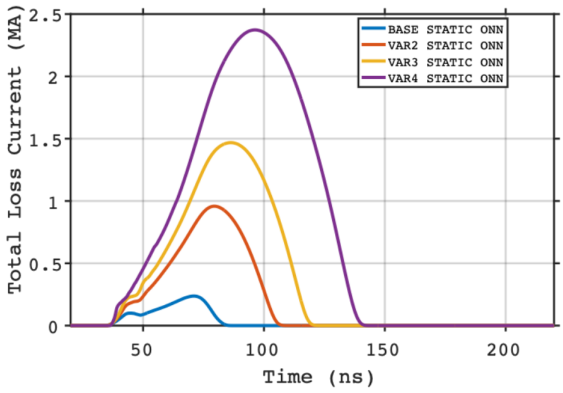

(b) SCREAMER: Individual Level A Domain

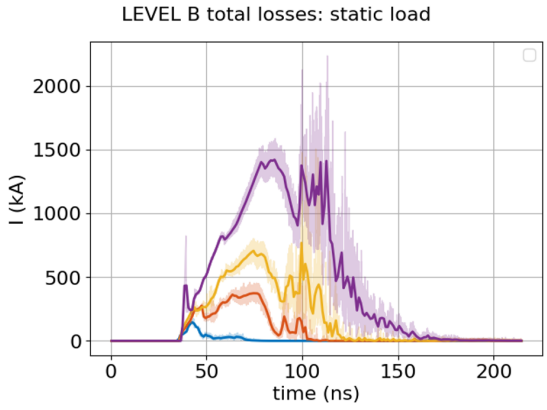

(c) Empire: Individual Level B Domain

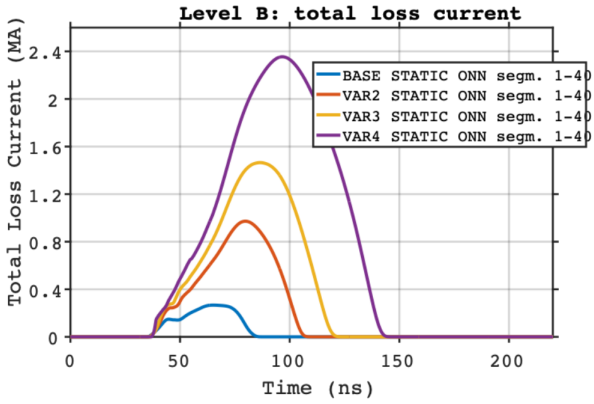

(d) SCREAMER: Individual Level B Domain

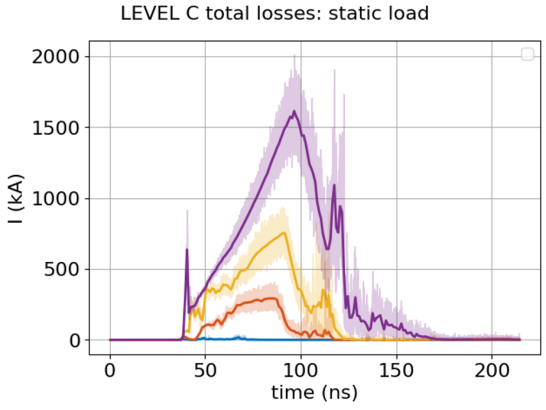

(e) Empire: Individual Level C Domain

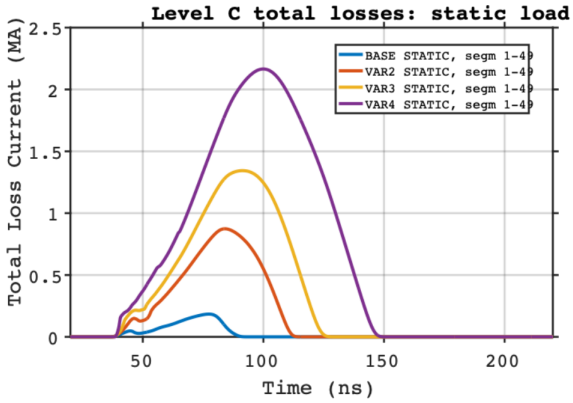

(f) SCREAMER: Individual Level C Domain

Figure 3-26. (Variable-impedance Level A, B, C Designs) Simulated anode losses in the main MITL region. In the Empire results, the semi-transparent data is the raw output whereas the dark line is 1-ns time-averaged data.

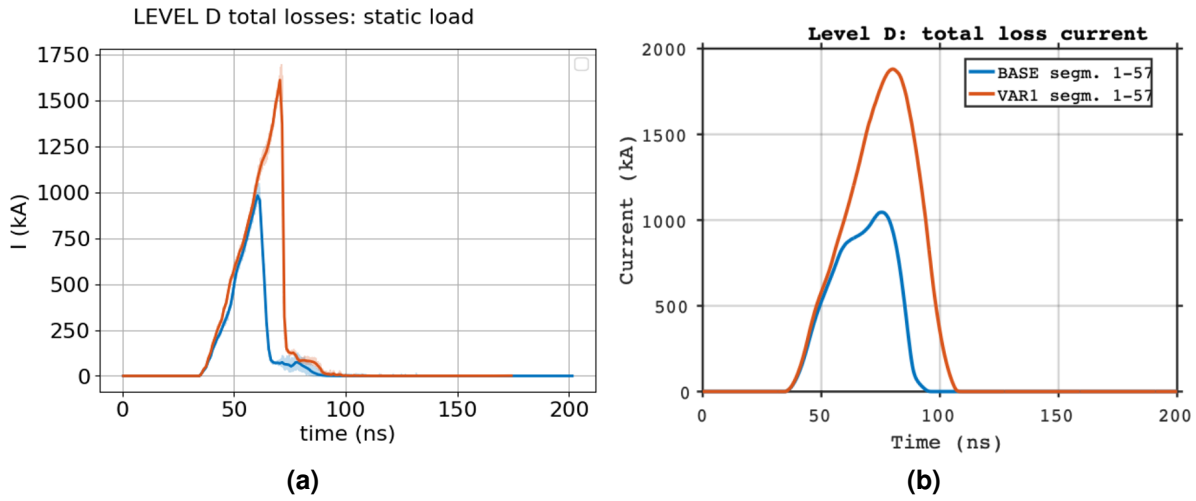

Figure 3-27. (Variable-impedance Level D Design) Simulated anode loss currents

In summary, for levels A, B, and C we find that `Variable2` and `Variable3` are safe MITL designs that meet design targets that meet or exceed the baseline load current targets. This grade of safety is made in spite of the (simulation) fact that anode plasma turns on at smaller radius the `Variable3` designs (Figure 3-28). As concerns levels B and C, the results suggests a converged trend at small radius (probably is real) whereas for level A the points where this occurs appear sporadic and should be attributed to PIC noise. That being pointed out, while the PIC simulations did turn on H+ emission for this design, the load current still met design targets. More analysis could clarify why that is, but one possiblity is anode plasma turned on later in the pulse than it does on `Variable4` so that its consequences on power flow may not have had enough time to grow and interfere significantly with delivering current to the load. Finally, we point out that while it was not simulated in Empire, the `Variable1` (see Tables 3-16 to 3-18), will also be a safe design since it is even less aggresive (a 20% inductance reduction compared to 30% and 40% reductions that produce safe designs as `Variable2` and `Variable3`. Thus, our full take-home from these studies is that `Variable1`, `Variable2`, `Variable3` for level A, B, and C can be recommended to try in a next evaluatory step (i.e., combined level simulations, Section 3.3).

As concerns level D, the single variable-impedance design studied (`Variable1`) was assessed by SCREAMER and Empire to be viable. Recalling that level D studies simulated an "Extended Level D" domain (Figure 3-7(d)), which includes the convolute and regions downstream, Figure 3-27 shows the physical accelerator load (combined current from all levels) for the constant baseline level D versus `Variable1` level D. The predicted load current meets the ≈ 25 MA load current we expect from Z today for the short circuit (static) load being simulated. There is a slight increase in current in the variable-impedance design that is due to the 19.51% inductance savings (cf. Figure 3-13(d))); this gain appears to be a prediction only in Empire and is probably due to how losses are modeled in the convolute circuit model (a value for `Zflow` was calibrated based on the constant-impedance Empire model). Note that the Empire determines the design is safe everywhere in the MITL region whereas SCREAMER predicts anode heating exceeds anode plasma thresholds ($\Delta T = 400\,^{\circ}\mathrm{C}$) at small radius. This is consistent with EM-PIC showing losses turn off sooner due to it self-consistently realizing magnetic insulation compared

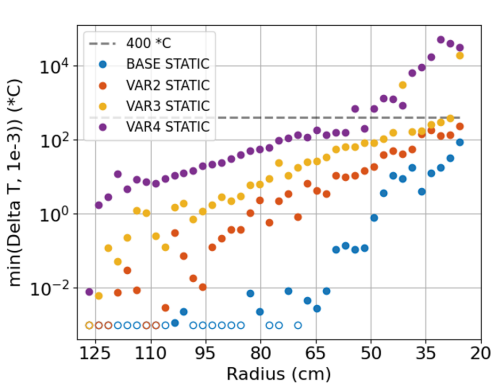

(a) Empire: Individual Level A Domain

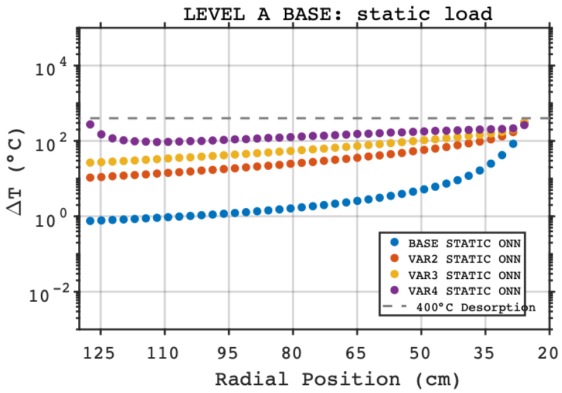

(b) SCREAMER: Individual Level A Domain

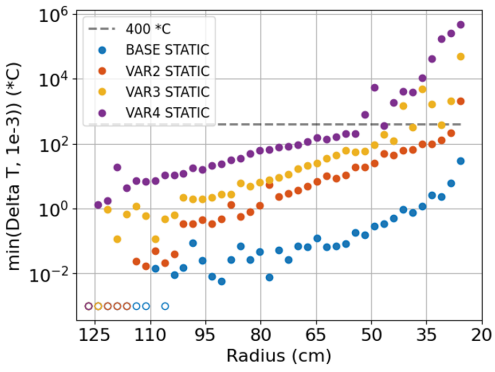

(c) Empire: Individual Level B Domain

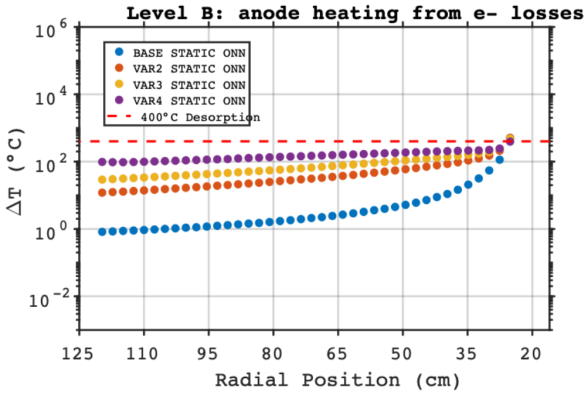

(d) SCREAMER: Individual Level B Domain

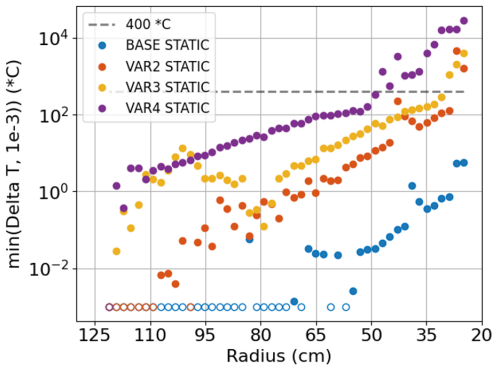

(e) Empire: Individual Level C Domain

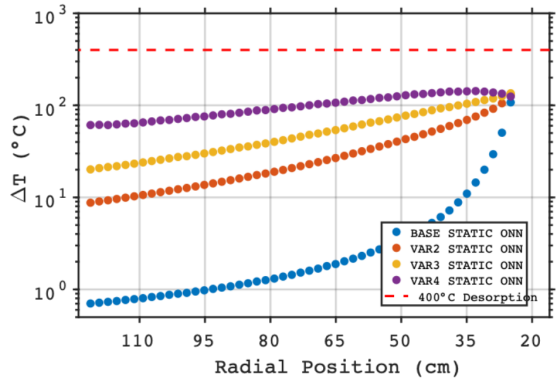

(f) SCREAMER: Individual Level C Domain

Figure 3-28. (Variable-impedance Level A, B, C Designs) Simulated anode temperature vs radius. On the Empire plots, open circles mark data whose values $\Delta T \approx 0$ deg, but which have been plotted at exactly $\Delta T = 10^{-3}$ to allow trends to be seen more clearly. Otherwise, the y-axis would need to span orders of magnitude to include negligible values (e.g., $\Delta T = 10^{-12}$).

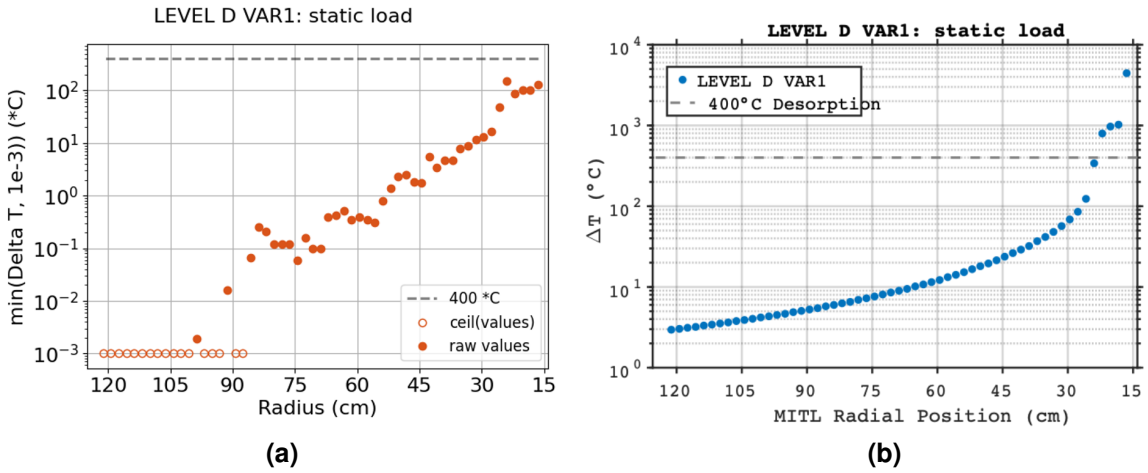

Figure 3-29. (Variable-impedance Level D Design) Simulated anode temperature vs radius.

to SCREAMER (Figure 3-27). Despite this, both codes assess that the load current design target is upheld so this design is viable.

Since the level D domain includes the convolute and regions downsream, it provides an opportunity to visualize MITL flow in constant- vs. variable-impedance systems for a domain that sees a real load. In particular, anode heating in the convolute region can be looked at as well as MITL flow characteristics before and after a retrapping wave which is an important operating prinicple for pulsed-power efficiency that is difficult to study from a theory standpoint.

We present select snapshots in time to show main features of the MITL flow. In Figures 3-30-3-31 we show a closeup view of the middle of MITL D showing baseline flow compared to the flow in a variable-impedance MITL. First, it is clear that before the trapping wave the insulated flow layer occupies more of the AK gap than in the constant-impedance case. However, after the retrapping wave both layers have enhanced insulation and the variable-impedance case has visibly smaller and more regular (more laminar) flow characteristics. This appears to be an advantage for *safely* designed variable-impedance MITLs.

Next, we point out that driving voltage is high enough to cause emission almost all the way upstream to the stack where gaps reach almost 50 cm. The magnetic insulation quality is very good and effectively zero losses occur in these regions.

Finally, we look at the flow in the downstream transition region into the post-hole convolute. Here, we also visualize surface temperature (dark red indicate anode plasma turn-on). While the flow characteristics are visually similar, there are differences in the early stage anode temperature profile, showing differences in hot spot distribution and that these hot spots set up earlier in the variable-impedance system compared to the baseline (Figures 3-33). However, by the time peak current is approached ($\approx$ 155 ns), the two outcomes are very similar (Figure 3-34) It has been emphasized in this report that details such as when anode plasma turns on is important. This concern is partially answered by seeing a gain in the machine load current for the variable-impedance design; differences in the transient anode plasma formation at least did not

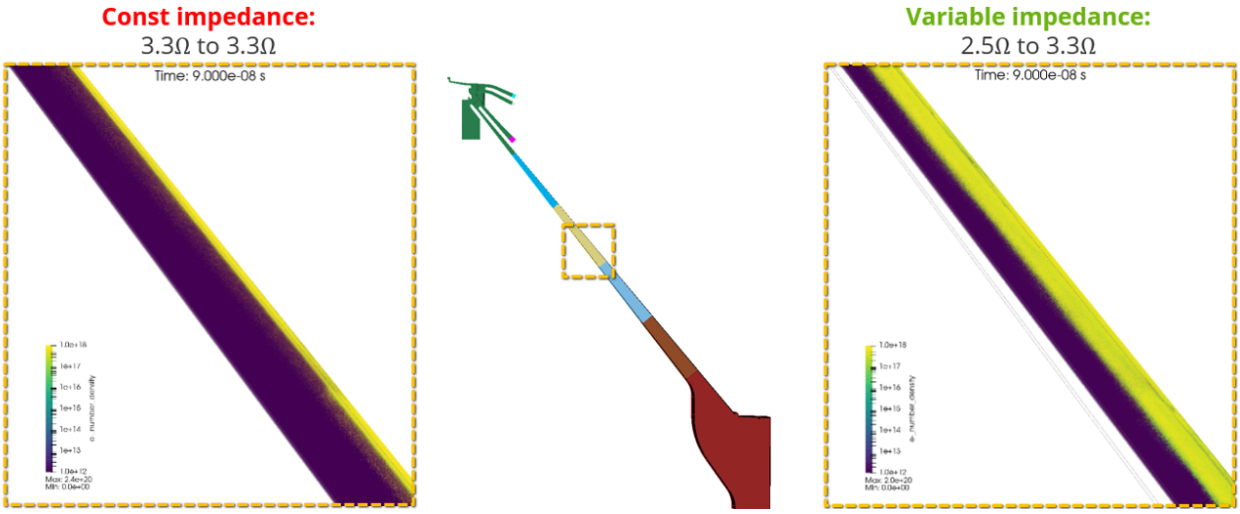

Figure 3-30. (Level D constant-impedance vs `Variable1`) electron flow prior to the retrapping wave in the middle of MITL D. The anode (respectively, cathode) is the top (respectively, bottom) surface.

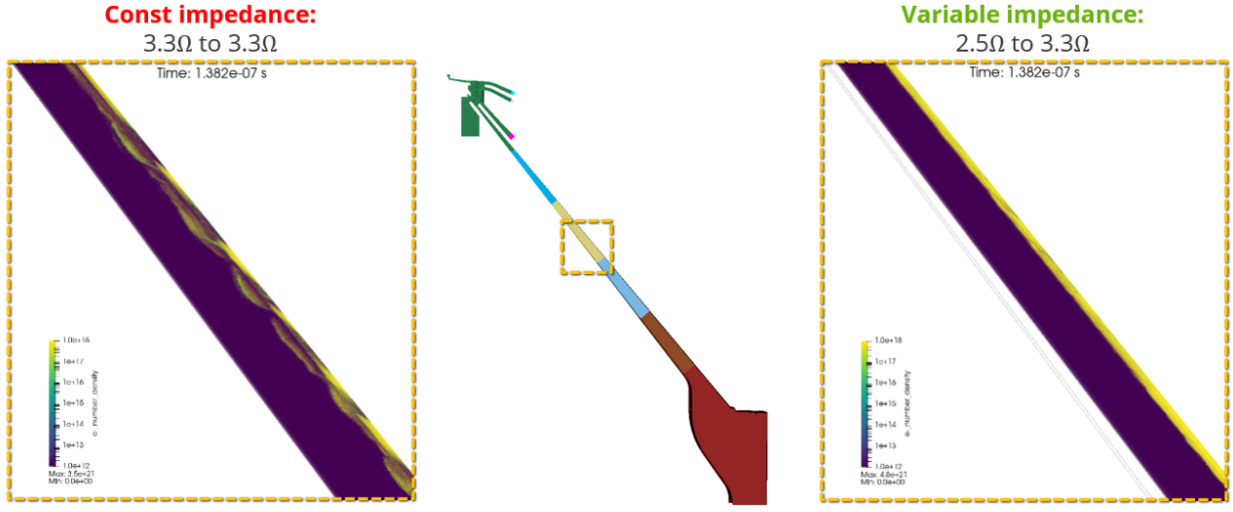

Figure 3-31. (Level D constant-impedance vs `Variable1`) electron flow after the retrapping wave in the middle of MITL D. the anode (respectively, cathode) is the top (respectively, bottom) surface.

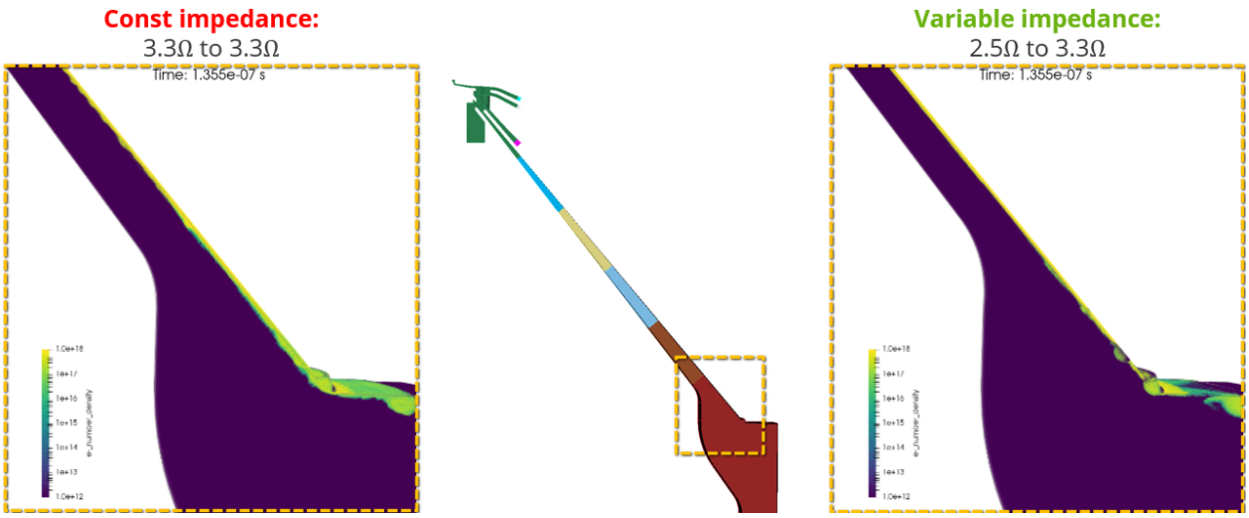

Figure 3-32. (Level D constant-impedance vs `Variable1`) electron flow at the start of MITL D. The anode (respectively, cathode) is the top (respectively, bottom) surface.

sabotage power flow and allowed us to meet (SCREAMER) or exceed (Empire) the machine load current of the constant-impedance case.

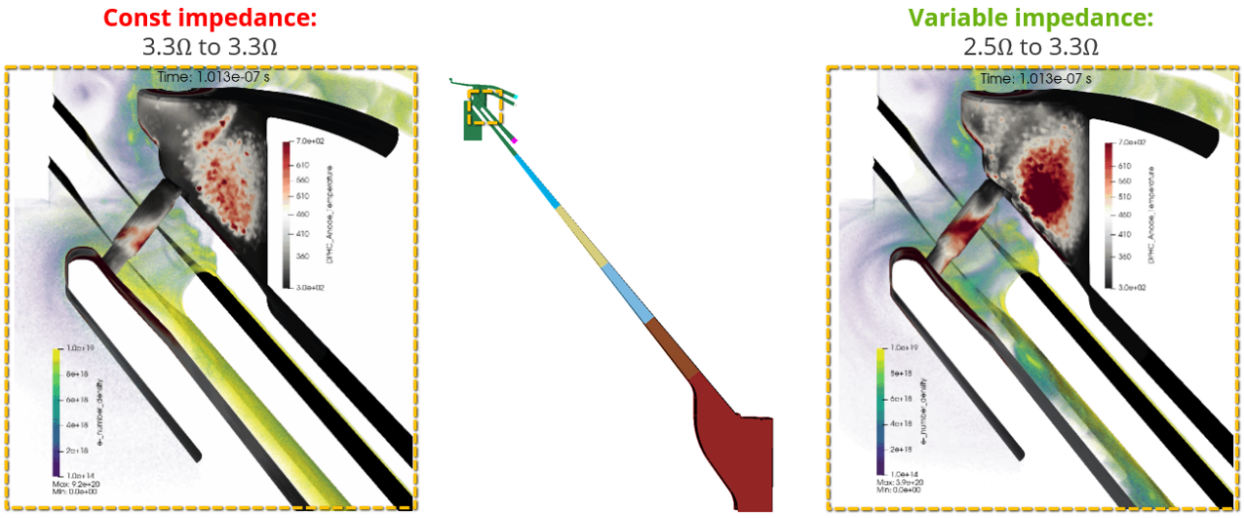

Figure 3-33. (Level D constant-impedance vs `Variable1`) electron flow and anode surface temperatures in the convolute region at select times. At this point in time, some differences in anode hot spot distribution and extent are clear. The two designs have slightly different transients in their heating profiles. The anode (respectively, cathode) is the top (respectively, bottom) surface.

With the discussion of design assessments finalized, we now take time to make general comments on trends we have observed in moving from constant-impedance to a variable-impedance MITL. First, in safe regimes the *load currents increase with more inductance savings* (Levels A, B, C: Figure 3-20; Level D: Figure 3-13(g,h) vs. Figure 3-27). Second, increasingly varable-impedance MITLs sharpen the pulse rise (Figures 3-20), this important result is shown in both Empire and SCREAMER. Third, *losses become both larger and more distributed for increasingly variable-impedance* MITLs. The loss *currents* are always higher in peak value (as is the

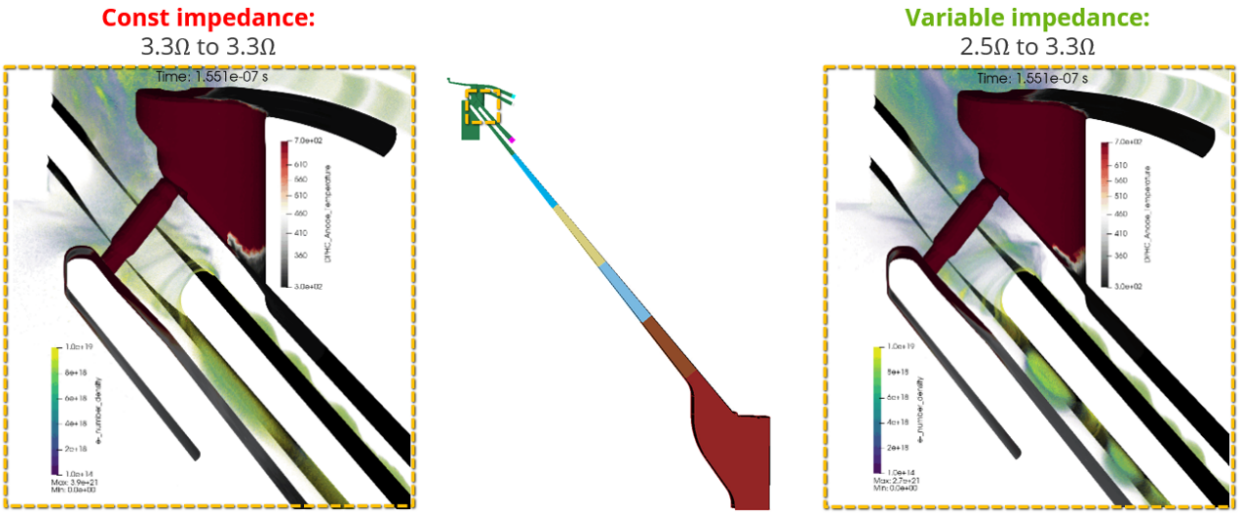

Figure 3-34. (Level D constant-impedance vs `Variable1`) electron flow and anode surface temperatures in the convolute region at select times. By this point in the pulse, anode hot spots are very similar (note: peak current is at ≈ 160 ns). The anode (respectively, cathode) is the top (respectively, bottom) surface.

cumulative charge lost to the entire anode Table 3-4), but the duration at a given radius is briefer (Level D example: Figure 3-36). Fourth, when operating in a safe mode (no anode plasma), early stage losses have *zero* effect on the peak current a MITL achieves once magnetic insulation is established. This is demonstrated by circuit simulation results shown in Figure 3-35 which compare load currents for cases with and without emission turned on for the same (baseline) MITL. This actionable information indicates that if a variable-impedance MITL design can tolerate early stage losses (no anode plasma results from anode heating), that we can reap the benefits of the increased current afforded by the inductive savings.

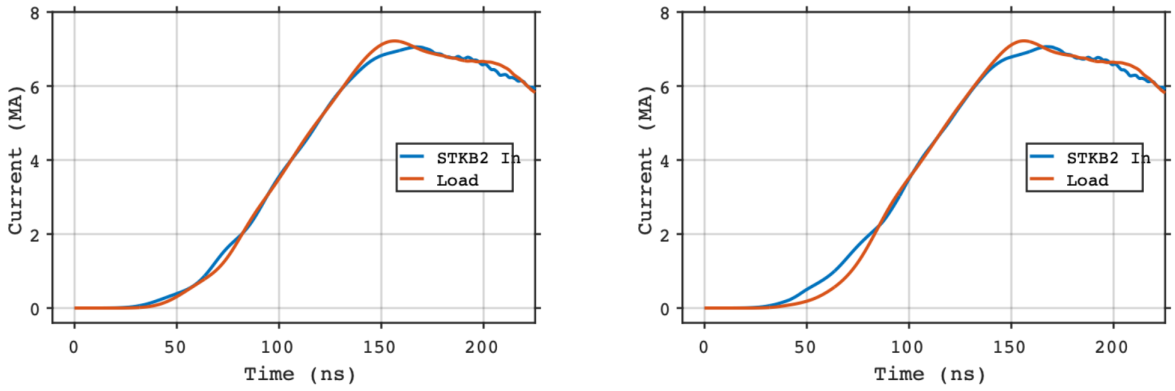

(a) SCREAMER: e^- emisson off **(b) SCREAMER: e^- emisson on**

Figure 3-35. (Constant-impedance level B) SCREAMER results show that turning on electron emission leads to early stage losses, but that these losses they have zero consequence on the peak load current achieved. Note that these predictions are valid for safe operating regimes (no anode plasma).

Fifth, and consistent with the losses becoming increasingly more distributed (point (2)), the anode

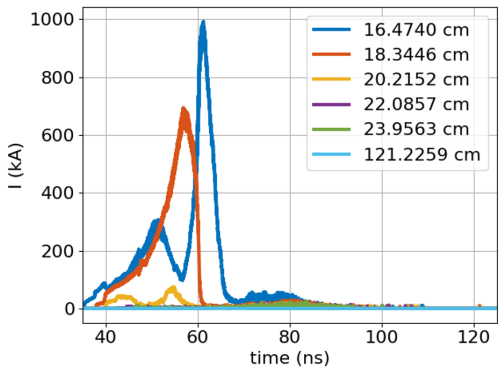

(a) Empire Level D Baseline: Figure 3-14(g) revisited

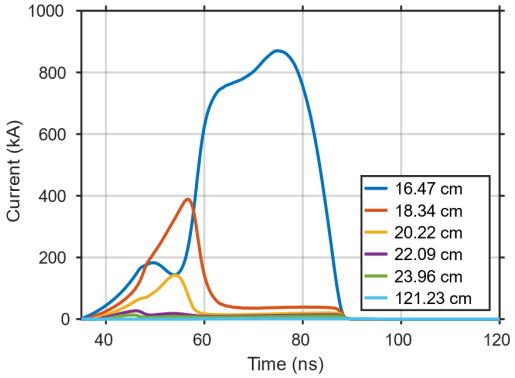

(b) SCREAMER Level D Baseline: Figure 3-14(h) revisited

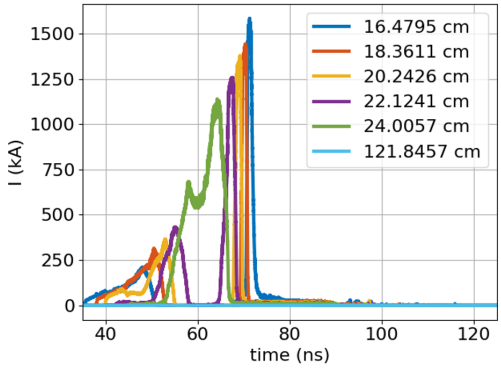

(c) Empire Level D `Variable1`

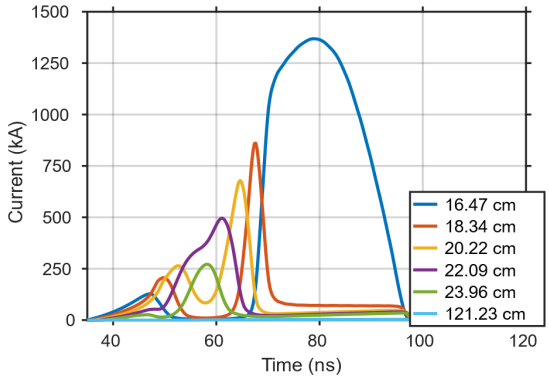

(d) SCREAMER Level D `Variable1`

Figure 3-36. (Level D: Baseline vs. `Variable1`) Simulated anode losses are shown at select locations throughout MITL D from simulations of the "Extended Level D" domain. The outer MITL extends from the upstream boundary at the vacuum flare exit ($R = 122.1612$ cm, gap $= 6.7337$ cm) downstream to the convolute entrance ($R = 15.5387$ cm, gap $= 0.8602$ cm) Note that the simulation domain is larger; extending upstream to the stack and downstream to the accelerator load.

Level	Design	Cumulative Charge loss (C)
A	Baseline	0.001585089
	`Variable2`	0.012559707
	`Variable3`	0.033304569
	`Variable4`	0.087516126
B	Baseline	0.001788067
	`Variable2`	0.014611554
	`Variable3`	0.034288979
	`Variable4`	0.087309889
C	Baseline	0.000221177
	`Variable2`	0.010827241
	`Variable3`	0.032388522
	`Variable4`	0.080044298
D	Baseline	0.015264254
	`Variable1`	0.029360212

Table 3-4. (All Levels, All Designs): Total charge lost to anodes. Note that in `Variable*` designs with index $\gtrsim$ 3 (Level dependent) anode plasma enhances the losses in a local region

heating vs. radius generally flattens with increasingly more variable-impedance MITLs. This trend is predicted by both codes in the regimes they agree in (safe operating regimes). Therefore, SCREAMER sees this trend in all results (Levels A, B, C: Figure 3-28(b,d,f); Level D: Figure 3-29(b) vs. Figure 3-15(h)). Empire also sees this pure flattening trend when comparing cases without anode plasma: Level D (cf. Figure 3-15(g,h) vs. Figure 3-29(a,b)) and level A (Figure 3-28(a), cf. curves for Baseline vs. `Variable2` vs. (debatable) `Variable3`). For all cases when anode plasma turns on (even if only in a small region), Empire predicts flattening but also an up-shifting of the entire anode temperature vs. radius curve (Level A: `Variable3-Variable4`; Levels B, C: `Variable2-Variable4`). We emphasize that anode plasma turn-on is not an immediately deal breaker, anode temperature at final simulation time is only one of many factors that determine a given design's grade of operational viablity.

In this section, we have shown that while there are many details that determine power flow efficiency of a given design, our results and analysis indicate there are key advantages (e.g., current gains, faster pulse rise) of the variable-impedance MITL concept. Our simulation survey of design space has resulted in the following designs recommended for further study: Designs `Variable1`, `Variable2`, `Variable3` are viable designs for MITLs A, B, and C, and `Variable1` is our recommendation for level D. As these designs were optimized one MITL at a time, and the extended level D domain gave a preview to the important interplay affecting power flow from the other levels (e.g., Figure 3-12(g,h)), the final assessment of design viability can only come from a combined ("all levels") simulations which includes the convolute and regions downstream. As emphasized in our design evaluations, it will be important to assess operating

characteristics using both circuit and EM-PIC modeling.

3.3. Combined Level Analysis

Based on the study of individual-level models (Section 3.2.2), a full VAR3−VAR3−VAR3−VAR1 (levels A, B, C, and D) Z model was proposed for the final evaluation. The top-level SCREAMER [15, 37] circuit diagram for the proposed all-levels model is shown in Figure 3-37. The model was built by replacing the baseline MITL circuit elements with the corresponding variable-impedance MITL elements, while the rest of the circuit elements remained unchanged. Because the innermost part of the outer MITL was kept unchanged, the only geometric change associated with the variable-impedance MITL is the reduction in the vacuum flare impedance. Preliminary studies indicated that this change in the vacuum flare geometry produces no discernible differences to circuit results nor does it affect the extent of agreement between circuit and Empire simulations[9]

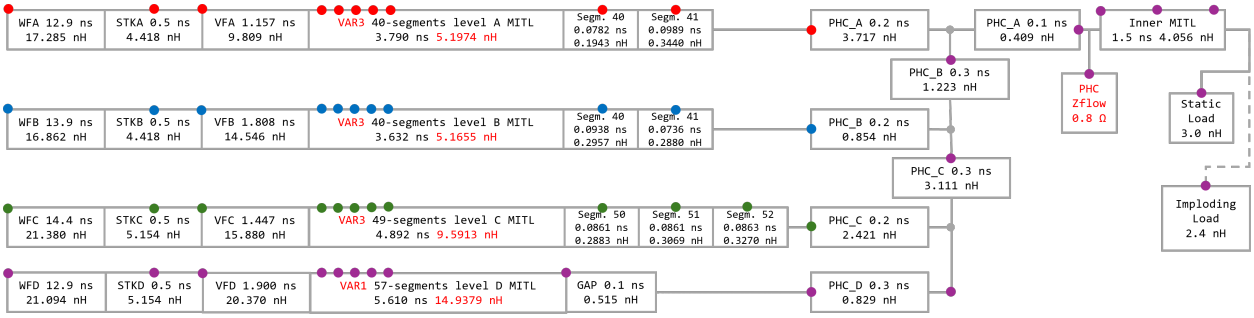

Figure 3-37. VAR3−VAR3−VAR3−VAR1 all-levels SCREAMER Z model

The inductance breakdown for the VAR3−VAR3−VAR3−VAR1 Z model is shown in Table 3-5. Comparison with the corresponding inductance breakdown for the baseline all-levels Z model (Table 1) shows that the proposed VAR3−VAR3−VAR3−VAR1 Z model provides approximately a 12% reduction across all levels in parallel (7.530 nH vs. 8.6000 nH) and an 8% reduction in the total vacuum inductance excluding the load (11.585 nHvs. 12.655 nH).

The outer MITL boundaries for the VAR3−VAR3−VAR3−VAR1 all-levels Z model for each individual levels as they were implemented in SCREAMER model are summarized in Figure 3-38. The boundaries were carefully evaluated in the Empire 3D model along the AK

[9]Empire models the full 3D geometry. Because all regions are connected in a continuous geometry model, changes we make in the main MITL region in order to define a variable-impedance MITL design require new transitions to be drawn between vacuum flare (VF) exit and the new gap at the entrance of the main MITL region for each design. This is not strictly necessary for a circuit model which has the flexiblity of allowing changes to be made on a segment-by-segment basis. Leaving the vacuum flare fixed while applying design changes to the main MITL region is a decision of expedience but was found in our back-to-back comparison study to be accurate. As this difference was found to be inconsequential on the circuit results, it was determined to not be worth the time investment to ensure 1:1 correspondence between circuit and Empire models at the VF level-of-detail. The person-hours savings is in not having to repeat (for each VF revision), segmenting the VF geometry, setting up and running Empire simulations to calculate inductances for each segment, and measuring pathlengths as in Section B.3. This was done once for the baseline VF and fixed at the circuit level.

A-level serial inductance (nH)	19.261
B-level serial inductance (nH)	21.149
C-level serial inductance (nH)	28.814
D-level serial inductance (nH)	36.652
All levels parallel (nH)	7.530
Inner MITL (nH)	4.056
Total vacuum excluding load (nH)	11.586

Table 3-5. Inductance breakdown of the `VAR3-VAR3-VAR3-VAR1` Z model.

midline. Similar to the baseline model, each MITL was divided into equally spaced segments ($\approx$ 0.1 ns) along the AK midline. Segments were modeled with MITL [38] circuit elements to account for pre-insulation electron losses, using a resolution time ten times smaller than the segment transition time. Total inductance was calculated as $L = \sum_i Z_i \tau_i$ and independently verified, showing excellent agreement.

	Outer R (cm)	Outer gap (cm)	Outer Zvac (Ω)	Inner R (cm)	Inner gap (cm)	Inner Zvac (Ω)
Level A (VAR3)	128.7487	2.2955	1.0690	24.6048	0.9356	2.2800
Level B (VAR3)	120.9057	2.2262	1.1040	23.9216	0.9456	2.3700
Level C (VAR3)	122.2593	3.1096	1.5250	23.9073	1.3031	3.2680
Level D (VAR1)	122.1612	5.0936	2.5000	15.5387	0.8602	3.3192

Figure 3-38. Geometry/impedance breakdown of the `VAR3-VAR3-VAR3-VAR1` Z model MITL regions.

The full geometry of each MITL segment, as implemented in the `VAR3-VAR3-VAR3-VAR1` all-levels SCREAMER model, is summarized in Appendix D. Notably, the Level D MITL has a markedly different geometry from the other levels. Level D was the first tested in Empire simulations, and there was insufficient time to redesign it for the full Z model. This discrepancy in geometry causes an imbalance in the current flowing out of each level and results in disproportionately large anode heating near the convolute, as seen in SCREAMER simulations. Our preliminary study indicates that the Level D anode heating can be mitigated by expanding its innermost gap and transitioning to a constant-gap section a short distance from the convolute, without sacrificing the current delivered to the load. Circuit simulations and analysis for the All-Levels domain have been completed for both the variable-impedance system and the constant-impedance (baseline) system with main highlights presented below.

The first major outcome is that in lossless circuit simulations, a 1.1 MA current gain in variable-impedance system compared to the constant-impedance (baseline) sytem is predicted.

This lossless simulation quantifies the gains in current we have succeeded in producing from reducing inductance across all 4 MITLs. When electron losses are turned on this gain diminishes to $\gtrsim 0.3$ MA.

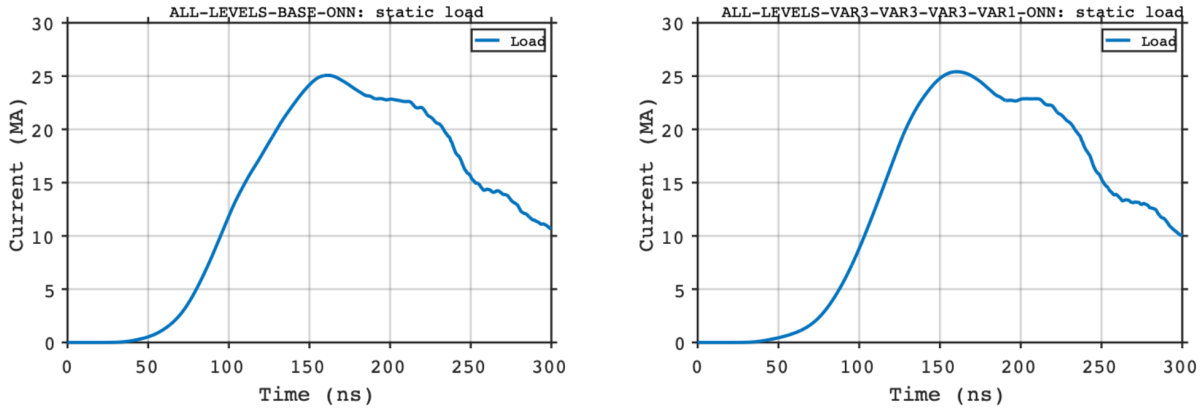

(a) Baseline **(b) VAR3-VAR3-VAR3-VAR1**

Figure 3-39. The load current in the VAR3-VAR3-VAR3-VAR1 system reaches an $\approx$ 0.3 MA peak current compared to the constant-impedance (baseline) system.

The second major outcome from circuit simulations is that the *variable-impedance system predicts lower stack voltage* (Figure 3-40). Levels C and D drop by ≈ 0.5 MV, or $\approx 10\%$ lower, whereas the stack voltages on levels A and B change shape but maintain peak values as the baseline. The feedback is more interesting: the stack voltage is virtually unchanged in the variable-impedance system compared to baseline if losses are turned off, this means that the change in MITL operating impedance in the variable-system due to electron flows is a larger effect than results from geometric modification alone.

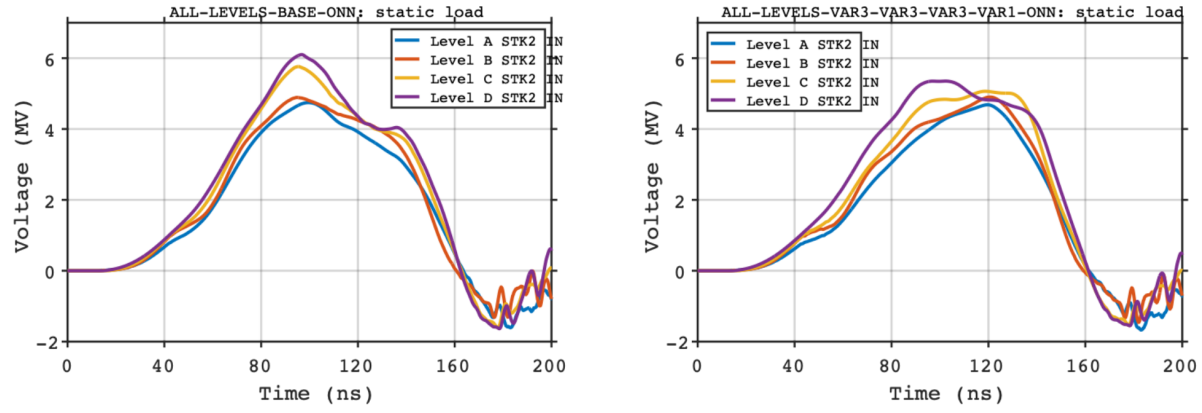

(a) Baseline: 1.0× driving voltage **(b) VAR3-VAR3-VAR3-VAR1: 1.0× driving voltage**

Figure 3-40. insert caption

These two sets of results combined provide design *options*: (1) an accelerator for the same current could be operated at lower stack voltage which has cost-savings (e.g., lower stack height), (2) increase the stack voltage to the same level as the baseline and deliver more current. To quantify

the gains afforded by the second option, circuit simulations of the variable-impedance system was run with 10% higher driving voltage. The results are shown in Figure 3-41

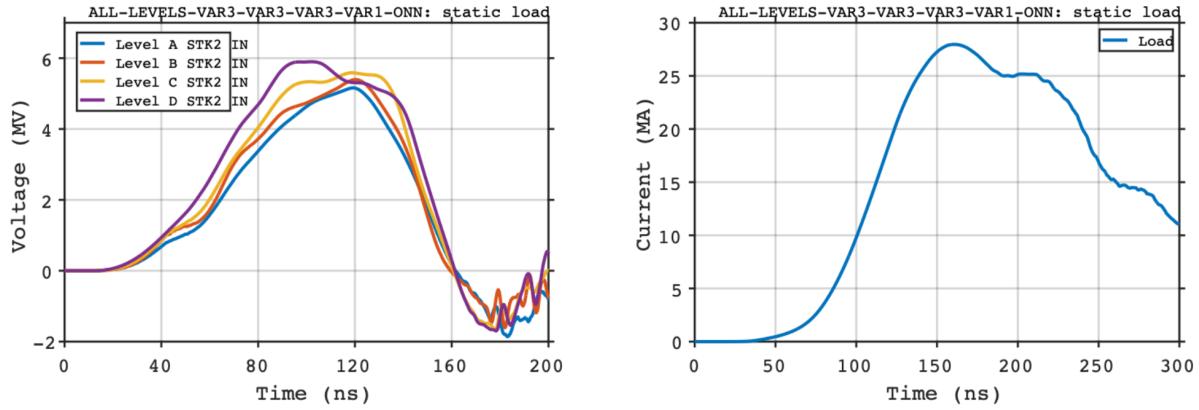

(a) Stack voltages ($1.1\times$ driving voltage) **(b) load current ($1.1\times$ driving voltage)**

Figure 3-41. `VAR3-VAR3-VAR3-VAR1`: Increasing the drive voltage by 10% restores the stack operating voltage to baseline (Panel (a)) and results in 2.9 MA load current gain.

This results in a 2.9 MA increase in current delivered to the load ($\approx$ 27.9 MA).

In the final stretch of this project, an Empire model of the All-Levels domain was completed (geometry, mesh, transmission line files, input decks). Preliminary simulation results been completed for the cases highlighted above in circuit simulations (baseline,`VAR3-VAR3-VAR3-VAR1`, and `VAR3-VAR3-VAR3-VAR1` with 10% driving voltage increase). However, time did not permit vetting these results to the extent required and therefore are not included in this report. Finally, alternative configurations (e.g., `VAR3-VAR3-VAR3-`*`VAR3`* or `VAR2-VAR2-VAR2-VAR2`) may have potential advantages and their operating characteristics should be carefully checked using both SCREAMER and Empire simulations. Circuit simulation studies for several combinations have already been completed for not only static loads, but imploding loads. We hope to confirm these exciting findings with full EM-PIC simulations.

4. NGPP 6-LEVEL

The baseline MITL design used in this study is from a conceptual NGPP point design, shown in Figure 4-1. This design features a six-level stack and MITL system, with insulator stack rings approximately 5.4 m in diameter. The dimensions of the insulator stack are primarily determined by water breakdown [44] and vacuum-insulator breakdown [43] criteria. The outer MITLs are conservatively designed to maintain a constant impedance of 3 Ω outside a radius of 20 cm. At a radius of 20 cm the MITLs transition to a constant gap of 1 cm. The outer MITLs end at a radius of 15 cm where they connect to triple-post-hole vacuum convolute current adder. The baseline MITL conductor profiles are shown in Figure 4-2. Although the point design is not optimized, it serves as a reasonable starting point for variable-impedance design studies.

4.1. NGPP circuit models

4.1.1. Simplified models for MITL evaluation

Simplified Bertha [12] circuit models are used to evaluate the NGPP MITL designs and to make direct comparisons with Empire PIC simulations. Each level of the stack and MITL is modeled independently, incorporating regions of the water flares, vacuum flares, MITLs, and load. The model is driven with an open-circuit voltage waveform, generated by the full circuit model of the point design, at the input to the water flares. A typical circuit model is shown in Figure 4-3. Circuit elements for the voltage input, water flare, and load are common to both Bertha and Empire simulations. The vacuum flare and MITLs are modeled as transmission line elements in Bertha and form the EM/PIC region of the Empire simulations.

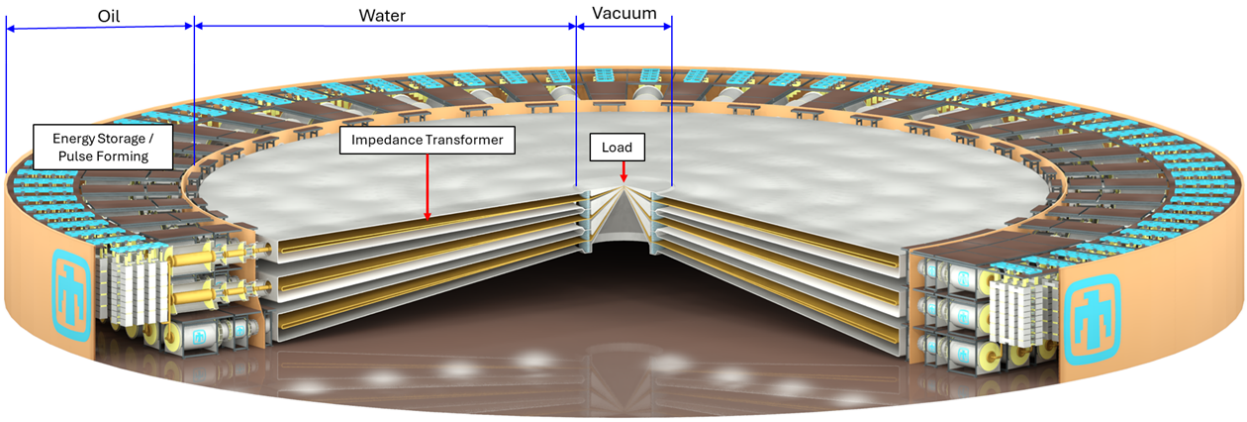

Figure 4-1. Rendering of a representative NGPP point design.

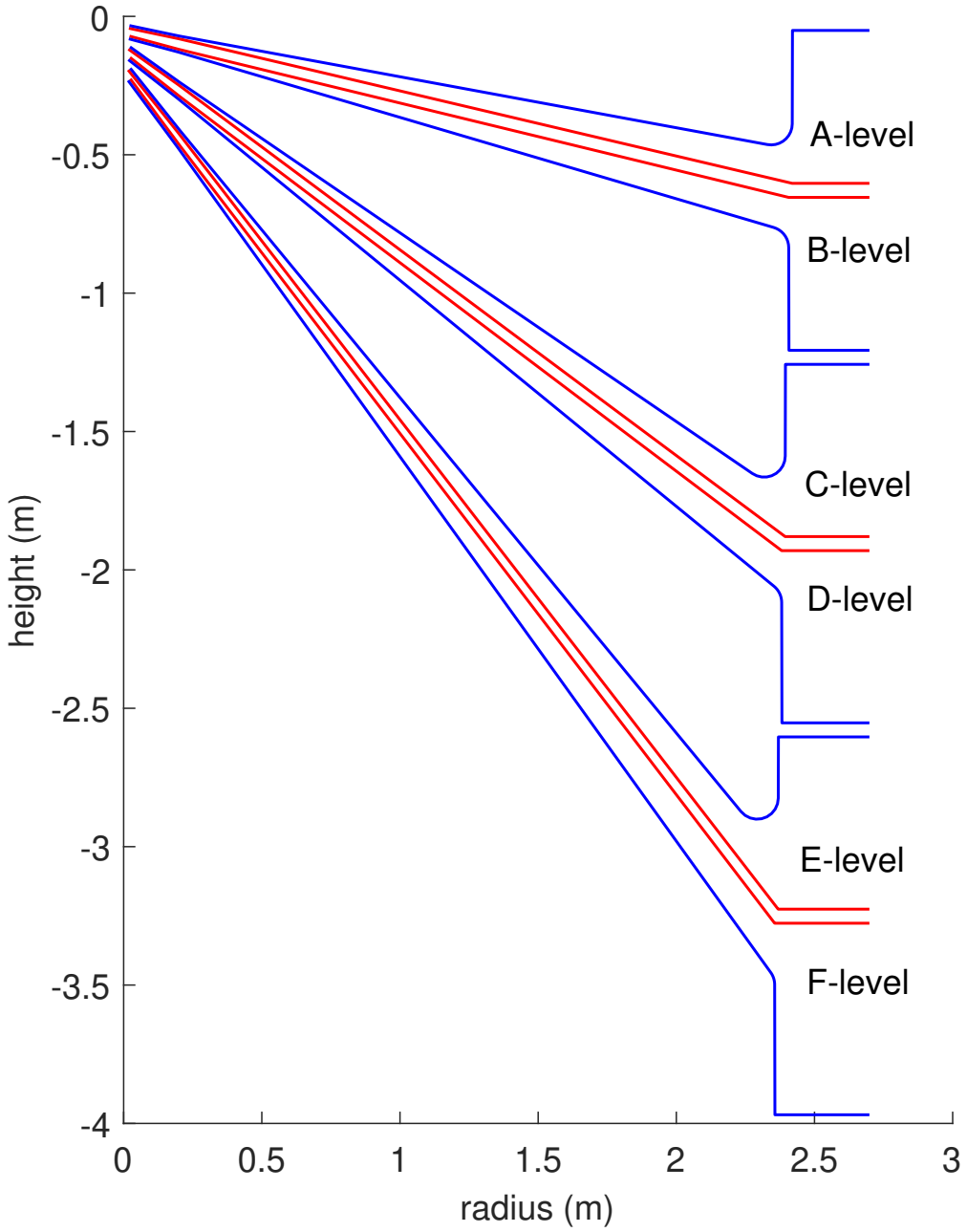

Figure 4-2. Baseline NGPP MITL conductor profiles. Anode conductors shown are in blue. Cathode conductors are shown in red.

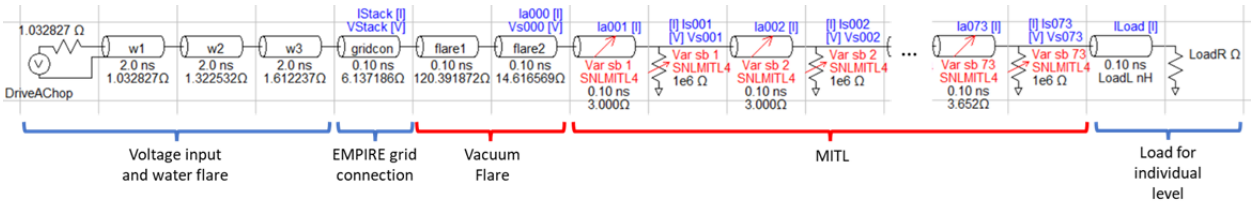

Figure 4-3. Typical NGPP MITL Bertha circuit model representation. Elements labeled with a blue bracket are common to both Bertha and Empire simulations. Elements labeled with a red bracket are a Bertha circuit model representation of the 3D domain modeled with Empire.

Level	Element 1	Element 2	Element 3	Element 4
A	1.032827 Ω 2.0 ns	1.322532 Ω 2.0 ns	1.612237 Ω 2.0 ns	
B	1.051139 Ω 2.0 ns	1.331688 Ω 2.0 ns	1.612237 Ω 2.0 ns	
C	1.111997 Ω 2.0 ns	1.464040 Ω 2.0 ns	1.816083 Ω 2.0 ns	
D	1.141787 Ω 2.0 ns	1.478935 Ω 2.0 ns	1.816083 Ω 2.0 ns	
E	1.207198 Ω 2.0 ns	1.410160 Ω 2.0 ns	1.613121 Ω 2.0 ns	1.816083 Ω 0.1 ns
F	1.334735 Ω 2.0 ns	1.563133 Ω 2.0 ns	1.791531 Ω 2.0 ns	2.019929 Ω 0.1 ns

Table 4-1. NGPP MITL water flare circuit element impedance and transit time. Levels A–D had 3 elements each. Levels E–F had 4 elements each.

Level	L (nH)	R (Ω)
A	14.83	0.4
B	20.20	0.4
C	23.74	0.4
D	26.48	0.4
E	28.43	0.4
F	31.67	0.4

Table 4-2. NGPP MITL load circuit inductance and resistance.

The input source impedance is matched to the input impedance of the water flare. The water flare elements are held constant for all simulations of a particular level. Transmission line parameters for the water flare elements for all levels are given in Table 4-1. The vacuum flare is modeled with lumped inductances, represented in Bertha as transmission line elements with a transit time of 1 time-step (0.1 ns) and the impedance determined by the inductance, $Z = \frac{L}{\tau}$, where L is the inductance and τ is the element transit time. The vacuum flare inductance varies slightly with changes to the MITL impedance profile. The MITLs are modeled using a series of pairs of elements: an ideal transmission line and a shunt resistor. A Bertha subroutine applies to all MITL element pairs. The MITL subroutine uses the voltage and current of the transmission line element, along with geometric parameters representing the circumference (or radius) and anode-cathode gap to determine when the electric field has exceeded an emission threshold and when magnetic insulation occurs. Local electron current losses prior to magnetic insulation are accounted for by adjusting the shunt resistor. After magnetic insulation, the subroutine calculates the electron flow current magnitude. Additional details on the MITL subroutine are given in Section 4.2. The load model consists of a fixed inductance and resistance. The load parameters for each level are shown in Table 4-2. These parameters were derived from full circuit simulations to best match voltage and current at the input to the vacuum flare.

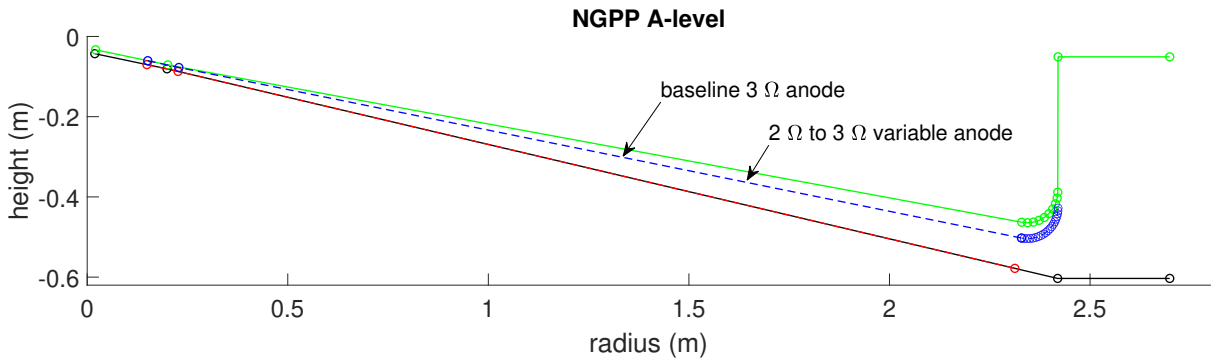

Figure 4-4. Typical NGPP variable impedance MITL design. Variable impedance designs were achieved by adjusting the MITL anode conductor to set a specified MITL input impedance at the transition from the vacuum flare. At small radius the anode-cathode gap was forced to be a minimum of 1 cm

4.1.2. Generating MITL circuit models

Variable impedance designs were generated using MATLAB, starting from the baseline geometry and adjusting the anode conductor to vary the MITL impedance. These designs were created using a linear variation in anode-cathode gap. Figure 4-4 illustrates the design process. The variable impedance MITL reduces the A-K gap in the transition from the vacuum flare to the MITL, compared to the baseline. This study did not consider the potential effects of lowering the inductance associated with the vacuum flare, insulator stack, and water flare.

Figure 4-5 depicts how the Bertha circuit elements were derived. The MITL region is divided into small segments with a transit time of 0.1 ns, the minimum time step used in all Bertha simulations. For each MITL region, the impedance, radius, and gap were determined for inputs to the MITL subroutine. The inductance of the vacuum flare regions was calculated through numerical integration of a triangular mesh in that region, given by $L = \frac{\mu_0}{2\pi}\int \frac{1}{r}\,dA$. The MITL element impedance and anode-cathode gap versus radius are shown in Figure 4-6 and Figure 4-7. The MITL impedance is given by,

$$Z = \frac{\eta_0}{2\pi}\frac{g}{r},$$

where $\eta_0 = 376.73\ \Omega$ is the impedance of free space, g is the anode-cathode gap, and r is the radius.

4.2. Bertha MITL subroutine

The Bertha MITL subroutine manages MITL physics, including local current losses prior to magnetic insulation and the calculations of electron flow current transport and shedding after magnetic insulation is established.

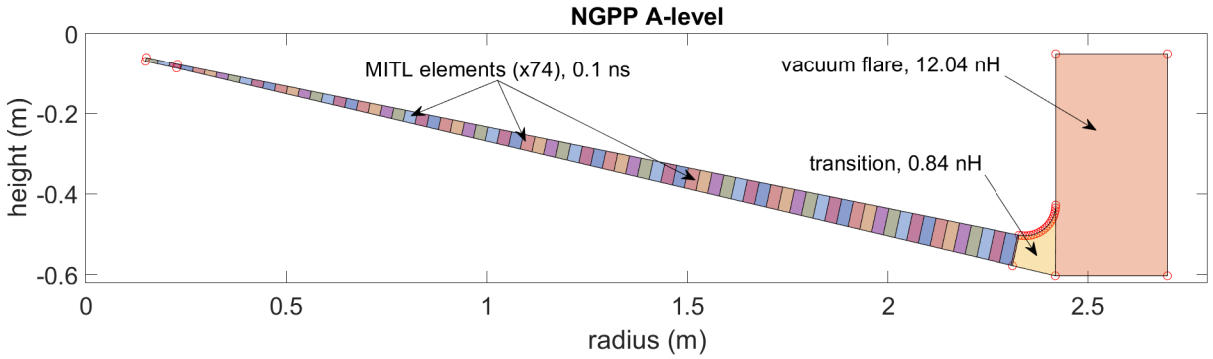

Figure 4-5. Typical NGPP MITL circuit element derivation from a MITL profile.

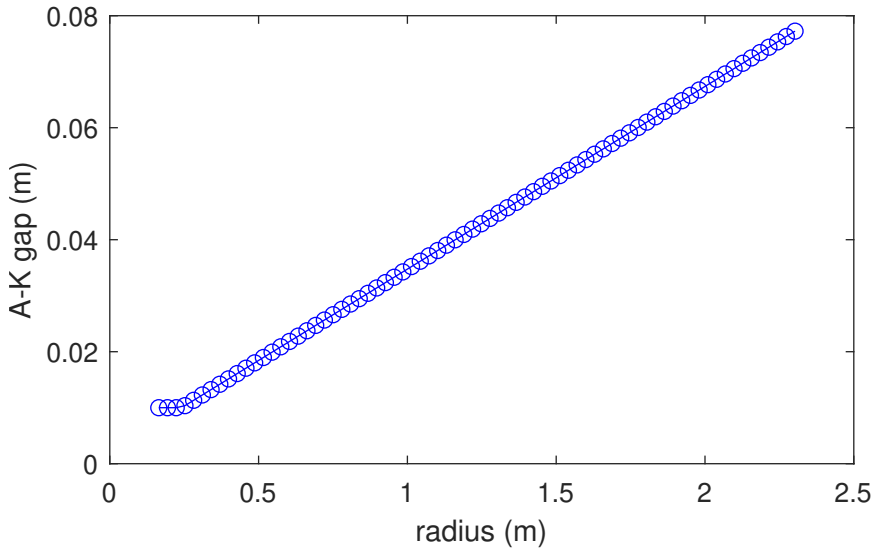

Figure 4-6. A-K gap versus radius for a 2 Ω to 3 Ω variable impedance MITL with a 1 cm minimum gap.

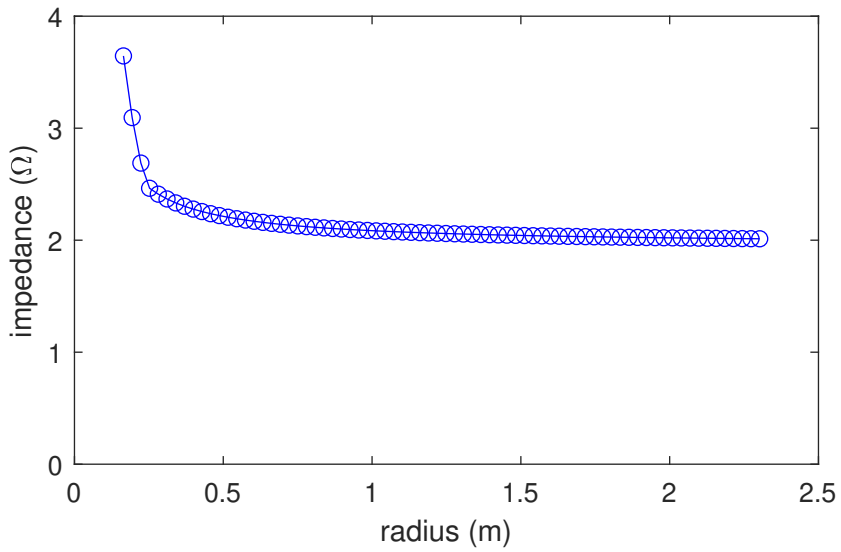

Figure 4-7. Impedance versus radius for a 2 Ω to 3 Ω variable impedance MITL with a 1 cm minimum gap.

4.2.1. Electron current losses prior to magnetic insulation

Electron current losses in the MITL prior to magnetic insulation can lead to anode heating and anode plasma formation. The electron loss current prior to magnetic insulation is calculated as the Child-Langmuir 1D space-charged-limited (SCL) current. The SCL current is reduced as the self-magnetic field in the MITL approaches and exceeds the critical magnetic field as discussed in Section III of [48]. During this project, differences in the loss model implementations between Bertha and Screamer were identified. Figure 4-8 shows the electron loss current density, normalized to the 1D Child-Langmuir space-charge limited current, versus the self-magnetic field, normalized to the single-particle critical magnetic field (see Eq. 5 in [48]). The third curve in Figure 4-8 shows an EH3 fit developed in Sec. V of [10] (called "Analytic fit" in that reference). All three of these curves were implemented in a Bertha subroutine to allow for comparisons to Empire simulations.

Electron emission is turned on when a specified threshold electric field is exceeded, typically 200 $\frac{\text{kV}}{\text{cm}}$ or 240 $\frac{\text{kV}}{\text{cm}}$. One of two methods is used to smooth the transition from non-emitting to emitting. The standard method in Bertha is to increase the SCL emission current linearly from zero to the full SCL current as the electric field rises from the threshold to a saturation electric field of 400 $\frac{\text{kV}}{\text{cm}}$. A second method, based on time, increases the loss current from zero to the full SCL current over 0.5 ns once the threshold electric field is exceeded.

4.2.2. Electron flow current after magnetic insulation

The electron flow current in the MITL after magnetic insulation is modeled based on either collisionless [22, 24] or collisional approaches [46]. The MITL subroutine in Bertha can transport and/or shed flow current throughout the series of MITL subroutine elements based on specified

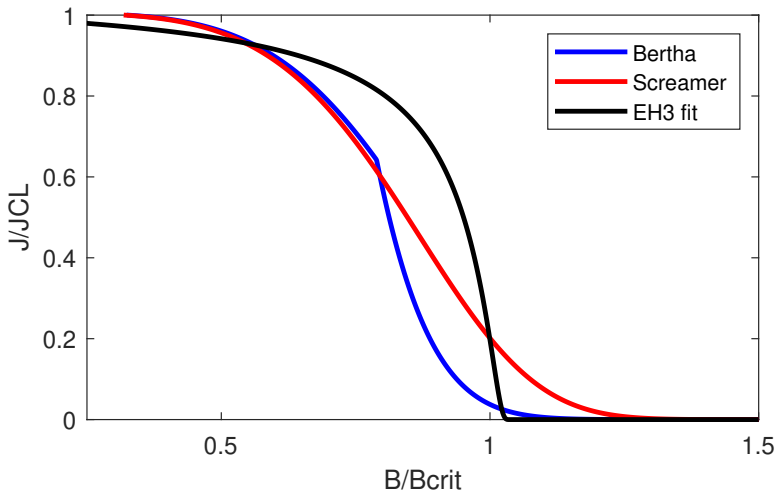

Figure 4-8. Uninsulated electron loss versus magnetic field. The EH3 fit is from reference [10].

inputs. For this project, it is assumed that the MITL electron flow current is not lost within the MITL or at the end of the MITL.

4.2.3. Anode heating due to uninsulated electron loss

The anode temperature rise is estimated from Ohmic heating and electron-energy deposition from the uninsulated electron loss current, given by:

$$\Delta T = \frac{\vartheta B^2}{2\mu_0 c_v} + \int_0^t \frac{V I_{\text{loss}}}{m_a c_v} dt. \tag{4.1}$$

The first term on the right side of Eq. 4.1 accounts for ohmic heating of the conductor as given by [45]. The second term accounts for the energy deposited by the uninsulated electron loss current. In this equation, the quantity V is the element voltage, I_{loss} is the uninsulated electron loss current, m_a is the anode electrode mass to which the electrons deposit energy, and c_v is the specific heat per unit volume of the conductor. The anode electrode mass varies with time and is given by:

$$m_a = A \frac{eV}{S_P} \cos\theta, \tag{4.2}$$

where S_P is the total stopping power of an electron given by Ref. [1], and θ is the electron angle of incidence, normal to the electrode surface, as calculated by Equations 27-29 in [10]. When determining the stopping power, the kinetic energy of the electron impacting the anode is assumed to be equal to the potential energy given by the element voltage, eV. As discussed in [10], the angle of incidence is undefined when $B > B_{\text{crit}}$, preventing additional temperature increases for the loss models discussed in Section 4.2.1. This was not significant for the analytic fit model from [10] which cuts off just above $B > B_{\text{crit}}$, but could be significant for the Screamer

and Bertha implementations. One method to address this this is to set a maximum angle of incidence as B approaches and exceeds B_{crit}, ensuring that all uninsulated electron loss contributes to anode heating.

4.3. Bertha Simulations of NGPP MITLs

Variable impedance MITL designs were simulated with Bertha for all six MITL levels. All designs enforced a 1 cm minimum gap and used a linear variation in anode-cathode gap. Other designs, such as a linear variation in impedance, were not simulated as part of this project. Table 4-3 through Table 4-8 list the MITL designs simulated for each level and their impact on MITL and total inductance. Figure 4-9 though Figure 4-14 show the load current, total uninsulated electron loss current, and temperature rise for all the MITL designs.

Trends in load current and loss current were consistent across all six levels. As the MITL input impedance decreases:

- The smaller anode-cathode gap at large radius reduces the total inductance.
- The total current loss prior to magnetic insulation increases.
- The duration of uninsulated electron loss current increases.
- The temperature in the MITL generally increases, except within the constant gap region.

Bertha predicts the temperature in the constant gap region decreases at the output of the MITL for more aggressive variable impedance MITL designs. This is explained by larger overall losses throughout the length of the MITL limiting $\mathrm{d}I/\mathrm{d}t$ at the MITL output early in time. Lower $\mathrm{d}I/\mathrm{d}t$ limits the voltage at the end of the MITL which suppresses the uninuslated electron losses early in time. This is one area where Empire and Bertha do not agree. Bertha does not model unstable electron flow current within the constant gap region that can result in additional heating of the anode after magnetic insulation is established.

The Bertha simulation results indicated that the “Variable 4” design with an input impedance of 1 Ω and an output impedance of 3 Ω produces the highest peak load current across all six MITL levels. These design reduce the total vacuum inductance by 23.3 % to 26.5 %, depending on the level. Although uninsulated electron loss current increases compared to the baseline, the entire length of the MITL becomes magnetically insulated prior to peak current.

The more aggressive “Variable 5” design significantly increases the magnitude and duration of the uninsulated electron loss current, resulting in the current loss throughout the entire load current rise time. The increased loss reduces the peak load current and increases the load current rise time.

MITL	Outer Z (Ω)	Inner Z (Ω)	Outer gap (cm)	MITL L (nH)	MITL ΔL/L	Vacuum L (nH)	Vacuum ΔL/L
Baseline MITL	3.0	3.0	11.39	22.25		50.31	
Variable 1	2.5	3.0	9.61	19.09	14.2%	46.97	6.6%
Variable 2	2.0	3.0	7.68	15.93	28.4%	43.63	13.3%
Variable 3	1.5	3.0	5.76	12.77	42.6%	40.30	19.9%
Variable 4	1.0	3.0	3.84	9.64	56.7%	37.00	26.5%
Variable 5	0.5	3.0	1.92	6.64	70.2%	33.84	32.7%

Table 4-3. NGPP level A MITL designs.

MITL	Outer Z (Ω)	Inner Z (Ω)	Outer gap (cm)	MITL L (nH)	MITL ΔL/L	Vacuum L (nH)	Vacuum ΔL/L
Baseline MITL	3.0	3.0	11.69	23.06	-	56.37	-
Variable 1	2.5	3.0	9.75	19.70	14.6%	52.93	6.1%
Variable 2	2.0	3.0	7.81	16.36	29.1%	49.54	12.1%
Variable 3	1.5	3.0	5.87	13.06	43.4%	46.18	18.1%
Variable 4	1.0	3.0	3.87	9.81	57.5%	42.85	24.0%
Variable 5	0.5	3.0	1.94	6.72	70.9%	39.68	29.6%

Table 4-4. NGPP level B MITL designs.

MITL	Outer Z (Ω)	Inner Z (Ω)	Outer gap (cm)	MITL L (nH)	MITL ΔL/L	Vacuum L (nH)	Vacuum ΔL/L
Baseline MITL	3.0	3.0	11.07	25.81	-	66.65	-
Variable 1	2.5	3.0	9.31	22.23	13.9%	62.72	5.9%
Variable 2	2.0	3.0	7.43	18.63	27.8%	58.78	11.8%
Variable 3	1.5	3.0	5.62	15.00	41.9%	54.84	17.7%
Variable 4	1.0	3.0	3.74	11.38	55.9%	50.92	23.6%
Variable 5	0.5	3.0	1.87	7.90	69.4%	47.17	29.2%

Table 4-5. NGPP level C MITL designs.

MITL	Outer Z (Ω)	Inner Z (Ω)	Outer gap (cm)	MITL L (nH)	MITL ΔL/L	Vacuum L (nH)	Vacuum ΔL/L
Baseline MITL	3.0	3.0	11.67	28.02		70.52	
Variable 1	2.5	3.0	9.75	24.00	14.3%	66.35	5.9%
Variable 2	2.0	3.0	7.82	19.99	28.7%	62.22	11.8%
Variable 3	1.5	3.0	5.88	15.99	42.9%	58.13	17.6%
Variable 4	1.0	3.0	3.90	12.01	57.1%	54.10	23.3%
Variable 5	0.5	3.0	1.96	8.20	70.7%	50.27	28.7%

Table 4-6. NGPP level D MITL designs.

MITL	Outer Z (Ω)	Inner Z (Ω)	Outer gap (cm)	MITL L (nH)	MITL ΔL/L	Vacuum L (nH)	Vacuum ΔL/L
Baseline MITL	3.0	3.0	10.91	32.85		81.10	
Variable 1	2.5	3.0	9.06	28.36	13.7%	76.07	6.2%
Variable 2	2.0	3.0	7.29	23.82	27.5%	71.01	12.4%
Variable 3	1.5	3.0	5.50	19.23	41.5%	65.94	18.7%
Variable 4	1.0	3.0	3.68	14.64	55.4%	60.89	24.9%
Variable 5	0.5	3.0	1.84	10.21	68.9%	56.05	30.9%

Table 4-7. NGPP level E MITL designs.

MITL	Outer Z (Ω)	Inner Z (Ω)	Outer gap (cm)	MITL L (nH)	MITL ΔL/L	Vacuum L (nH)	Vacuum ΔL/L
Baseline MITL	3.0	3.0	11.44	36.37		87.60	
Variable 1	2.5	3.0	9.57	31.17	14.3%	82.16	6.2%
Variable 2	2.0	3.0	7.68	25.97	28.6%	76.76	12.4%
Variable 3	1.5	3.0	5.79	20.79	42.8%	71.42	18.5%
Variable 4	1.0	3.0	3.87	15.65	57.0%	66.17	24.5%
Variable 5	0.5	3.0	1.95	10.74	70.5%	61.19	30.1%

Table 4-8. NGPP level F MITL designs.

4.4. Empire Simulations of NGPP MITLs

In this section we describe our setup and simulation results for NGPP MITLs.

The particular NGPP design under investigation is one consisting of six levels, labeled A through F starting from the top level. We divide the designs in two categories: (i) constant impedance MITLs and (ii) variable impedance MITLs, see sections 4.4.1, 4.4.2.

4.4.1. Constant-Impedance Designs

The constant impedance design is designated as a "baseline." The baseline design was chosen to have constant impedance of 3 Ω in the straight section of the MITL until the AK gap becomes as small as 1 cm, after which the MITL has a constant gap section until it connects to the convolute. Such design was inspired by the highly successful outer MITLs of the Z machine at Sandia National Laboratories.

We approach the design first from a circuit element simulation viewpoint with BERTHA, then set up PIC simulations with Empire. Additionally, we divide the problems into six individual level problems, each level being separately simulated but accounting for the other levels by attaching a specific circuit at the "load side" of the MITL; thus, each level accounts for the presence of all other levels, the convolute, as well as the load.

Level	Empire	Bertha
A	35.51	35.48
B	36.15	36.13
C	42.93	42.94
D	44.03	44.04
E	52.65	52.68
F	55.90	55.93

Table 4-9. NGPP MITL levels inductance (nH) comparison between Empire and Bertha.

Parameter	Value
Number of elements	2.5-5 million
Wedge angle	0.5 degrees
Resolution (port side)	4-5 mm
Resolution (load side)	400-500 μm
Time step size	1-4 $\times$ 10^{-13} s
Simulation time	200 ns
SCL threshold	20 MV/m
Thermal desorption threshold	400 °C

Table 4-10. Typical Empire simulation parameters.

Since the load at the generator appears predominantly inductive, we first compared overall MITL inductance for each individual level. The results in Table 4-9 show excellent agreement between the two codes.

Typical Empire simulation parameters are given in Table 4-10. In the Empire setup we assume azimuthal symmetry and accordingly, only simulate a small 3D angular wedge. Space-charge limited emission (SCL) of electrons from the cathode contribute to anode temperature increase (ohmic heating is also included but is a much smaller contributor). For all six levels of the baseline design, the anode temperature does not exceed 400°C and accordingly, thermal desorption does not modify the results. In the next section on variable impedance MITL design, however, thermal desorption plays a major role and is always included.

A set of simulations was performed to determine viability of the baseline NGPP design. The conclusion was that the base design is safe and delivers peak current as expected, i.e., in agreement with circuit element simulations with Bertha. The following figures illustrate this.

Figures 4-15 to 4-20 typically show excellent agreement with Bertha simulations. Small exceptions can be seen in the voltages on the load side as well as in the loss currents. The latter are difficult to predict around the theoretical Hull cutoff magnetic field even with the recently revised model EH3, due to the fact that turbulent electron dynamics in PIC simulations is not included in circuit element models.

4.4.2. Variable-Impedance designs

The advantages of variable impedance MITL designs were addressed in Sec. 3.2.2. Here we consider variable impedance NGPP MITL designs for levels A and F. Level A is considered since it has the smallest inductance (cf. Table 4-9) and delivers the largest currents to the load, which also leads to the best (self-)magnetic insulation. Level F is the opposite limit, i.e., has the weakest magnetic insulation and delivers the smallest current to the load. These two levels are in this sense bounding the parameter design space.

We present two examples of level A variable impedance designs, with impedance changing between 1-3 Ω (1 Ω being the impedance at the outer radius of the MITL) and a design with impedance change between 2-3 Ω. The next figures demonstrate the crucial importance of thermal desorption.

Figure 4-21 (a) shows that load current delivery is unacceptably low, with more than 3 MA lower peak current than the stack current. Due to the large current loss in the first $\sim$ 100 ns of the pulse (panel (b)) the anode temperature is increased well beyond the thermal desorption threshold (panel (c)) leading the contaminant release from the anode surface (modeled in Empire as H+ ion injection). This design is obviously unacceptable.

We explored a less aggressive level A MITL design with impedance variation between 2-3 Ω. The results are shown in Figure 4-22. This design shows full current delivery (panel(a)), much reduced current loss (panel (b)), and temperature *not* exceeding 400 °C. In fact, peak current is increased compared to the constant impedance MITL design, as expected.

Next we looked at NGPP MITL level F variable impedance designs. The design with 1-3 Ω impedance change showed severely degraded current delivery to the load, worse than that for level A. A less aggressive impedance variation design, between 2-3 Ω, showed also worse current delivery due to thermal desorption. An even less aggressive design was explored, with impedance change between 2.5-3 Ω. The results from this simulation are shown in Figure 4-23. Although current delivery does not appear degraded compared to BERTHA (panel(a)), anode temperature exceeds thermal desorption close to the convolute. For practical purposes, one would prefer to have some safety margin. For this reason, even this less aggressive MITL design for level F is likely not viable.

4.5. Conclusions

Designs for NGPP outer MITLs were explored. It was shown that the baseline design with constant MITL impedance was acceptable and performed as predicted by the circuit element code Bertha, with thermal desorption not contributing to current loss.

Designs with variable impedance MITLs were explored from a more aggressive impedance change in the range 1-3 Ω to less aggressive change in the range 2.5-3 Ω. PIC simulations were performed for levels A and F, as the two limits of the property of magnetic insulation. It was determined that in most of these designs thermal desorption played a crucial role in current delivery to the load. Both levels A and F with the more aggressive design 1-3 Ω registered large

current losses and were deemed unacceptable. For level A, a design with 2-3 Ω impedance variation change was shown to be acceptable with anode temperature not exceeding 400 °C. For level F no variable impedance design was found that kept the anode temperature below thermals desorption threshold. A less aggressive design with 2.5-3 Ω showed minimal current delivery degradation but since thermal desorption still turned on, no safety margin existed for practical implementation.

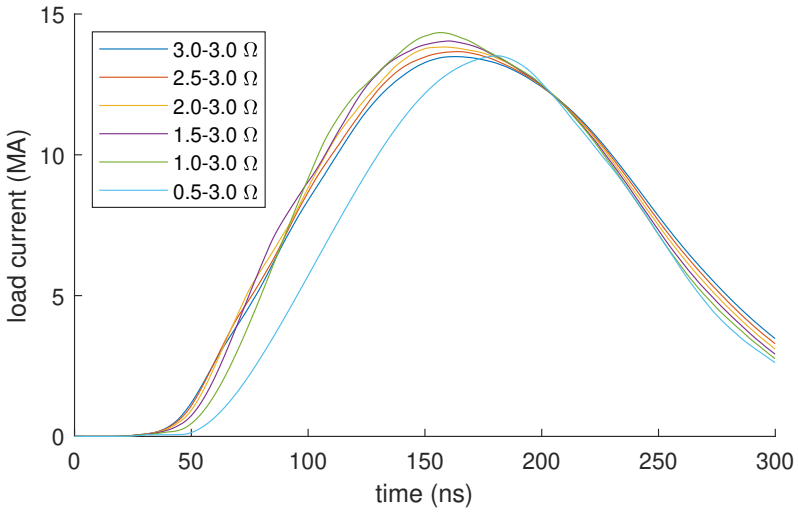

(a) load current

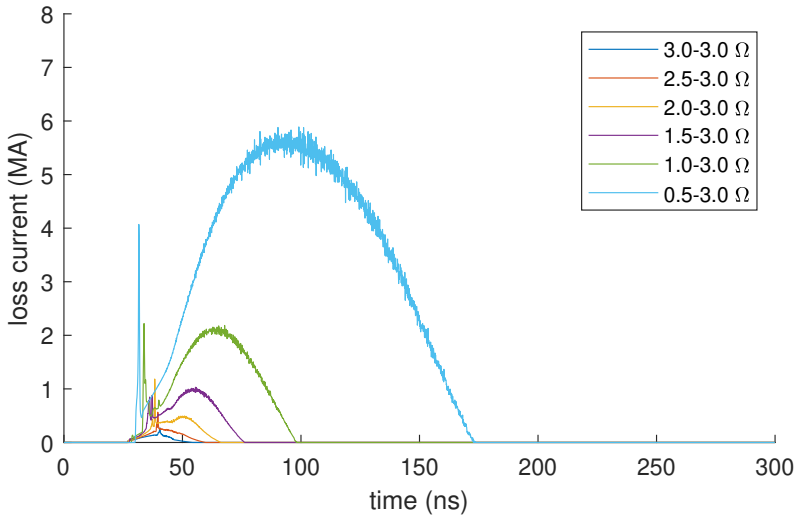

(b) loss current

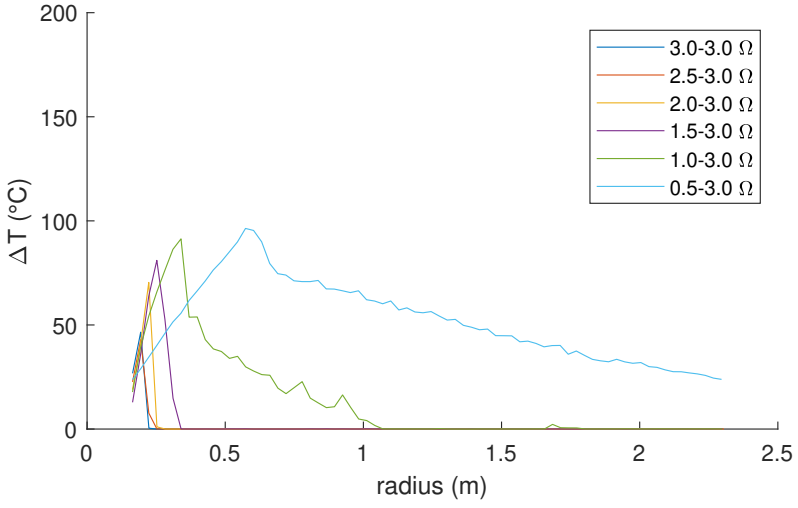

(c) temperature

Figure 4-9. NGPP MITL level A Bertha simulation results.

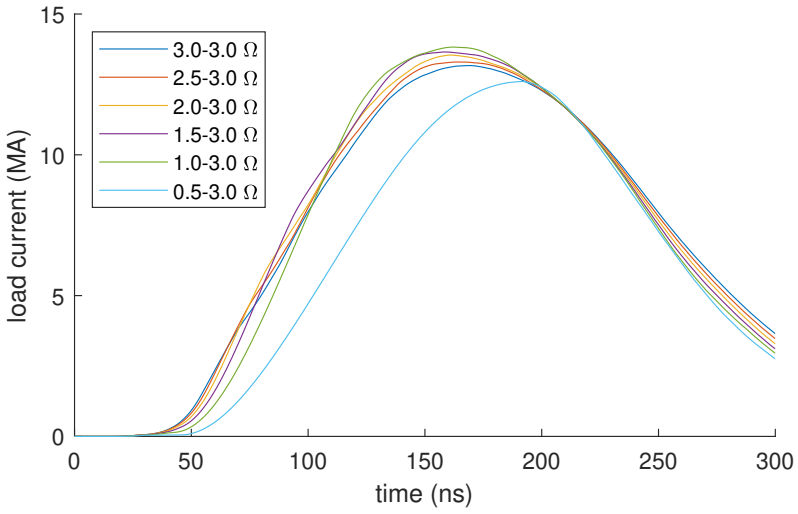

(a) load current

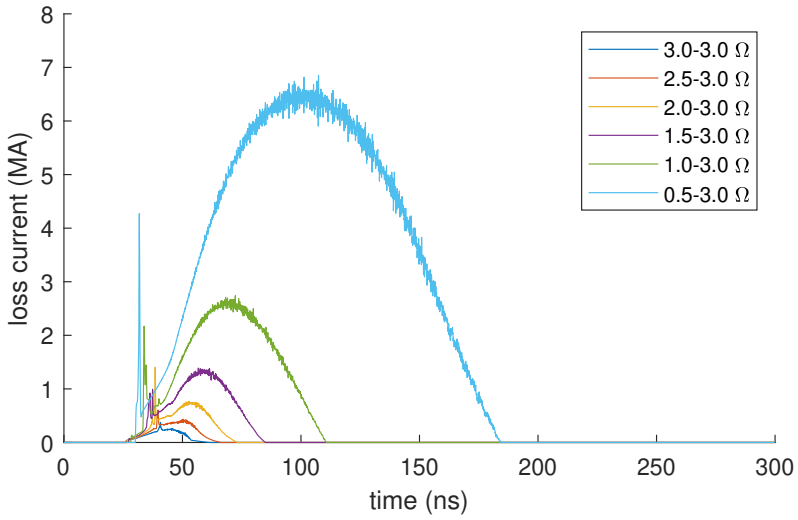

(b) loss current

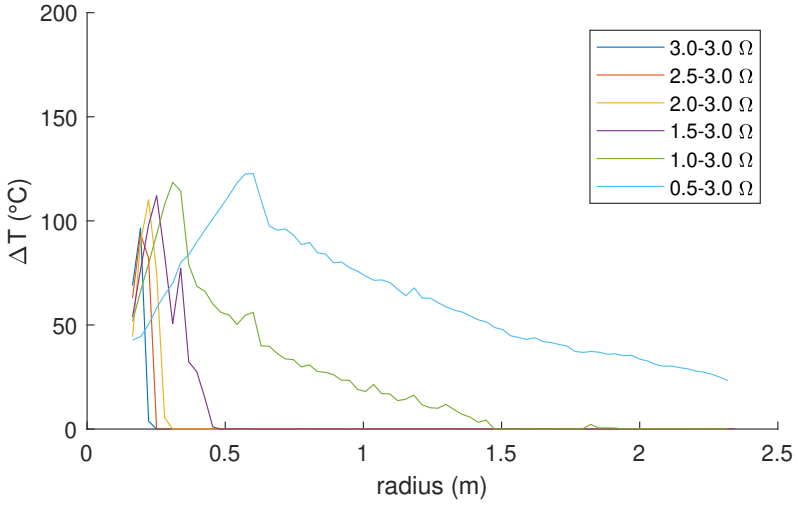

(c) temperature

Figure 4-10. NGPP MITL level B Bertha simulation results.

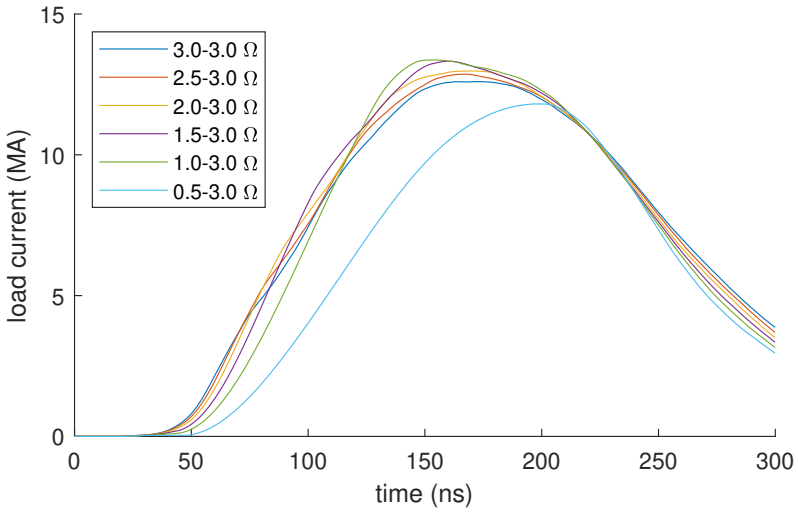

(a) load current

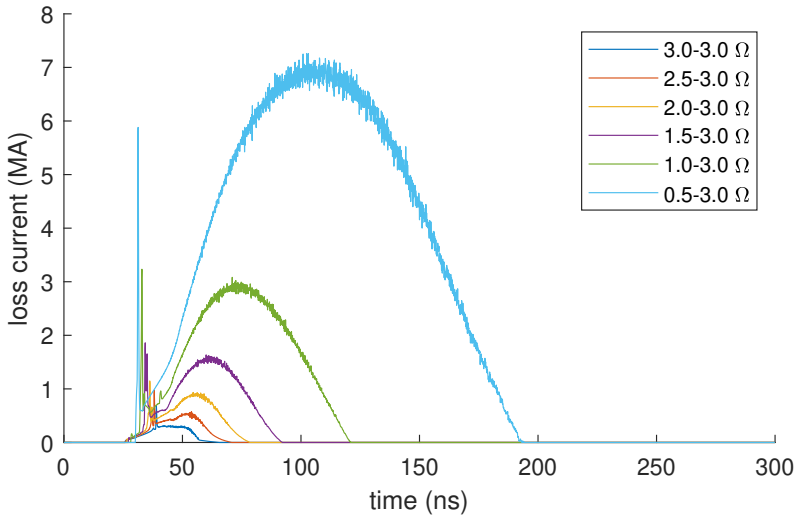

(b) loss current

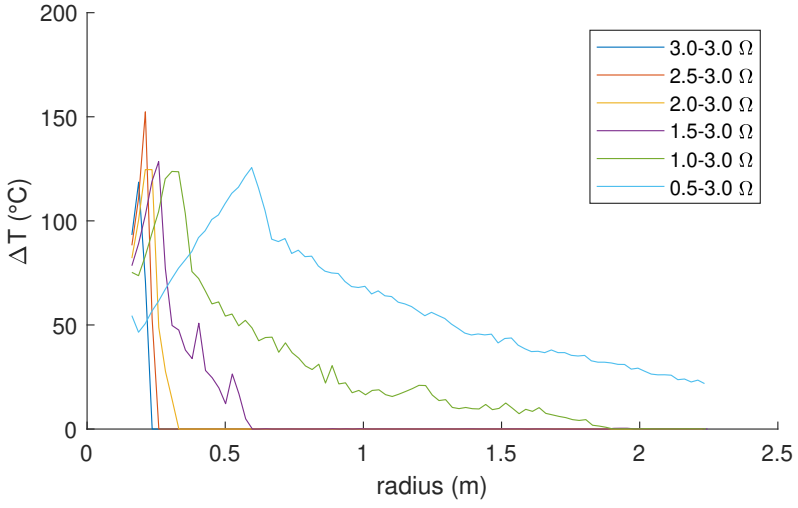

(c) temperature

Figure 4-11. NGPP MITL level C Bertha simulation results.

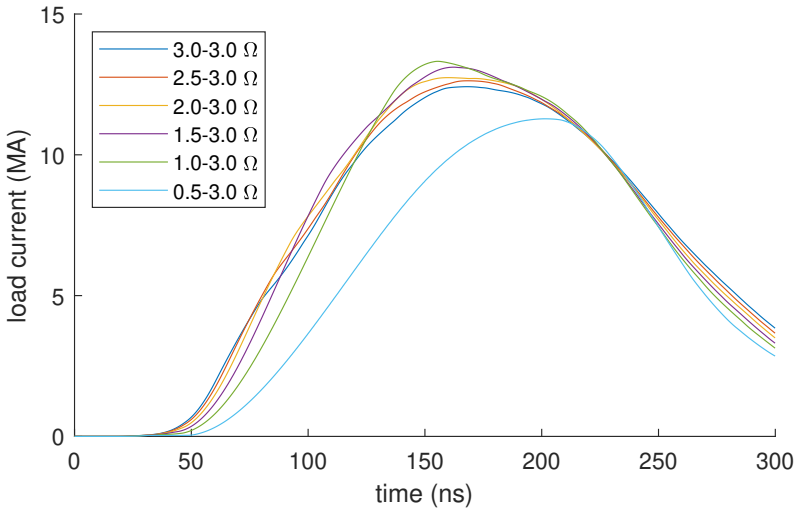

(a) load current

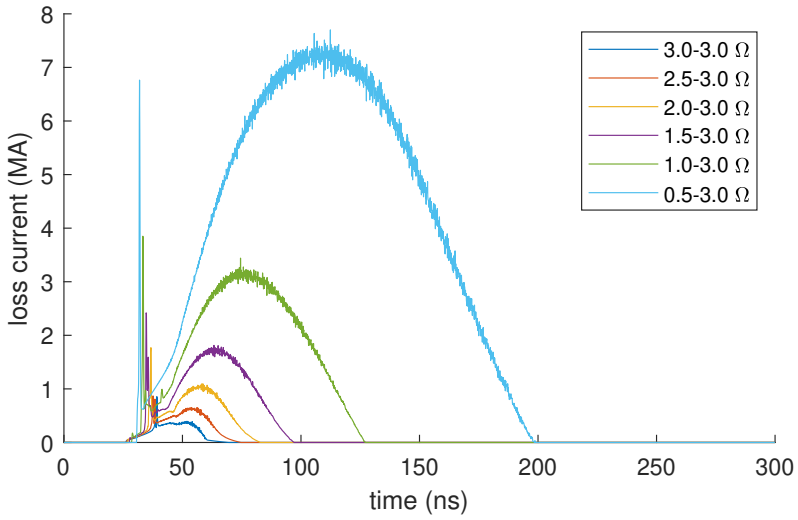

(b) loss current

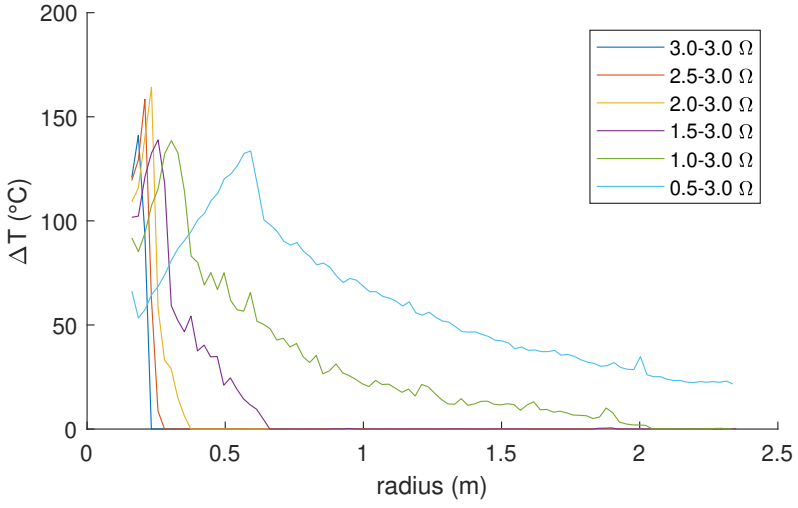

(c) temperature

Figure 4-12. NGPP MITL level D Bertha simulation results.

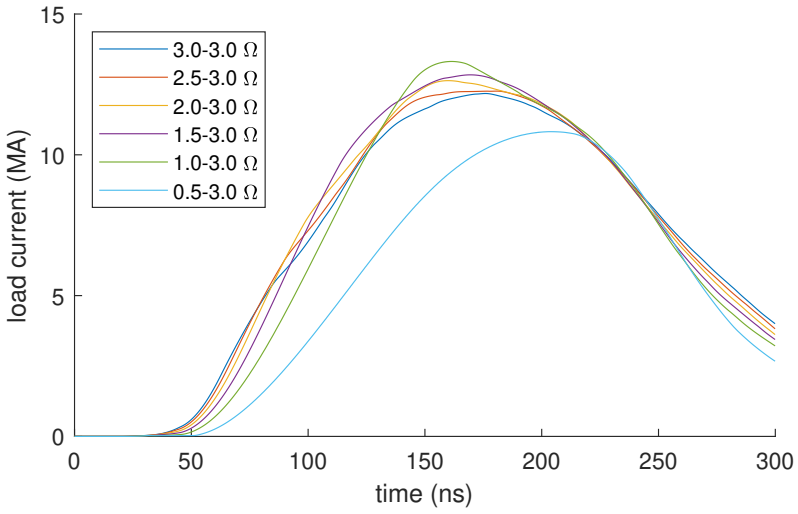

(a) load current

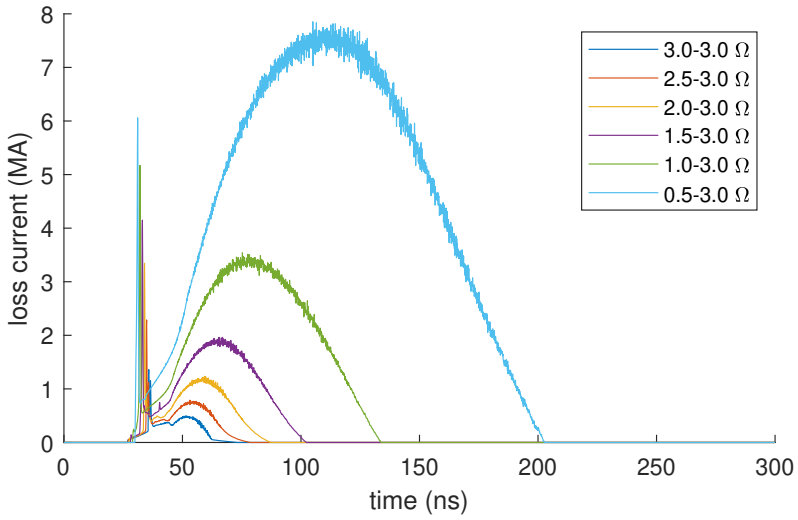

(b) loss current

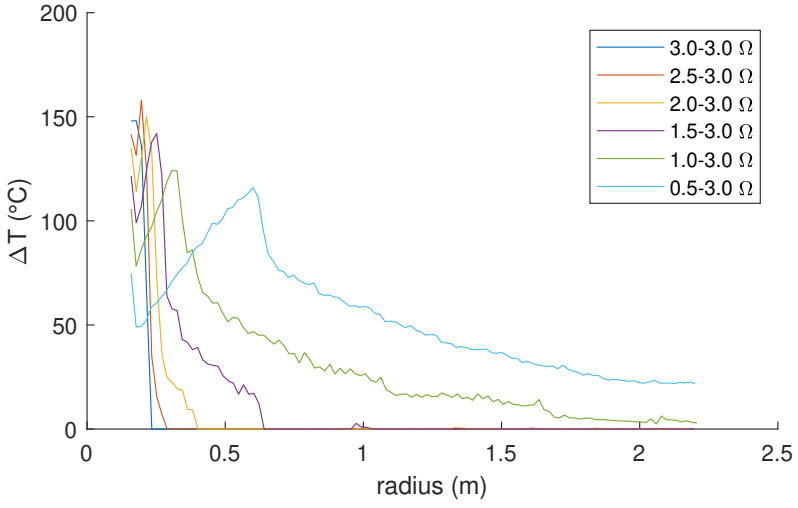

(c) temperature

Figure 4-13. NGPP MITL level E Bertha simulation results.

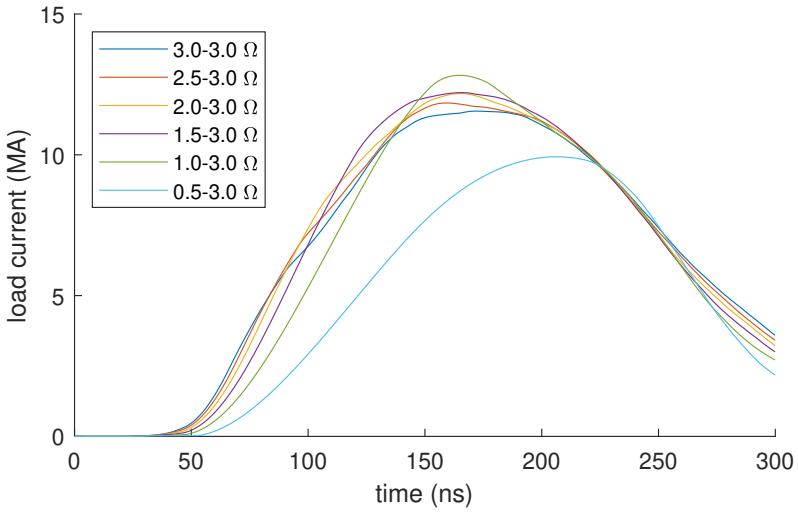

(a) load current

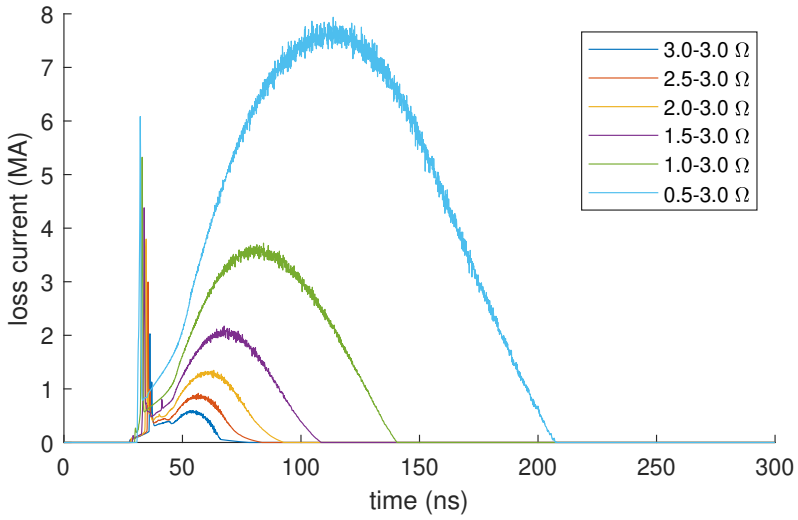

(b) loss current

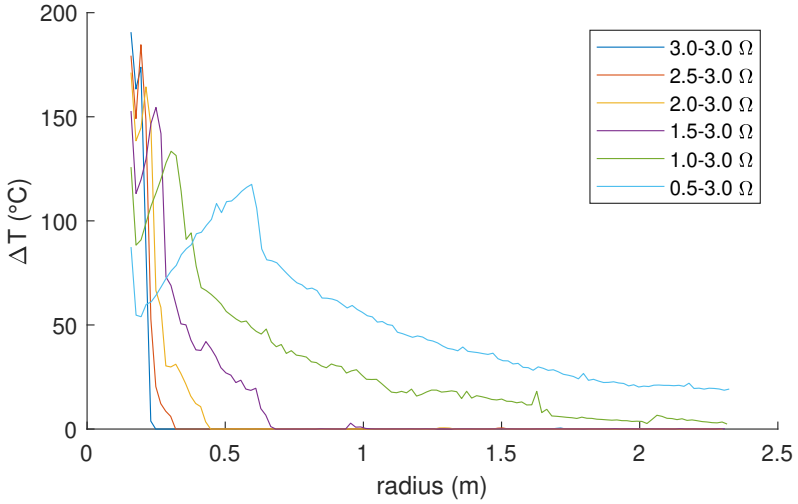

(c) temperature

Figure 4-14. NGPP MITL level F Bertha simulation results.

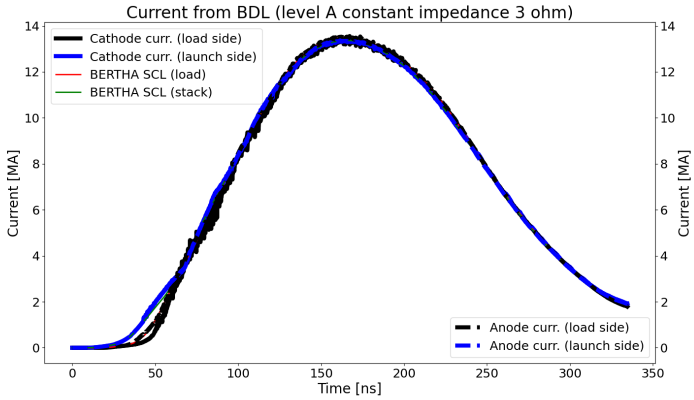

(a) load current

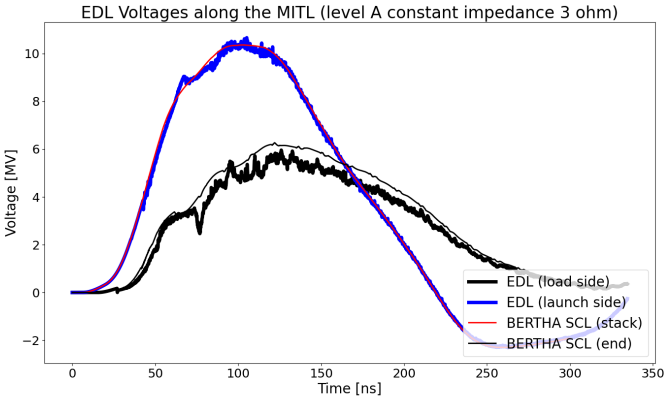

(b) voltages

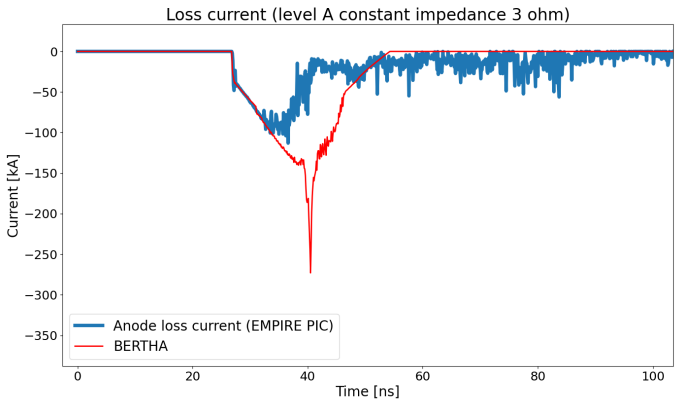

(c) loss current

Figure 4-15. NGPP MITL level A constant impedance Empire and Bertha simulation results.

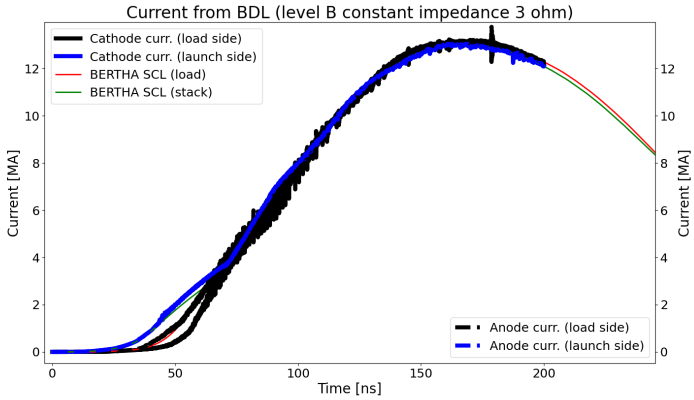

(a) load current

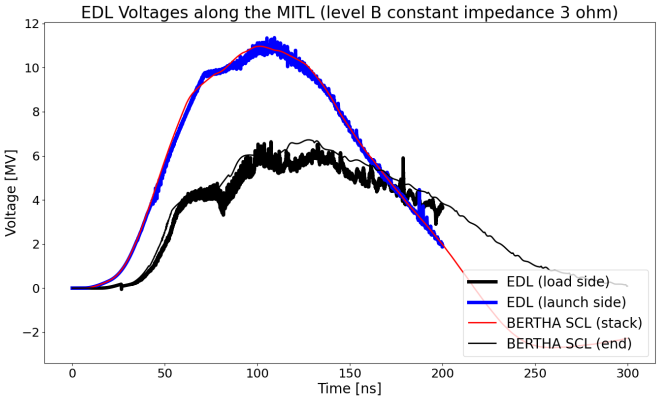

(b) voltages

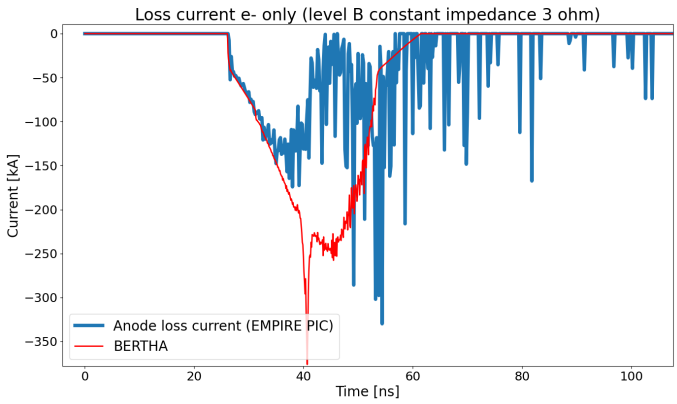

(c) loss current

Figure 4-16. NGPP MITL level B constant impedance Empire and Bertha simulation results.

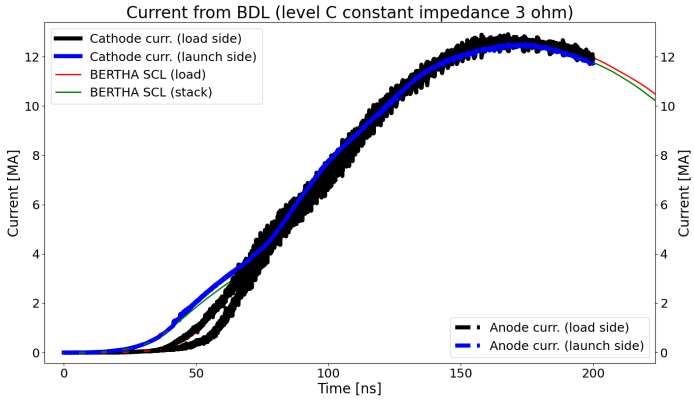

(a) load current

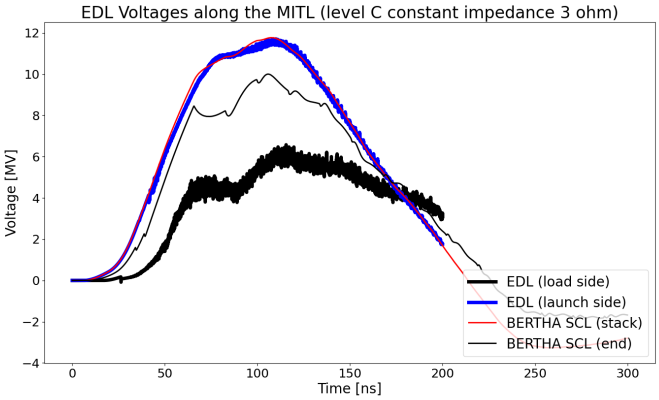

(b) voltages

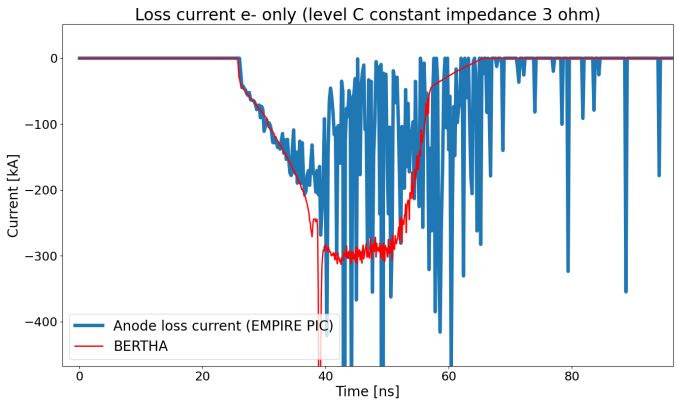

(c) loss current

Figure 4-17. NGPP MITL level C constant impedance Empire and Bertha simulation results.

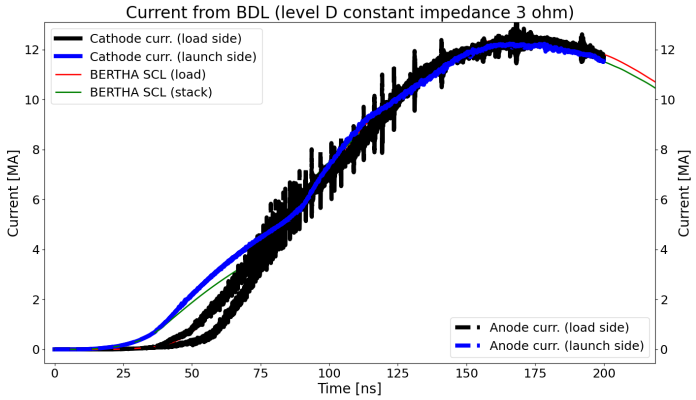

(a) load current

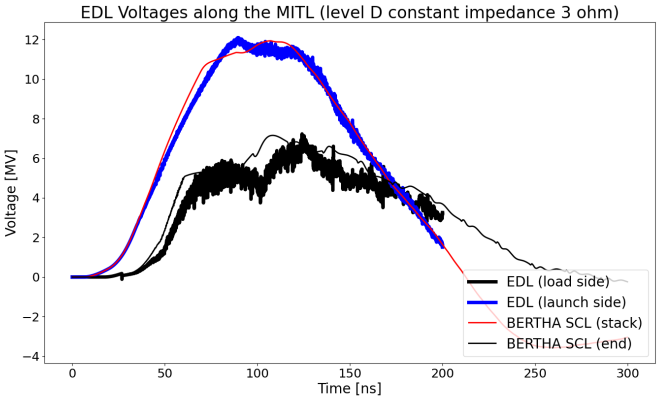

(b) voltages

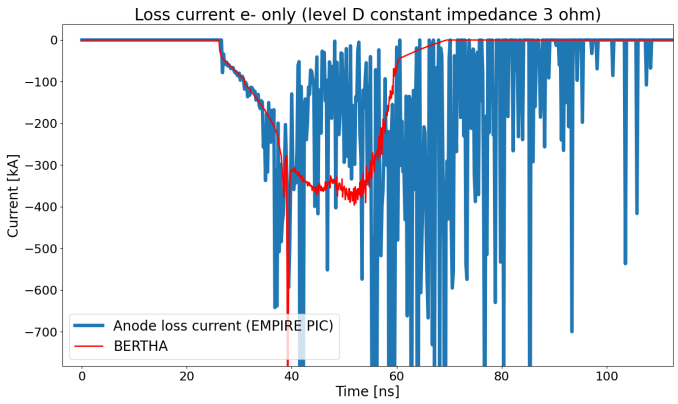

(c) loss current

Figure 4-18. NGPP MITL level D constant impedance Empire and Bertha simulation results.

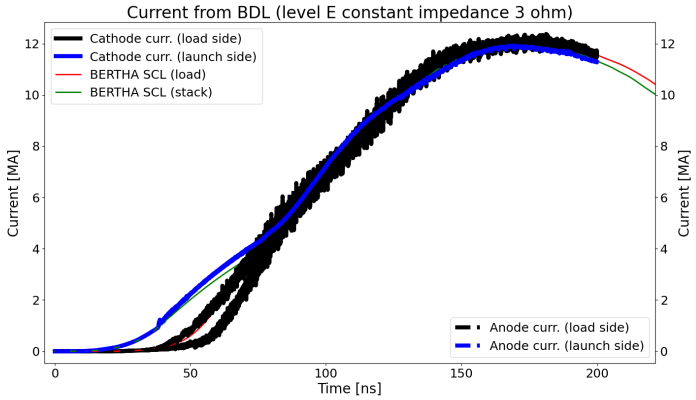

(a) load current

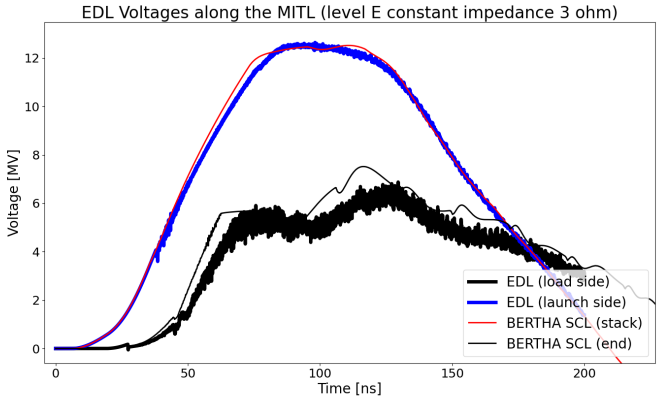

(b) voltages

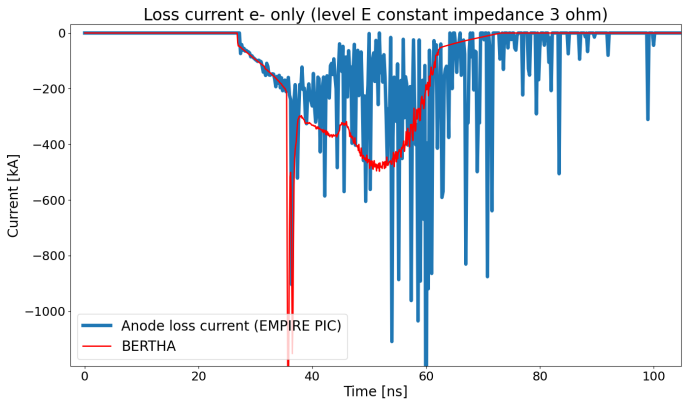

(c) loss current

Figure 4-19. NGPP MITL level E constant impedance Empire and Bertha simulation results.

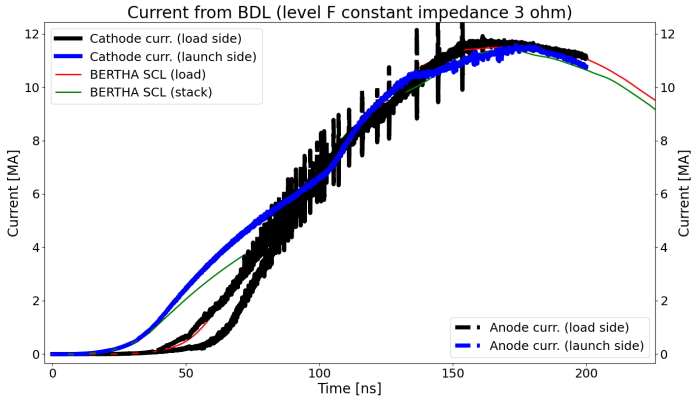

(a) load current

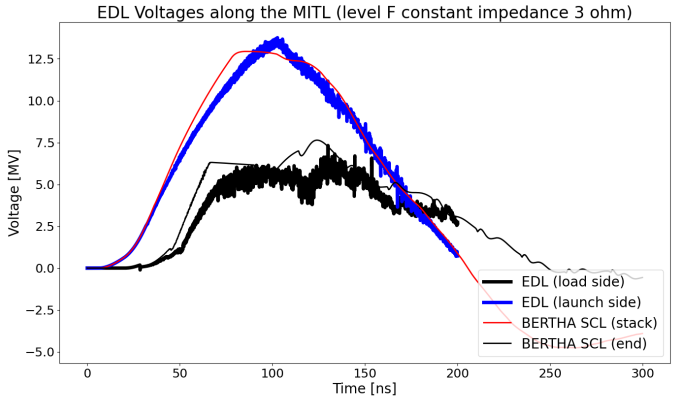

(b) voltages

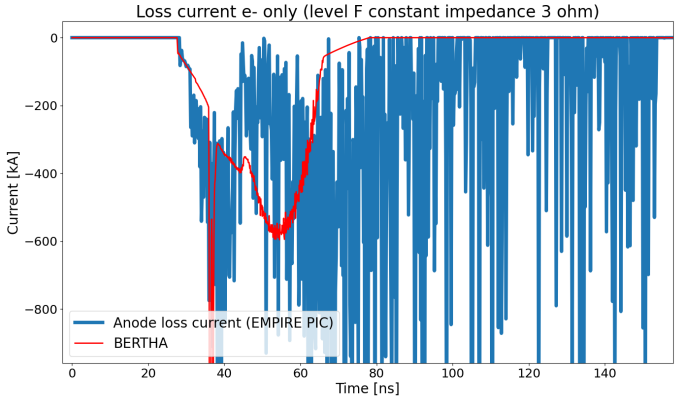

(c) loss current

Figure 4-20. NGPP MITL level F constant impedance Empire and Bertha simulation results.

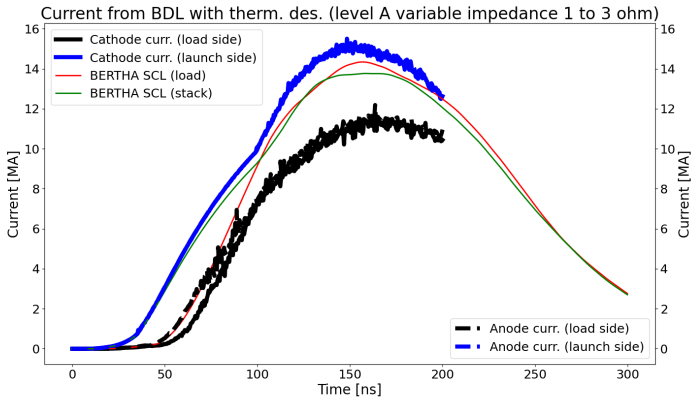

(a) load current

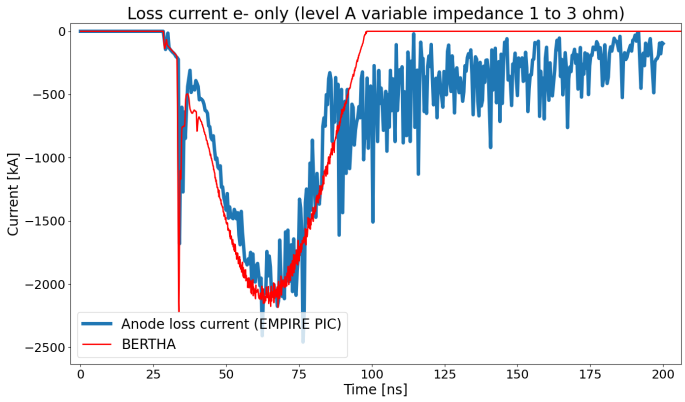

(b) loss current

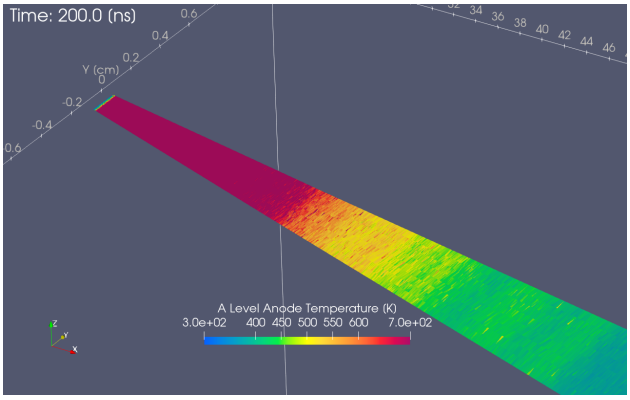

(c) anode temperature

Figure 4-21. NGPP MITL level A variable impedance 1-3 Ω Empire simulation results.

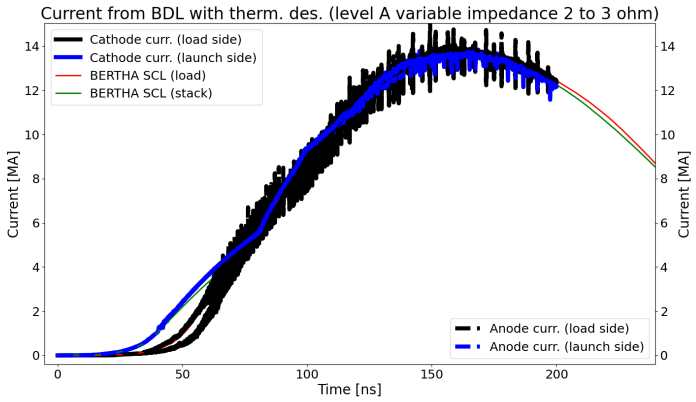

(a) load current

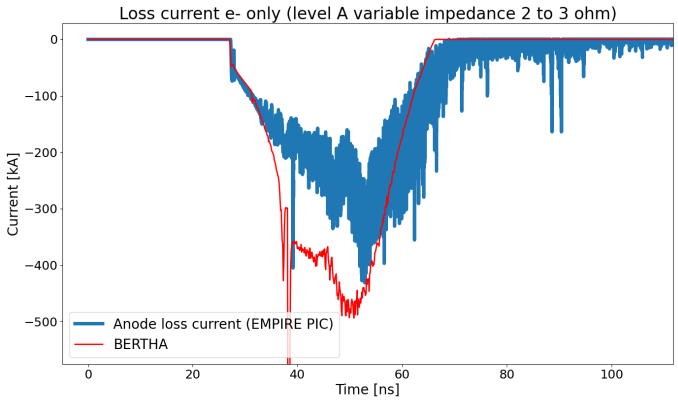

(b) loss current

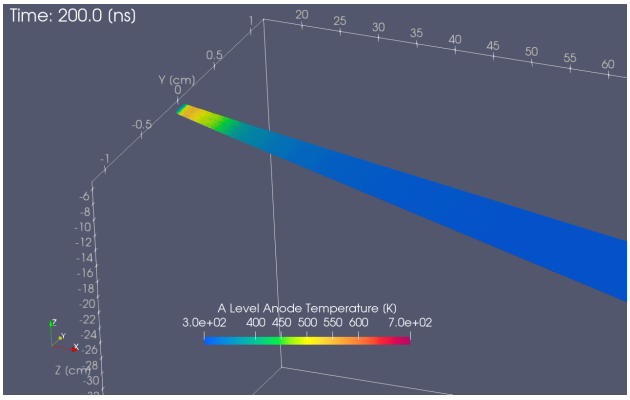

(c) anode temperature

Figure 4-22. NGPP MITL level A variable impedance 1-3 Ω Empire simulation results.

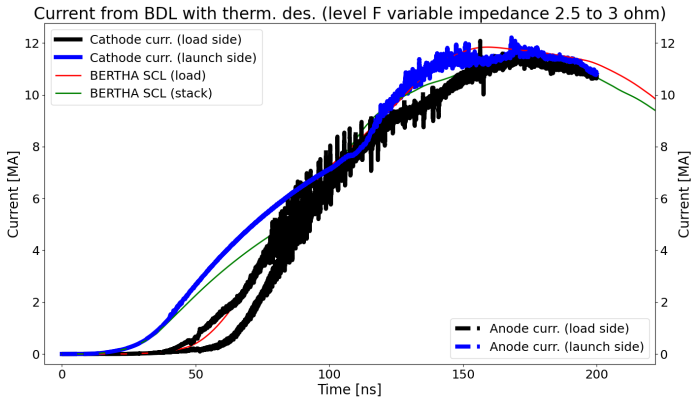

(a) load current

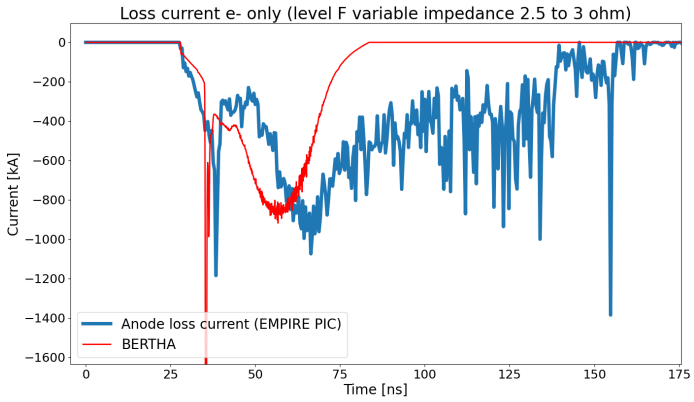

(b) loss current

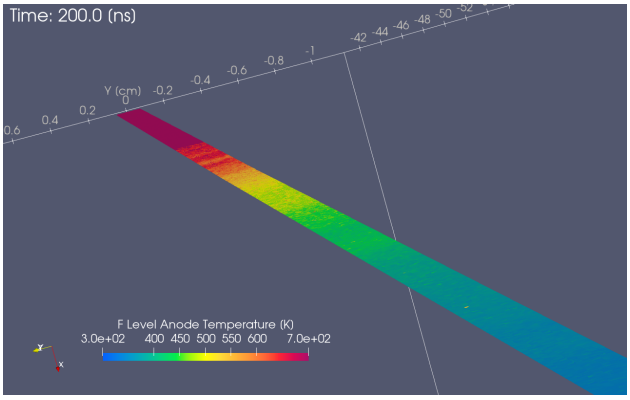

(c) anode temperature

Figure 4-23. NGPP MITL level F variable impedance 2.5-3 Ω Empire simulation results.

5. REDUCED DIMENSION THEORY AND SIMULATIONS

Modeling Z and NGPP provides useful calculations for specific designs. To provide additional insight we also studied magnetically-insulated transmission lines (MITLs) in a simplified two-dimensional (2D) planar geometry. Additional detail not reproduced here may be found published in Ref. [8]. First-principles, equilibrium theory and 2D Empire simulations were used as reduced dimension modeling tools. The main risk of using reduced dimension modeling is oversimplification. Early simulations lacked several fine-tuning controls and were indeed oversimplified. The journey toward an enhanced simulation model is detailed in Sec. 5.1. The theoretical model used was Brillouin flow theory from Lau et al., Ref. [17]. Section 5.2 recapitulates the key ideas from the reference and also updates conical MITL flow theory from Creedon, Ref. [6], using the modern formalisms of Lau et al., Ref. [17], to facilitate use for Z and NGPP designs. Finally, findings from 2D simulation and theory are presented.

5.1. Source and Load Impedances

Source and load impedances were initially set to vacuum impedance. However, as MITL operating impedance was better understood, eventually both of these were changed to vary independently.

Source impedance controls how power enters the MITL. The simple transmission line model used to couple the source to the Empire domain treats source impedance as a voltage divider [19], the main effect of choosing source impedance not matched to MITL operating impedance is higher or lower voltage coupled to the MITL (cf. Eq. (5.11)).

Load impedance affected MITL flow conditions in specific ways described in subsequent sections. Notably, leaving load impedance at vacuum impedance always meant load impedance was higher than MITL operating impedance. Either impedance or transmission line type boundary conditions could have been used to control load impedance.

5.2. Reduced Dimension Theory

Theory has the advantage of being universal for any MITL which adheres sufficiently well to the underlying assumptions. Naturally, “sufficiently well” can be difficult to quantify and well-diagnosed experiments are required to discover model deficiencies. Two theoretical models are described here: planar MITL flow in Subsection 5.2.1 and simple impedance transitions in Subsection 5.2.2.

5.2.1. Planar MITL Flow

In the absence of collisions, electron acceleration is governed by the Lorentz force $\mathbf{F}$,

$$m\frac{d\mathbf{v}}{dt} = -e\left(\mathbf{E}+\mathbf{v}\times\mathbf{B}\right) \equiv \mathbf{F} \tag{5.1}$$

with electron mass m, electron velocity $\mathbf{v}$, time t, elementary charge e, electric field $\mathbf{E}$, and magnetic field $\mathbf{B}$. There exists a force-free condition in Eq. 5.1:

$$|\mathbf{v}| = |\mathbf{E}|/|\mathbf{B}|. \tag{5.2}$$

One equilibrium state for electron dynamics in MITLs is this force-free or "drift" flow, also called Brillouin flow[5], where any given electron moves at constant $\mathbf{v}$ purely in the downstream direction. Since velocity is constant, electric potential ϕ (i.e., $\mathbf{E} = -\nabla\phi$) must also be constant. Thus, Brillouin flow is also sometimes called "parapotential"[6] flow. Lau et al.[17] derives relativistic Brillouin flow theory using a more modern framework while recovering exactly the seminal Creedon result[9].

The essential details of Lau et al.[17] are recapitulated for planar geometries. First, no vector notation is used since all vector quantities are reduced to a single component: velocity downstream in $\hat{z}$, electric field from cathode to anode in $\hat{x}$, and magnetic field into the page in $\hat{y}$. The magnetic vector potential $\mathbf{A}$ (i.e., $\mathbf{B} = \nabla\times\mathbf{A}$) is introduced, with only the $\hat{z}$ component surviving (i.e., we write $A =\equiv A_z$). Second, several dimensionless variables (overbars) are used:

$$\bar{v} = v/c;\ \bar{\phi} = e\phi/\left(mc^2\right);\ \bar{A} = eA/\left(mc\right);\ \bar{I} = e\mu_0 I/\left(mc\right) \tag{5.3}$$

with vacuum permeability μ_0 and current I. Electric and magnetic fields can also be nondimensionalized by scaling to an arbitrary physical scale, x_s:

$$\bar{E} = ex_sE/\left(mc^2\right);\ \bar{B} = ex_sB/\left[mc\right];\ \bar{n} = e^2x_s^2n/\left(\varepsilon_0mc^2\right);\ \bar{x} = x/x_s \tag{5.4}$$

with electron number density n, vacuum permittivity ε_0, and position x. For planar geometry, Lau et al.[17] favored $x_s \equiv D$ where D is the gap distance, such that $\bar{x} = 0$ is the cathode and $\bar{x} = 1$ is the anode. Given boundary conditions

$$\bar{\phi}_{\bar{x}=0} = \bar{A}_{\bar{x}=0} = 0;\ \bar{\phi}_{\bar{x}=1} = \bar{V}_a;\ \bar{A}_{\bar{x}=1} = \bar{A}_a, \tag{5.5}$$

two quantities can be calculated:

$$\chi_b = \tanh^{-1}\left[\frac{\left(\bar{V}_a+1\right)\bar{A}_a - \sqrt{\bar{A}_a^2 - \bar{V}_a^2 - 2\bar{V}_a}}{\bar{A}_a^2+1}\right] \tag{5.6}$$

and

$$\kappa = \bar{V}_a/\sinh\left(\chi_b\right) + \chi_b - \tanh\left(\chi_b\right)/2. \tag{5.7}$$

While Lau et al.[17] have many results which can be useful for interpreting MITL flow, we focus here on the three quantities most readily observed in experiment: voltage, captured as a boundary condition (Eq. 5.5); cathode current I_c, and anode current I_a. The dimensionless currents are

$$\bar{I}_c = \bar{w}\kappa \tag{5.8}$$

with MITL width $\bar{w} = w/D$ and

$$\bar{I}_a = \bar{w}\kappa\cosh\left(\chi_b\right). \tag{5.9}$$

5.2.2. MITL Impedance Transitions

Operational impedance Z_{op} is defined as

$$Z_{\text{op}} \equiv V_a / I_a. \tag{5.10}$$

In context with another MITL section, source impedance, or load impedance, the series impedance reflection coefficient Γ is often applicable.

$$\Gamma = \frac{Z_2 - Z_1}{Z_2 + Z_1} \tag{5.11}$$

is the reflection coefficient going from section 1 to section 2. The transmitted voltage is the same as the sum of incident V_{in} and reflected voltages, leading to equilibrium voltage V_{eq}

$$V_{\text{eq}} = V_{\text{in}} (1 + \Gamma) \tag{5.12}$$

given an ideal source and sink. Similarly,

$$I_{\text{eq}} = I_{\text{in}} (1 - \Gamma) \tag{5.13}$$

with incident current $I_{\text{in}} \equiv V_{\text{in}} / Z_{\text{source}}$, where Z_{source} is the ideal source impedance. As described in Ref. [8], MITL electron flow can also act in parallel to the load such that

$$Z_{\text{load,effective}} = \left[Z_{\text{load}}^{-1} + Z_{\text{parallel}}^{-1} \right]^{-1}. \tag{5.14}$$

This parallel or lossy impedance pathway splits the current while maintaining voltage, allowing a MITL to efficiently transmit power toward any load, even an open circuit. This is not the same as *delivering* power efficiently to the load, electrons will be delivered to the anode only for a sufficiently high Z_{load}. The reason for this parallel pathway is detailed in Ref. [8]; for this Report, suffice to say that Z_{op} from Eq. 5.10 has a global maximum. Equation 5.12 says voltage is constant across any transition and in fact guarantees that voltage is constant over the whole system in equilibrium. Since Eq. 5.13 yields the same conclusion for current, effective impedance must be the same at all points. One way for this condition to be satisfied when $Z_{\text{source}} = Z_{\text{load}} > Z_{\text{op,max}}$ is for a parallel load impedance to exist.

In simpler terms, the arguments above explain why some MITL-driven systems are lossy, especially large impedance loads. This also implies that the ideal matched-impedance load would have $Z_{\text{load}} > Z_{\text{op}}$; however, this is only possible when $Z_{\text{parallel}} \equiv \infty$. As will be shown, losses to the anode are not the only form of Z_{parallel} and, as such, Z_{parallel} actually drives $Z_{\text{load,effective}}$ down when a matched-impedance load is attempted. Fortunately, low $Z_{\text{load}} \ll Z_{\text{op}}$ drives an easily-characterized "load-limited"[28] MITL mode where $Z_{\text{op}} \to Z_{\text{load}}$ in equilibrium, simplifying analysis greatly for load-limited systems such as ZX and NGPP.

In contrast to the complicated relationship between Z_{op} and Z_{load}, Z_{source} couples simply with the rest of the system according to Eqs. 5.11-5.13, where $Z_1 \equiv Z_{\text{source}}$ and $Z_2 \equiv Z_{\text{op,final}}$ once impedance transition and MITL-load interactions are accounted for. As will be observed later,

$Z_{\text{op,final}}$ is generally close to, but not exactly at, the smallest $Z_{\text{op,max}}$ for any MITL section. While the differences between $Z_{\text{op,final}}$ and $Z_{\text{op,max}}$ can be small, the difference is observed and calculated consistently[26, 27] and must be considered for MITL designs with large Z_{load}. The differences observed in this report should not be used as-is for ZX or NGPP analysis, since planar geometry (here) and cylindrical geometry (Refs. [26, 27]) have opposite trends for which branch of the solution $Z_{\text{op,final}}$ occupies. Small Z_{load} leads to $Z_{\text{op}} \rightarrow Z_{\text{load}}$, a far easier condition to calculate and one which circuit codes are well-equipped to handle.

6. CONCLUSIONS & FUTURE WORK

This project has revisited the longstanding design principle that efficient power flow in the magnetically-insulated transmission lines (MITLs) of pulsed-power drivers require *constant* geometric impedance by undertaking a directed study of the variable-impedance MITLs concept. Towards this end, we have presented a number of work products:

First, contributions to variable-impedance MITL equilibrium theory were developed. This has resulted in one journal article submission.

Second, we evaluated the variable geometric impedance MITLs concept through modeling and simulation (circuit modeling and high fidelity electromagnetic particle-in-cell (EM-PIC)). In this pursuit, we have delivered the first detailed characterizations of this MITL technology applied to systems relevant to Sandia's pulsed power program (Z) and roadmap (Next-Generation Pulsed Power (NGPP)).

For the NGPP system, a point design having six levels was selected for this work. The baseline design is conservative, employing 3 Ω constant-impedance MITLs for most of its length (250 cm $\gtrsim R \lesssim$ 25 cm). Because of large system, a set of decoupled problems (one for each level) was designed to make the problem size feasible for electromagnetic particle-in-cell simulations and to allow focused design work without extra variables (i.e., feedback from other levels). A circuit and electromagnetic particle-in-cell (EM-PIC) model was developed for each constant-impedance MITL for our simulation studies. Baseline operating performance as characterized by both Bertha (circuit) and Empire (EM-PIC) simulations were presented for all MITLs (levels "A" through "F"). The two sets of results show excellent agreement, confirming load current targets are met for each level while maintaining safe operation (e.g., minimal anode heating). For the variable-impedance study, at least five designs were fully vetted using Bertha for every level (i.e., at least 30 designs total). Each design is a linear taper geometry that reduces total MITL inductance more aggressively than the previous one (all results are provided in this report). Encouraging candidates for level A (highest current line) and level F (highest inductance line) were selected for evaluation using EM-PIC simulations. In most of these designs, Empire simulations predicted significant losses primarily due to anode plasma turn-on which circuit simulations cannot currently model. In this way, most designs considered viable according to circuit simulations were ultimately found to be non-viable when simulated with the higher level of detail (and more physics) enabled by the EM-PIC simulations. In spite of these challenges, we were able to iterate between circuit and EM-PIC codes to find a viable design for each level (A and F) that both Empire and Bertha agree meet design targets. For level A, this is a linear taper design varying between 2-3 Ω along its length. This design did not turn on anode plasma anywhere. For level F, a design with 2.5-3 Ω showed minimal current delivery degradation, but anode plasma does turn on so this design likely has no safety margin.

For the Z system, our technical approach was similar. First, a set of equivalent decoupled problems (one for each level) was consistently set up. Unlike NGPP, Z as it exists today is not strictly constant impedance [33], therefore our first step was to revise the MITL geometries to have constant impedance. Our variable-impedance studies were then perturbations from this baseline and, as for NGPP, we focused on the parameter space of linear tapers. Note that this first step was undertaken in order to maximize the utility of our results. If we only considered variable-impedance designs on top of Z as it exists today, our results would be an optimization for this specific system. By deliberately designing a constant impedance system our results is a broader comment, speaking to the advantages of variable-impedance MITLs *as a concept* compared to constant-impedance MITLs.

We established reliable SCREAMER single-level models for each Z level (MITLs "A" through "D"), which show excellent agreement with Empire for the baseline case and satisfactory agreement for variable-impedance cases. When discrepancies arise, they are mostly due to anode plasma turn-on, which is incuded in Empire as H+ emission but which cannot be modeled in SCREAMER. These comparisons provide confidence that SCREAMER can reliably predict Z performance in safe mode without H+ emission.

SCREAMER simulation results were completed for single-level models for 5 cases of increasing variable-impedance MITL designs (20%, 30%, 40%, 50%, 60%) for levels A, B, and C. Additionally, 1 variable-impedance design was completed for level D. Empire simulations were completed for single-level models for 3 down-selected variable-impedance designs for levels A, B, C and 1 variable-impedance design for level D. As with NGPP, it was found that anode plasma is a crucial factor in determining a safe design in a variable-impedance parameter space. Based on the study of individual-level models, SCREAMER and Empire identify several safe designs. We propose a combined variable-impedance system `VAR3-VAR3-VAR3-VAR1` (40%-40%-40%-20% inductance reductions for levels A, B, C, D, respectively) should be pursued as combined simulation ("full Z model") that includes the convolute and regions downstream in order to confirm viability and directly measure stack voltages and machine load current. In the final stretch of this project, SCREAMER simulations were completed for the full Z (baseline and the proposed variable-impedance system). The results are encouraging but, as we have experienced in this project work, must be confirmed in EM-PIC simulations.

The first priority for future work is to set up a baseline all-levels Z model in Empire and to establish agreement with the SCREAMER model. Once established, the analysis can be extended to the variable all-levels configuration. The most notable result from all-levels SCREAMER simulations that must be confirmed in Empire is the reduction in insulator stack voltage in the variable-impedance MITL model relative to the baseline. When extended to future pulsed power (e.g., ZX, NGPP), this reduction presents two options: (1) operate the stack at a lower voltage, thereby reducing the overall cost for the target load current, or (2) increase the stack voltage to the same level as in the baseline model (constant-impedance MITL) to achieve additional current.

The next notable result is the reduction in current rise time—for the `VAR3-VAR3-VAR3-VAR1` all-levels Z model, the current rise time (10-90%) is reduced by up to 12%. When extended to NGPP, this reduction can further relax the strict requirements on stack voltage ($V \sim LdI/dt$), thereby reducing the pulsed-power risks associated with NGPP construction.

The variable-impedance MITL design [39, 36] is a new concept that enables controlled manipulation of the initial electron losses in the outer MITL and can be tested on Z today. We encourage follow-on work (both modeling and simulation and experiment) to explore other potential configurations for a future Z upgrade. Our preliminary results are very encouraging for the all-levels VAR2 and VAR3 full Z models.

BIBLIOGRAPHY

[1] M. J. BERGER, J. S. COURSEY, M. A. ZUCKER, AND J. CHANG, *ESTAR, PSTAR, and ASTAR: Computer programs for Calculating Stopping-power and Range Tables for Electrons, Protons, and Helium Ions*, 2016-12-01 2005.

[2] M. T. BETTENCOURT, D. A. BROWN, K. L. CARTWRIGHT, E. C. CYR, C. A. GLUSA, P. T. LIN, S. G. MOORE, D. A. O. MCGREGOR, R. P. PAWLOWSKI, E. G. PHILLIPS, ET AL., *EMPIRE-PIC: A performance portable unstructured particle-in-cell code*, Communications in Computational Physics, 30 (2021).

[3] C. K. BIRDSALL AND A. B. LANGDON, *Plasma Physics via Computer Simulation*, Series in Plasma Physics, Taylor & Francis, New York, 1st ed., 2005.

[4] D. D. BLOOMQUIST, R. W. STINNETT, D. H. MCDANIEL, J. R. LEE, A. W. SHARPE, J. A. HALBLEIB, L. G. SCHLITT, P. W. SPENCE, AND P. CORCORAN, *Saturn: A large area x-ray simulation accelerator*, sand report, Sandia National Laboratories, Albuquerque, NM, dec 1987.

[5] L. BRILLOUIN, *A theorem of Larmor and its importance for electrons in magnetic fields*, Physical Review, 67 (1945), p. 260.

[6] J. M. CREEDON, *Relativistic Brillouin flow in the high ν/γ diode*, J. Appl. Phys., 46 (1975), p. 2946.

[7] ——, *Magnetic cutoff in high-current diodes*, J. Appl. Phys., 48 (1977), p. 1070.

[8] A. M. DARR, *Theory and simulation of gap distance transitions in planar magnetically insulated transmission lines*, Submitted to Phys. Rev. Accel. Beams Letters, (2025).

[9] A. M. DARR AND K. L. CARTWRIGHT, *Mutually magnetically insulated two-species Brillouin flow*, Physics of Plasmas, 30 (2023), p. 053105.

[10] E. G. EVSTATIEV ET AL., *Nonlocal, diamagnetic electromagnetic effects in magnetically insulated transmission lines*, Physics of Plasmas, 32 (2025), p. 062707.

[11] D. D. HINSHELWOOD, *BERTHA — A versatile transmission line and circuit code*, NRL Memorandum Report 5185 ADA135024, Naval Research Lab., Washington, DC (USA), Nov 1983.

[12] ——, *Naval Research Laboratory Memorandum Report No. 5185*, report, 1983.

[13] R. W. HOCKNEY AND J. W. EASTWOOD, *Computer Simulation Using Particles*, CRC Press, Mar. 2021.

[14] B. T. HUTSEL, P. A. CORCORAN, M. E. CUNEO, M. R. GOMEZ, M. H. HESS, D. D. HINSHELWOOD, C. A. JENNINGS, G. R. LAITY, D. C. LAMPPA, R. D. MCBRIDE, J. K. MOORE, A. MYERS, D. V. ROSE, S. A. SLUTZ, W. A. STYGAR, E. M. WAISMAN, D. R. WELCH, AND B. A. WHITNEY, *Transmission-line-circuit model of an 85-TW, 25-MA pulsed-power accelerator*, Phys. Rev. Accel. Beams, 21 (2018), p. 030401.

[15] M. L. KIEFER AND M. M. WIDNER, *Screamer—a single-line pulsed-power design tool*, in 5th IEEE Pulsed Power Conference (PPC), 1985.

[16] G. R. LAITY, A. C. ROBINSON, M. E. CUNEO, M. K. ALAM, K. R. BECKWITH, N. L. BENNETT, M. T. BETTENCOURT, S. D. BOND, K. COCHRANE, L. CRISCENTI, ET AL., *Towards predictive plasma science and engineering through revolutionary multi-scale algorithms and models (final report)*, tech. rep., Sandia National Laboratories (SNL-NM), Albuquerque, NM (United States); Sandia National Laboratories, SNL California, 12 2020.

[17] Y. Y. LAU, D. A. PACKARD, C. J. SWENSON, J. W. LUGINSLAND, D. LI, A. JASSEM, N. M. JORDAN, R. D. MCBRIDE, AND R. M. GILGENBACH, *Explicit Brillouin flow solutions in magnetrons, magnetically insulated line oscillators, and radial magnetically insulated transmission lines*, IEEE Transactions on Plasma Science, (2021), pp. 1–20.

[18] R. D. MCBRIDE, W. A. STYGAR, M. E. CUNEO, D. B. SINARS, M. G. MAZARAKIS, J. J. LECKBEE, M. E. SAVAGE, B. T. HUTSEL, J. D. DOUGLASS, M. L. KIEFER, B. V. OLIVER, G. R. LAITY, M. R. GOMEZ, D. A. YAGER-ELORRIAGA, S. G. PATEL, B. M. KOVALCHUK, A. A. KIM, P.-A. GOURDAIN, S. N. BLAND, S. PORTILLO, S. C. BOTT-SUZUKI, F. N. BEG, Y. MARON, R. B. SPIELMAN, D. V. ROSE, D. R. WELCH, J. C. ZIER, J. W. SCHUMER, J. B. GREENLY, A. M. COVINGTON, A. M. STEINER, P. C. CAMPBELL, S. M. MILLER, J. M. WOOLSTRUM, N. B. RAMEY, A. P. SHAH, B. J. SPORER, N. M. JORDAN, Y. Y. LAU, AND R. M. GILGENBACH, *A primer on pulsed power and linear transformer drivers for high energy density physics applications*, IEEE Transactions on Plasma Science, 46 (2018), pp. 3928–3967.

[19] D. MCGREGOR, E. PHILLIPS, D. SIRAJUDDIN, AND T. POINTON, *Variational, stable, and self-consistent coupling of 3D electromagnetics to 1D transmission lines in the time domain*, Journal of Computational Physics, 451 (2022), p. 110856.

[20] D. A. O. MCGREGOR, D. SIRAJUDDIN, AND E. G. GEOFFREY, *Multi-mode transmission lines*, (2021).

[21] C. W. MENDEL AND S. E. ROSENTHAL, *Modeling magnetically insulated devices using flow impedance*, Phys. Plasmas, 2 (1995), p. 1332.

[22] C. W. MENDEL AND S. E. ROSENTHAL, *Dynamic modeling of magnetically insulated transmission line systems*, Physics of Plasmas, 3 (1996), pp. 4207–4219.

[23] C. W. MENDEL, D. B. SEIDEL, AND S. E. ROSENTHAL, *A simple theory of magnetic insulation from basic physical considerations*, Laser and Particle Beams, 1 (1983), pp. 311–320.

[24] C. W. MENDEL JR. AND D. B. SEIDEL, *Flow impedance in a uniform magnetically insulated transmission line*, Physics of Plasmas, 6 (1999), pp. 4791–4793.

[25] C. E. MYERS, *Using scaled power flow experiments at 20 MA to establish the efficacy of load current delivery on a > 50 MA next-generation pulsed power facility*, in 2021 American Physical Society Division of Plasma Physics (APS-DPP), no. SAND2021-14005C, Pittsburgh, PA, USA, nov 2021.

[26] P. F. OTTINGER AND J. W. SCHUMER, *Magnetically insulated ion flow theory*, Physics of Plasmas, 13 (2006), p. 063101.

[27] P. F. OTTINGER, J. W. SCHUMER, D. D. HINSHELWOOD, AND R. J. ALLEN, *Generalized model of magnetically insulated transmission line flow*, IEEE Transactions on Plasma Science, 36 (2008), pp. 2708–2721.

[28] R. C. PATE, J. C. PATTERSON, M. C. DOWDICAN, J. J. RAMIREZ, D. E. HASTI, K. M. TOLK, J. W. POUKEY, L. X. SCHNEIDER, S. E. ROSENTHAL, AND T. W. L. SANFORD, *Self-magnetically insulated transmission line (MITL) system design for the 20-stage Hermes-III accelerator*, in Proc. 6th IEEE Int. Pulsed Power Conf., 1987, pp. 478–481.

[29] J. J. RAMIREZ ET AL., *The HERMES-III program*, in Proceedings of the 6th IEEE Pulsed Power Conference, Arlington, VA, USA, jun 1987, IEEE, pp. 294–297.

[30] D. E. RUIZ, P. F. SCHMIT, M. R. WEIS, K. J. PETERSON, AND M. K. MATZEN, *Exploring the parameter space of MagLIF implosions using similarity scaling. III. rise-time scaling*, Physics of Plasmas, 30 (2023), p. 032709.

[31] D. E. RUIZ, P. F. SCHMIT, D. A. YAGER-ELORRIAGA, M. R. GOMEZ, M. R. WEIS, C. A. JENNINGS, A. J. HARVEY-THOMPSON, P. F. KNAPP, S. A. SLUTZ, D. J. AMPLEFORD, K. BECKWITH, AND M. K. MATZEN, *Exploring the parameter space of MagLIF implosions using similarity scaling. II. current scaling*, Physics of Plasmas, 30 (2023), p. 032708.

[32] D. E. RUIZ, P. F. SCHMIT, D. A. YAGER-ELORRIAGA, C. A. JENNINGS, AND K. BECKWITH, *Exploring the parameter space of MagLIF implosions using similarity scaling. i. theoretical framework*, Physics of Plasmas, 30 (2023), p. 032707.

[33] R. SHAPOVALOV, *ZR MITL D-level geometry observations, dec-22-2022*, internal memo, (2022).

[34] R. V. SHAPOVALOV, R. B. SPIELMAN, AND S. A. SLUTZ, *Reduction of electron losses with voltage prepulse in magnetically insulated transmission lines*, Physics of Plasmas, 32 (2025), p. 092707.

[35] D. B. SINARS, M. A. SWEENEY, C. S. ALEXANDER, D. J. AMPLEFORD, T. AO, J. P. APRUZESE, C. ARAGON, D. J. ARMSTRONG, K. N. AUSTIN, T. J. AWE, A. D. BACZEWSKI, J. E. BAILEY, K. L. BAKER, C. R. BALL, H. T. BARCLAY, S. BEATTY, K. BECKWITH, K. S. BELL, J. F. BENAGE, N. L. BENNETT, K. BLAHA, D. E. BLISS, J. J. BOERNER, C. J. BOURDON, B. A. BRANCH, J. L. BROWN, E. M. CAMPBELL, R. B. CAMPBELL, D. G. CHACON, G. A. CHANDLER, K. CHANDLER, P. J. CHRISTENSON, M. D. CHRISTISON, E. B. CHRISTNER, R. C. CLAY, K. R. COCHRANE, A. P. COLOMBO, B. M. COOK, C. A. COVERDALE, M. E. CUNEO, J. S. CUSTER, A. DASGUPTA, J.-P. DAVIS, M. P. DESJARLAIS, I. D. DOLAN, J. D. DOUGLASS, G. S.

DUNHAM, S. DUWAL, A. D. EDENS, M. J. EDWARDS, E. G. EVSTATIEV, B. G. FARFAN, J. R. FEIN, E. S. FIELD, J. A. FISHER, T. M. FLANAGAN, D. G. FLICKER, M. D. FURNISH, B. R. GALLOWAY, P. D. GARD, T. A. GARDINER, M. GEISSEL, J. L. GIULIANI, M. E. GLINSKY, M. R. GOMEZ, T. GOMEZ, G. P. GRIM, K. D. HAHN, T. A. HAILL, N. D. HAMLIN, J. H. HAMMER, S. B. HANSEN, H. L. HANSHAW, E. C. HARDING, A. J. HARVEY-THOMPSON, D. HEADLEY, M. C. HERRMANN, M. H. HESS, C. HIGHSTRETE, O. A. HURRICANE, B. T. HUTSEL, C. A. JENNINGS, O. M. JOHNS, D. JOHNSON, M. D. JOHNSTON, B. M. JONES, M. C. JONES, P. A. JONES, P. E. KALITA, R. J. KAMM, J. W. KELLOGG, M. L. KIEFER, M. W. KIMMEL, P. F. KNAPP, M. D. KNUDSON, A. KREFT, G. R. LAITY, P. W. LAKE, D. C. LAMPPA, W. L. LANGSTON, J. S. LASH, K. R. LECHIEN, J. J. LECKBEE, R. J. LEEPER, G. T. LEIFESTE, R. W. LEMKE, W. LEWIS, S. A. LEWIS, G. P. LOISEL, Q. M. LOOKER, A. J. LOPEZ, D. J. LUCERO, S. A. MACLAREN, R. J. MAGYAR, M. A. MANGAN, M. R. MARTIN, T. R. MATTSSON, M. K. MATZEN, A. J. MAURER, M. G. MAZARAKIS, R. D. MCBRIDE, H. S. MCLEAN, C. A. MCCOY, G. R. MCKEE, J. L. MCKENNEY, A. R. MILES, J. A. MILLS, M. D. MITCHELL, N. W. MOORE, C. E. MYERS, T. NAGAYAMA, G. NATONI, A. C. OWEN, S. PATEL, K. J. PETERSON, T. D. POINTON, J. L. PORTER, A. J. PORWITZKY, S. RADOVICH, K. S. RAMAN, P. K. RAMBO, W. D. REINHART, G. K. ROBERTSON, G. A. ROCHAU, S. ROOT, D. V. ROSE, D. C. ROVANG, C. L. RUIZ, D. E. RUIZ, D. SANDOVAL, M. E. SAVAGE, M. E. SCEIFORD, M. A. SCHAEUBLE, P. F. SCHMIT, M. S. SCHOLLMEIER, J. SCHWARZ, C. T. SEAGLE, A. B. SEFKOW, D. B. SEIDEL, G. A. SHIPLEY, J. SHORES, L. SHULENBURGER, S. C. SIMPSON, S. A. SLUTZ, I. C. SMITH, C. S. SPEAS, P. E. SPECHT, M. J. SPEIR, D. C. SPENCER, P. T. SPRINGER, A. M. STEINER, B. S. STOLTZFUS, W. A. STYGAR, J. W. THORNHILL, J. A. TORRES, J. P. TOWNSEND, C. TYLER, R. A. VESEY, P. E. WAKELAND, T. J. WEBB, E. A. WEINBRECHT, M. R. WEIS, D. R. WELCH, J. L. WISE, M. WU, D. A. YAGER-ELORRIAGA, A. YU, AND E. P. YU, *Review of pulsed power-driven high energy density physics research on Z at Sandia*, Physics of Plasmas, 27 (2020), p. 070501.

[36] R. B. SPIELMAN, *Pulsed-power innovations needed for next-generation, high-current drivers*, in 2021 IEEE 23rd International Conference on Pulsed Power (PPC), September 2021, pp. 1–6.

[37] R. B. SPIELMAN AND Y. GRYAZIN, *Screamer v4.0 — a powerful circuit analysis code*, in 2015 IEEE Pulsed Power Conference (PPC), 2015, pp. 1–6.

[38] R. B. SPIELMAN, M. L. KIEFER, K. L. SHAW, K. W. STRUVE, AND M. M. WINDER, *Screamer manual*. `https://www.isu.edu/iac/research/screamer/`, 2020. [Accessed 18 09 2025].

[39] R. B. SPIELMAN AND D. B. REISMAN, *On the design of magnetically insulated transmission lines for z-pinch loads*, Matter and Radiation at Extremes, 4 (2019), p. 027402.

[40] B. S. STOLTZFUS, W. A. STYGAR, M. L. WISHER, D. B. REISMAN, J. J. LECKBEE, K. N. AUSTIN, G. C. BLEIER, E. W. BREDEN, R. J. FOCIA, D. L. HUBER, B. T. HUTSEL, D. M. JARAMILLO, O. JOHNS, D. J. LUCERO, G. R. MCKEE, T. D. MULVILLE, D. MURON, M. E. SAVAGE, M. E. SCEIFORD, AND C. TURNER, *Creating*

the foundation of next generation pulsed-power accelerator technology, SAND Report SAND2016-9670, Sandia National Laboratories, Albuquerque, NM, 2016.

[41] W. STYGAR, M. CUNEO, D. HEADLEY, H. IVES, R. LEEPER, M. MAZARAKIS, C. OLSON, J. PORTER, T. WAGONER, AND J. WOODWORTH, *Architecture of petawatt-class Z-pinch accelerators*, Physical Review Special Topics Accelerators and Beams, 10 (2007), p. 030401.

[42] W. A. STYGAR, T. J. AWE, J. E. BAILEY, N. L. BENNETT, E. W. BREDEN, E. M. CAMPBELL, R. E. CLARK, R. A. COOPER, M. E. CUNEO, J. B. ENNIS, D. L. FEHL, T. C. GENONI, M. R. GOMEZ, G. W. GREISER, F. R. GRUNER, M. C. HERRMANN, B. T. HUTSEL, C. A. JENNINGS, D. O. JOBE, B. M. JONES, M. C. JONES, P. A. JONES, P. F. KNAPP, J. S. LASH, K. R. LECHIEN, J. J. LECKBEE, R. J. LEEPER, S. A. LEWIS, F. W. LONG, D. J. LUCERO, E. A. MADRID, M. R. MARTIN, M. K. MATZEN, M. G. MAZARAKIS, R. D. MCBRIDE, G. R. MCKEE, C. L. MILLER, J. K. MOORE, C. B. MOSTROM, T. D. MULVILLE, K. J. PETERSON, J. L. PORTER, D. B. REISMAN, G. A. ROCHAU, G. E. ROCHAU, D. V. ROSE, D. C. ROVANG, M. E. SAVAGE, M. E. SCEIFORD, P. F. SCHMIT, R. F. SCHNEIDER, J. SCHWARZ, A. B. SEFKOW, D. B. SINARS, S. A. SLUTZ, R. B. SPIELMAN, B. S. STOLTZFUS, C. THOMA, R. A. VESEY, P. E. WAKELAND, D. R. WELCH, M. L. WISHER, AND J. R. WOODWORTH, *Conceptual designs of two petawatt-class pulsed-power accelerators for high-energy-density-physics experiments*, Phys. Rev. ST Accel. Beams, 18 (2015), p. 110401.

[43] W. A. STYGAR ET AL., *Flashover of a vacuum-insulator interface: A statistical model*, Physical Review Special Topics - Accelerators and Beams, 7 (2004), p. 070401. PRSTAB.

[44] ——, *Water-dielectric-breakdown relation for the design of large-area multimegavolt pulsed-power systems*, Physical Review Special Topics - Accelerators and Beams, 9 (2006), p. 070401. PRSTAB.

[45] ——, *Energy loss to conductors operated at lineal current densities <10 MA/cm: Semianalytic model, magnetohydrodynamic simulations, and experiment*, Phys. Rev. ST Accel. Beams, 11 (2008), p. 120401.

[46] W. A. STYGAR, T. C. WAGONER, H. C. IVES, P. A. CORCORAN, M. E. CUNEO, J. W. DOUGLAS, T. L. GILLILAND, M. G. MAZARAKIS, J. J. RAMIREZ, J. F. SEAMEN, D. B. SEIDEL, AND R. B. SPIELMAN, *Analytic model of a magnetically insulated transmission line with collisional flow electrons*, Physical Review Accelerators and Beams, 9 (2006), p. 090401.

[47] J. P. VANDEVENDER, *Gas-breakdown-inhibited, low-leakage current, magnetically insulated switches*, J. Appl. Phys., 50 (1979), p. 3928.

[48] J. P. VANDEVENDER ET AL., *Requirements for self-magnetically insulated transmission lines*, Phys. Rev. ST Accel. Beams, 18 (2015), p. 030401.

APPENDIX A. Converting Lumped Circuit Element Parameters to Distributed Transmission Line Parameters

The 1D circuit capability we use in Empire is actually a transmission line model; this requires *distributional* (per unit length) parameters $\{\ell_i, L_{\ell,i}, C_{\ell,i}\}$ where L_ℓ (H/m) and C_ℓ (F/m) are the inductance and capacitance per length ℓ_i for the *i*th segment of the circuit.

Circuit codes such as SCREAMER and Bertha have elements that use lumped (integrated over distance) parameters such as $\{\tau_i, Z_i\}$ where τ_i and Z_i is the length (in units of time) and impedance for the *i*th segment. The following relationships allow translating between one set of parameters and the other

$$\ell_i = v_i \tau_i \tag{A.1}$$

$$C_\ell = \frac{\tau}{Z_i \ell_i} \tag{A.2}$$

$$L_\ell = \frac{Z_i \tau_i}{\ell_i} \tag{A.3}$$

where *i* indexes a circuit segment.

APPENDIX B. Inductance calculations using Empire

Circuit models require lumped inductances to describe corresponding changes to power flow as a segmented 1D circuit. For regions in our designs having simple geometries (e.g., the "main MITL" regions of each level), analytic formulas for simle shapes (e.g., trapezoid) were used to directly calculate inductances for each segment of the main body. For nontrivial geometries, we employed two approaches. For the Z inner MITL and load regions, we use an analytic approach proposed by McBride et al. [18] valid for arbitrary shapes in axisymmetric configurations. For regions of the outer MITL having nontrivial geometries, we used Empire to calculate inductances L from from simulation output (simulated diagnostics for total magnetic energy in a volume and field line integrals). These were used for both the downstream transition segments (which generally have curved boundaries), and the vacuum flare regions (which are generally irregular).

B.1. Z inner MITL and load

The inner MITL and load regions is shown Figure B-1.

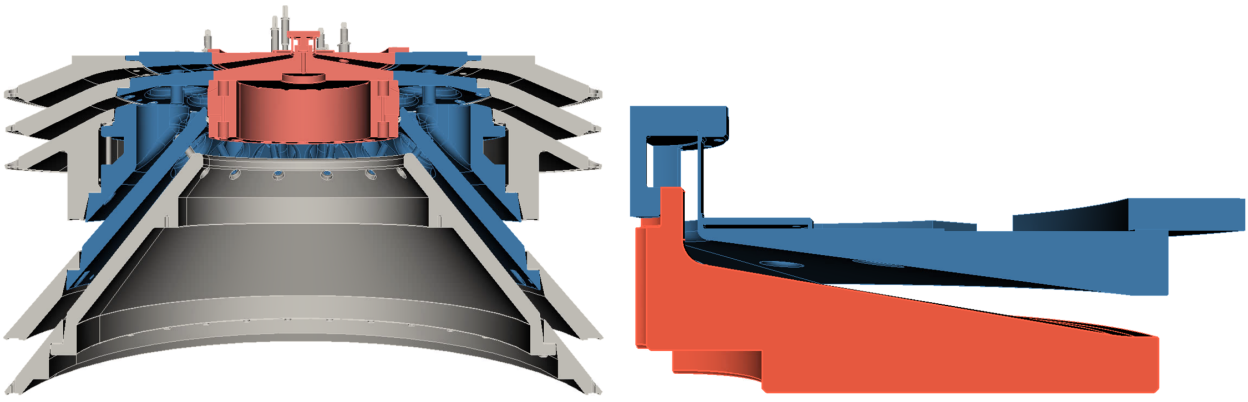

(a) (b)

Figure B-1. Clarifying inner MITL vs. upstream regions. A CAD rendering of the convolute hardware is shown in panel (a) which includes the post-hole convolute region (PHC, colored in steel blue) and the inner plates of the outer MITLs (top to bottom: A, B, C, and D). The inner MITL and load (panel (b); salmon colored) start downstream of the PHC which occupies regions at smaller radius. radius)

These regions of the SCREAMER model was ported from a legacy Bertha Z circuit model [14], and so had values pre-defined values for both the inner MITL and load segments. In our early simulations of the baseline system comparing Empire and SCREAMER, we realized this region in the circuit was a source of discrepancy that needed to be corrected. The reason is that, while

the baseline SCREAMER model did describe a 31-cm convolute (just as the Empire domain does), this circuit model was probably not the exact hardware set used in the Z shot series Empire was modeling (the "Powerfow 18a" shot series). Therefore, we checked the inductances in order to reconcile any differences.

The inductance of arbitrary axisymmetric profiles can be determined by the following calculation which was outlined in McBride et al. [18]:

$$L = \frac{\mu_0}{2\pi} \int_{z_{bot}}^{z_{top}} dz \ln \left[\frac{R_{upstream}(z)}{R_{downstream}(z)} \right] \tag{B.1}$$

We use Equation (B.1) to calculate lumped inductances of the "inner MITL" and "load" regions which, for specificity, are defined as the regions covered in Figure B-2(a,b), respectively.

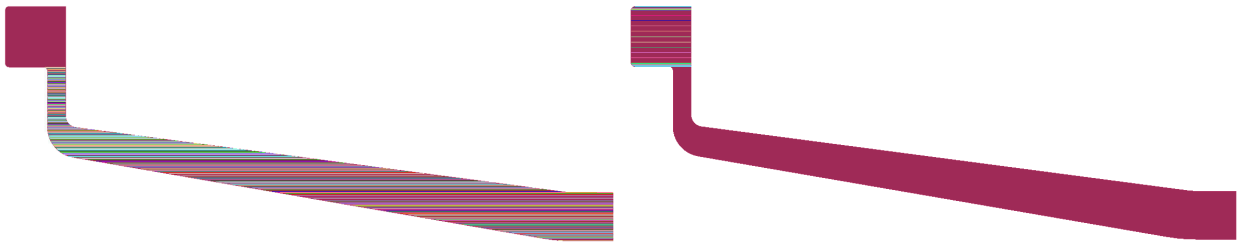

(a) inner MITL **(b)** load

Figure B-2. A 2D slice of the axisymmetric volume covering (a) inner MITL region and (b) load. Apre-pro scripting was used in a Cubit journal file to automatically draw any number of horizontal lines (providing local measurments for $R_{out} = R_{out}(z)$, $R_{in} = R_{in}(z)$) throughout the region. Contributions to the inductance integral (B.1) **were calculated in each loop of this procedure, and summed to produce the total inductance.**

The results are reported in Table B-1. Since these inductance values correspond to the same geometry that Empire models, we label this as "Empire" in the table, but note that the calculation as analytic as above.

Model	Inner MITL (nH)	Load (nH)	Total (nH)
Empire	3.27	2.92	20.96
SCREAMER	4.06	1.7	20.53

Table B-1. Inductances used in the inner MITL and load regions for each model.

Before we performed these inductance calculations as above, we explored adjusting the load inductance in SCREAMERto determine what value produced agreement with Empire, electromagnetic (lossless) simulations. The result of this excerise are reported in the same table (labeld as "SCREAMER"). While these values converged on could be more fine-tuned if desired, the total inductance of 20.53 nH compares very well with the calculation from the actual Empire geometry which was 20.96 nH and confirms the hypothesis for our original discrepancies, that inductances in the regions approaching the load were the cause. We could have decided to use the

Empire values for both regions in the SCREAMER model to make the correspondence truly one-to-one; however, the outcome of this load inductance calibration in SCREAMER produced such good agreement that it was decided there was no reason to revise the model parameters further in this region and that redistributing virtually the same total inductance sligthly differnet will not lead to consequential differences in the simulations.

B.2. Z vacuum flare for each level

2D profiles for each vacuum flare (VF) geometry were partitioned into 4 (at most 5) segments (Figure B-3). The inductances were calculated using Empire by setting up a simulation which drives the corresponding 3D electromagnetic domain (the volume generated by sweeping this 2D profile through an angle $\Delta\phi$) with a source voltage which smoothly ramps up rapidly (≈ 0.1 ns) to steady state. Empire diagnostic output was written for the `total_magnetic_energy` in the volume ($U_B = \int dV \frac{B^2}{2\mu_0}$) and a line integral diagnostic for the magnetic field at the anode (`BDL` $= \int_a \mathbf{B} \cdot d\boldsymbol{\ell}$) which is a proxy for the anode current[1] $I_a = \frac{1}{\mu_0}$`BDL` $\cdot \frac{\Delta\phi}{360^\circ}$. Periodic field conditions were used, and the simulation duration was ensured to be 10 times the transit time of EM waves through the domain, using time steps satisfying the speed-of-light $CFL < 1$ (a value of $CFL = 0.7$ was chosen).

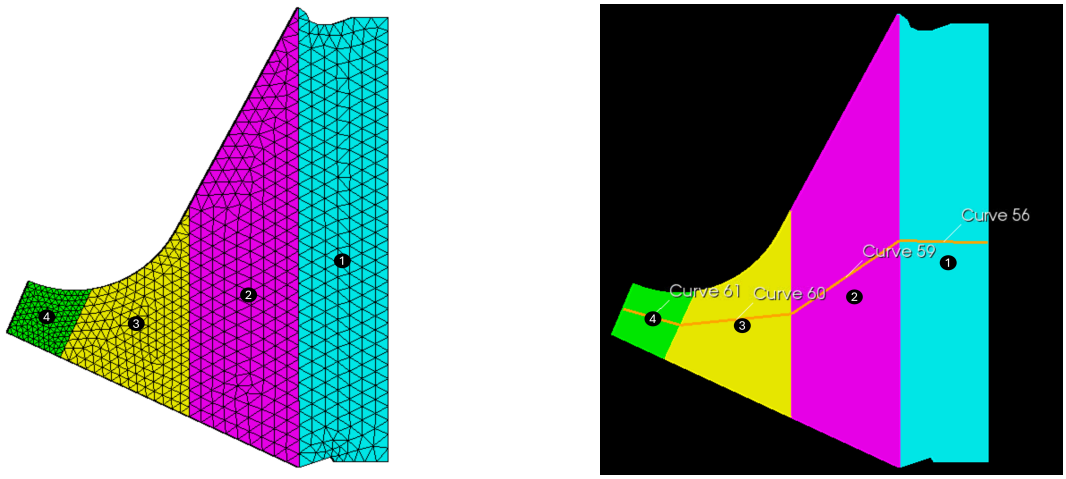

(a) **(b)**

Figure B-3. (*Example*: level A) vacuum flare segmentation for circuit modeling. Panel (a) shows the main segmentation and simulation mesh; panel (b) shows how transit time was measured (shown as gold lines drawn between midpoints of each segment boundary) which was done in the geometry/meshing creation software CUBIT. Note that each segment is simulated separately.

Note that we confirmed that summing segment inductances was consistent with the Empire result for the non-segmented volume. Thus, the decision to segment the volume is not for Empire 's

[1] i.e., from Ampere's law in integral form `BDL` $\equiv \oint \mathbf{B} \cdot d\boldsymbol{\ell} = \int_\Omega \mu_0 \mathbf{J}_a \cdot d\mathbf{A} = \mu_0 I_{a\in\Omega}$. When the simulated domain Ω is wedge-periodic having angular extent $\Delta\phi$, we calculate the total current by scaling by the n-fold symmetry factor $360^\circ/\Delta\phi$. Finally, the accuracy of this calculation is increased by designing the simulation for this calculation to reach steady state ($\partial_t \to 0$) causing the displacement field term in Ampere's law to become negligible ($\partial_t D \to 0$).

sake, it is purely to enable a higher "resolution" description from the 1D circuit perspective. The calculated inductances the value obtained at late time (steady state, see Figure B-4

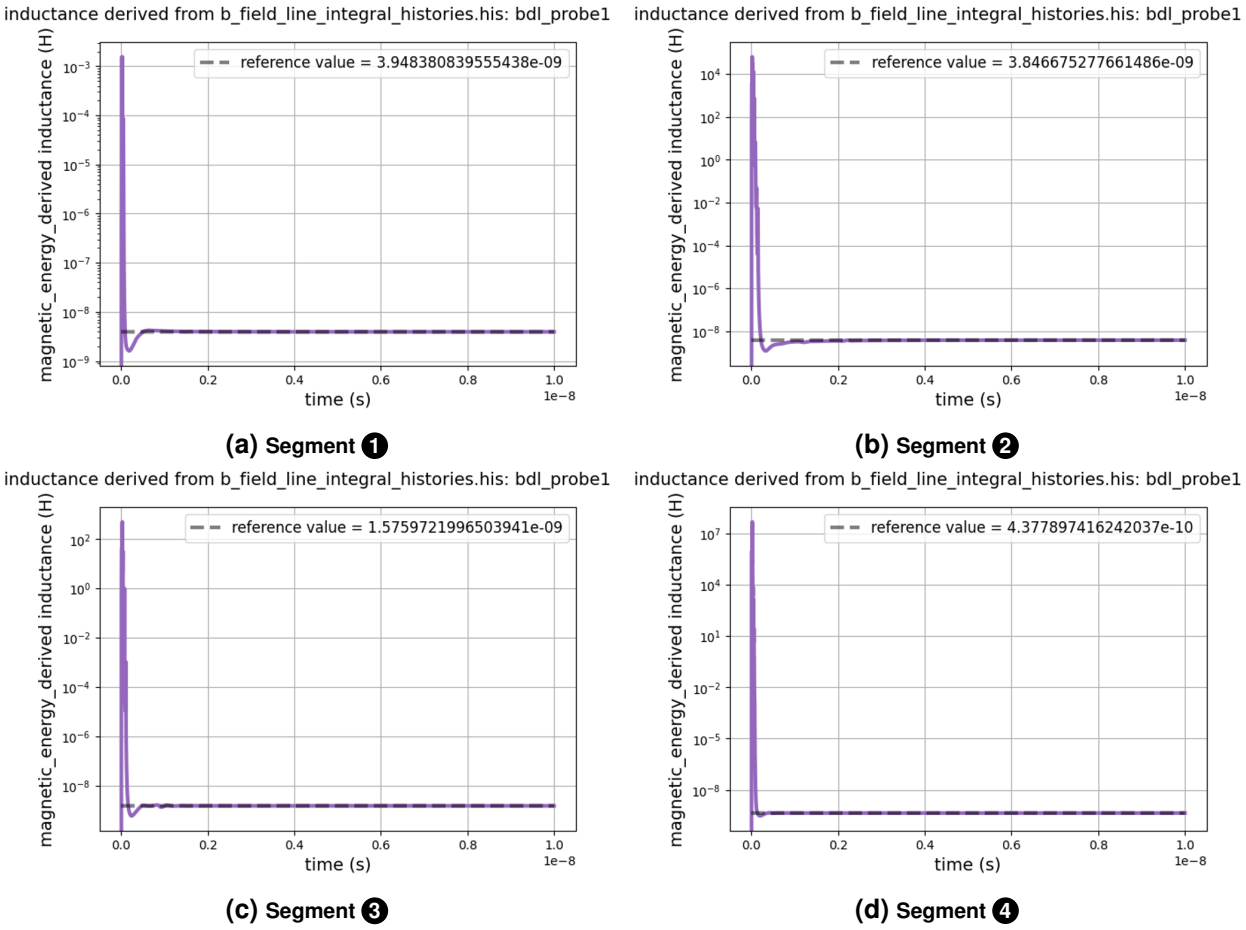

Figure B-4. (*Example*: level A) inductance vs. time plots for each segment of the VF (Figure B-3). The simulation is driven to steady state and the "final inductance" we use is the mean value over the last 10 time steps (typically 3000 time steps in total for a simulation). This value is reported in the legend as "reference value."

B.3. Z vacuum flare for each level

APPENDIX C. Decoupling Z MITLs into individual level domains

C.1. Approach

Accelerators like Z and NGPP combine several individual lines in the convolute (current adder) region just upstream of the single "inner MITL" which deliveres the combined current to a target (load). The presence of this combination region means the system is fundamentally a 3D problem (with periodicity restricted by the 12-point rotational symmetry of the post-hole hardware, i.e., 30°).

Characterizing operating performance of various designs for the outer MITLs using EM-PIC requires modeling the entire vacuum domain to track all these details. Modeling this 3D region for all levels (0.06 cm $\lesssim R \lesssim$ 150 cm, $0 \leq \phi \leq n \cdot 30°$, $n \in \mathbb{N}$) requires meshes having at least 500M elements at minimum[1]. In this team's experience, PIC simulations of power flow in MITLs modeling emission from electrode plasma, but not their expansion, require simulations at coarsest: $\Delta x \lesssim 300\mu$m cells near the emitting surfaces to resolve (or at least ballpark) the correct magnetic insulation layer thickness in AK gaps spanning 1 cm to 10 cm, 10^{-13} second time steps to resolve $\min(\omega_{pe}, \Delta t_{speed-of-light\,CFL}, \Delta t_{particle\,CFL})$[2]

For our performance-portable, massively-parallel particle-in-cell code, this would require 50k compute-cores ($\sim$ 10k mesh elements per core) and 24 wall-hours to complete a single simulation. This utilization is > 70% of the total compute-nodes available on any of the unclassified high performance computing (HPC) clusters available at Sandia Nationa Laboratories. The problem size might be argued as feasible from an individual standpoint, but HPCs are a shared resource for the entire lab and so does not represent a reasonable job size to submit to the laboratories' supercomputers. Furthermore, we would potentially need to run several simuations to vet candidate variable-impedance designs. A smaller size problem is needed.

This issue of problem size was solved in the following way. Noting that it is the convolute that couples individual MITL levels togeher, circuit simulations were used extensibly to calculate an equivalent lumped inductance (convolute+load) $L = \int V(t)dt/I$ seen by each level individually. This results in the following table

[1] this is using judicious meshing decisions and exploiting advantages afforded by our unstructured (simplex) meshes which allow non-uniform cell sizes to mesh the domain.

[2] ω_{pe} being the electron plasma frequency, $\Delta t_{particle\,CFL} = \{\Delta t : c\Delta t/\Delta x < 1\}$ is the time step restriction satisfying the Courant–Friedrichs–Lewy ("CFL") condition for electromagnetic waves (speed of light), and $\Delta t_{speed-of-light\,CFL} = \{\Delta t : v_{max}\Delta t/\Delta x < 1\}$ is the time step restriction satisfying the CFL condition for the velocity spread in the macroparticle population. Both of these numbers can be interpreted as the dimensionless unit corresponding to number of cells the corresponding entity (EM wave or particle) is transported in a time step. Explicit codes require resolving these conditions to maintain numerical stability.

The last column of the table gives an option to model an approximation to an imploding load in Empire using existing capabilities. Namely, a constant L-dot resistance ($R_{\dot{L}}$) value was chosen produces good agreement with the rise to and peak value of the load current according to the circuit model. This presents an option to extend the impact of the Empire results for Z presneted in this reporting to a more realistic load (time did not allow for this path to be seen through to its end, our partially complete portfolio of results covering this imploding load approimation not included here (at least for Empire). This work studied the short circuit load (referred to as a "static load" in this document since $\dot{L} = 0$), which corresponds to the smae load circuit but with $R_{\dot{L}} = 0$.

An analogous modeling approach is used for the even larger domains describing the NGPP system.

C.2. *Example*: cross-code verification of decoupled level A model (Empire vs. Bertha)

The decoupled problem for level A using the geometry for Z today (i.e., not strictly constant impedance) was set up in both Bertha and Empire . The results are shown in Figure C-1

A significant cost-savings afforded by this model is that by lumping the convolute into a 1D transmission line model, the remainder of the 3D domain is in a purely axisymmetric region of the machine. In principal, this allows us to choose the angular extent of our domain freely rather than at strict multiples $n \cdot 30^\circ$ ($n \in \mathbb{N}$) to satisfy the machine periodicty (or $n \cdot 15^\circ$ for an approximation to periodicity which is mirror symmetry). Evidence supporting this modeling freedom is shown in Figure C-2 which shows identical load current predictions for the case of a 15° vs. 2.5° domain which is an angle 6 times smaller.

We take advantage of this modeling freedom in both Z and the NGPP systems simulated, using 2.5° and as skinny as 0.5° degree "wedge" domains, respectively, without loss of fidelity.

Level	Convolute+Load Inductance (nH)	Load "L-dot" Resistance (Ω)
A	26.70	0.08
B	28.38	0.08
C	44.26	0.08
D	45.65	0.08

Table C-1. (Individual load circuits for each level of Z) Bertha was used to calculate the total inductance (second column) actualy "seen" by each level individual. For the case of an imploding load, a constant L-dot resistance ($R_{\dot{L}}$) value is chosen that approximated the rise to and peak value of the load current according to the circuit model. For a short circuit load (referred to as a "static load" in this document since $\dot{L} = 0$), the load circuit is the same except ith $R_{\dot{L}} = 0$

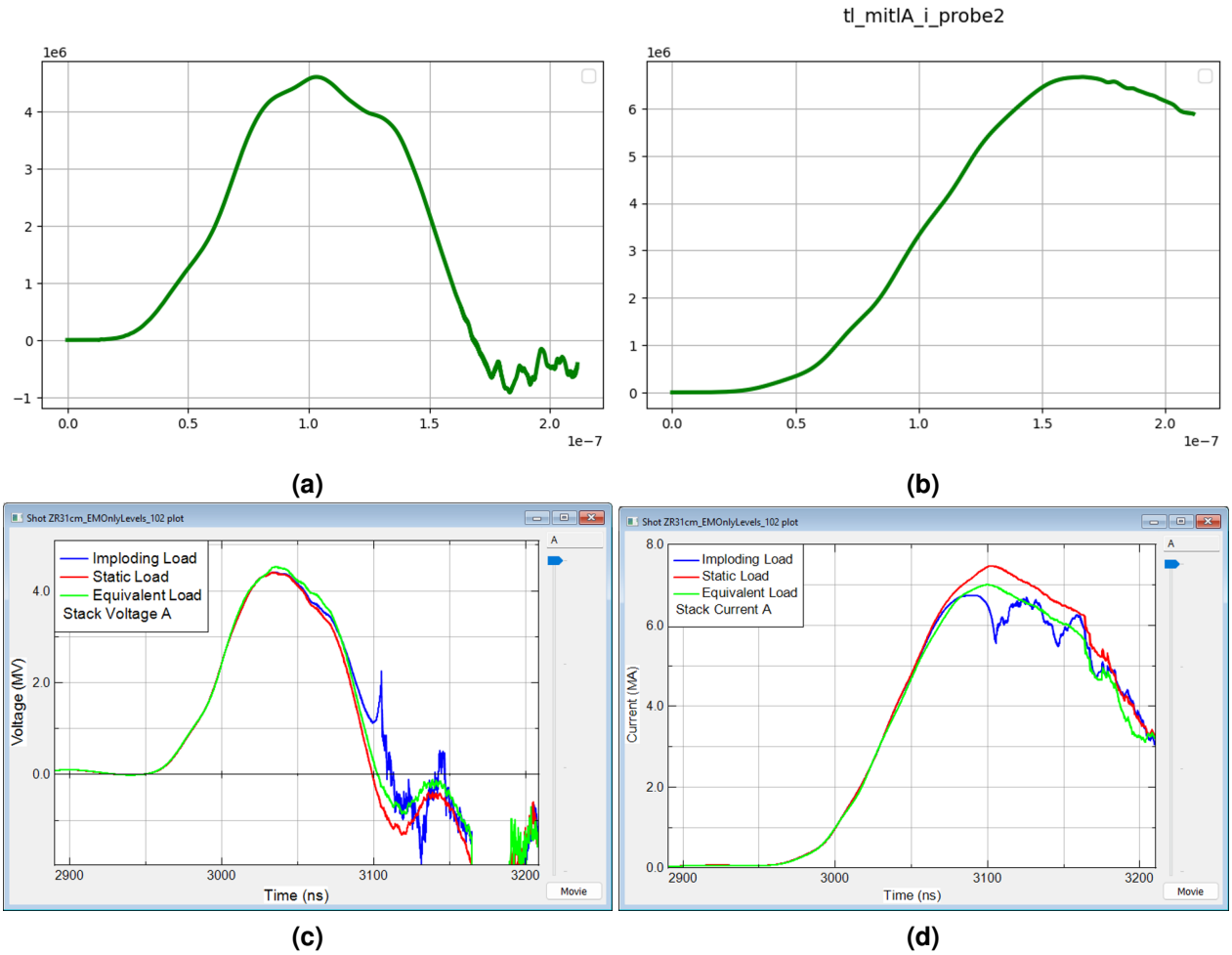

Figure C-1. (*Z today* subproblem A: Bertha vs Empire) Results from simulating a 3D EM model in Empire (top row) is compared to the equivalent Bertha model ("simplified model" in the legend; bottom row). The results show good agreement which indicates the model has been consistetnly set up in Empire. With this benchmark, we are positioned to proceed with setting up models of interest (Constant baseline version and variable-impedance versions) for our design study. Note: the comparison is Bertha , this is not a mistype. The model was subsequently ported to SCREAMER which was used as the circuit simulation code for the remainder of the Z studies (constant baseline and all variable impedance cases). This comparison is shown using the "L-dot" load (compare green curves on top row plots with green curves on bottom row plots); the agreement also holds for the static load case.

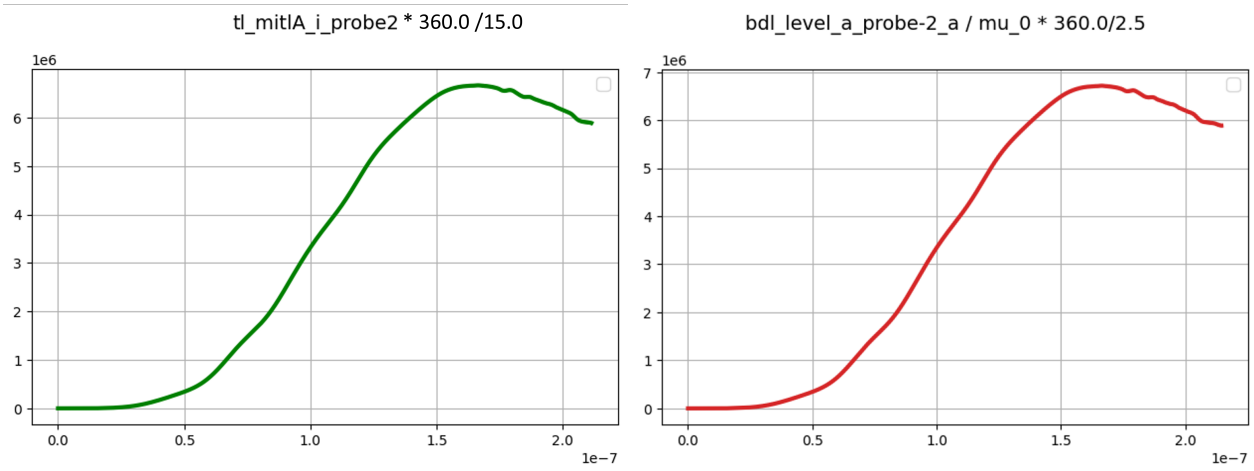

(a) **(b)**

Figure C-2. (simulated level A load current: $15°$ vs. $2.5°$ wedge domains) Empire results from a 3D EM simulation using a $15°$ (panel (a)) or a $2.5°$ (panel (b)) wedge domain are indistinguishable. This indicates that significant computational expense can be saved by reducing the wedge domain angle. This comparison is shown using the "L-dot" load; the agreement also holds for the static load case.

C.3. *Example*: cross-code verification of decoupled level D model (Empire vs. Bertha)

The decoupled problem for level D using the geometry for Z today (i.e., not strictly constant impedance) was set up in both Bertha and Empire . The results are shown in Figure C-3

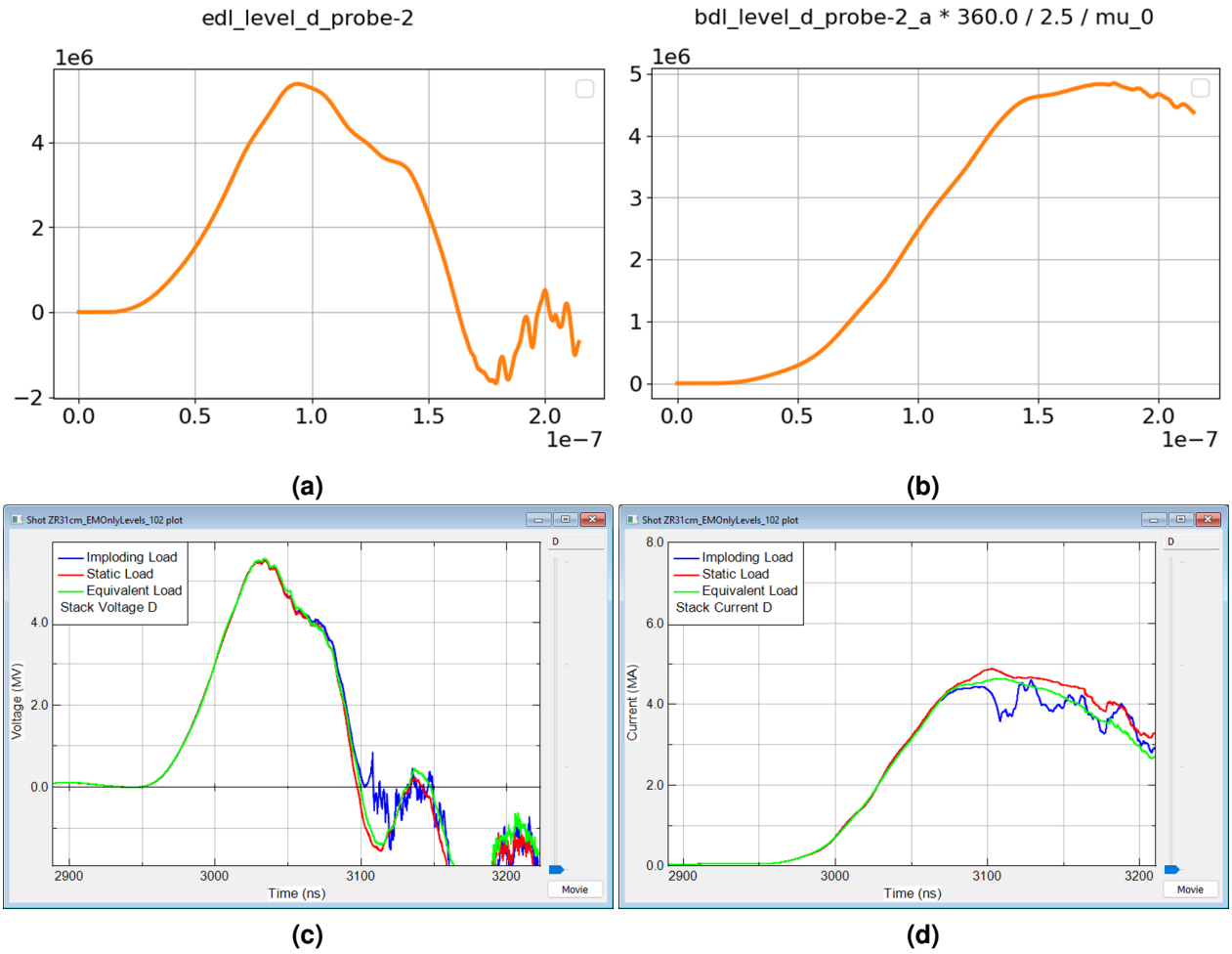

Figure C-3. (*Z today subproblem D*: Bertha vs Empire) Results from simulating a 3D EM model in Empire (top row) is compared to the equivalent Bertha model ("simplified model" in the legend; bottom row). The results show good agreement which indicates the m odel has been consistetnly set up in Empire . With this benchmark, we are positioned to proceed with setting up models of interest (Constant baseline version and variable-impedance versions) for our design study. Note: the comparison is Bertha , this is not a mistype. The model was subsequently ported to SCREAMER which was used as the circuit simulation code for the remainder of the Z studies (constant baseline and all variable impedance cases). This comparison is shown using the static load (compare orange curves on top row plots with red curves on bottom row plots); the agreement also holds for the "L-dot" load case.

APPENDIX D. SCREAMER Circuit Model Details Summaries

D.1. Constant-Impedance MITLs

D.1.1. *input file stub*: Constant-Impedance (Baseline) All-Levels Z Model

```
Z Variable LDRD  --  ALL LEVELS
! R. V. Shapovalov 02-Sep-2025 16:03:53
! This deck was created with MATLAB using the following inputs:
!!  Work folder = /Users/rsha/Documents/Work/LDRD-Power-Flow/ZRMITL-Variable-v60
!!  Sim. folder = Shots_all_levels/
!!  Matlab file = deck_all_levels.m
!!  top_branch = D-level
!!  vdrive = Empire
!!  fl_convolute = large
!!  fl_inner_MITL = large
!!  fl_load = SHORT30
!!  R_vsource = 0.712
!!  zflow = 0.800

!!  Level A MITL
!!  fl_MITLA_type = BASE
!!  fl_MITLA_za = ZA2280
!!  fl_MITLA_emiss = ONN

!!  Level B MITL
!!  fl_MITLB_type = BASE
!!  fl_MITLB_za = ZA2370
!!  fl_MITLB_emiss = ONN

!!  Level C MITL
!!  fl_MITLC_type = BASE
!!  fl_MITLC_za = ZA3268
!!  fl_MITLC_emiss = ONN

!!  Level D MITL
!!  fl_MITLD_type = BASE
!!  fl_MITLD_za = ZA3305
!!  fl_MITLD_emiss = ONN

!! Write main MITL boundaries for later read-in
!!      Keyword   N-segm        angle        Ra-cm        Rb-cm        ga-cm        gb-cm  res-fac turn-kV/cm
!!  MITLA-bound       40   23.8784103   128.748700    24.604800     4.895837     0.935630       10        200
!!  MITLB-bound       40   27.0302828   120.905700    23.921600     4.779081     0.945557       10        200
!!  MITLC-bound       49   47.8832194   122.259300    23.907300     6.663666     1.303052       10        200
!!  MITLD-bound       57   50.6591000   122.161200    15.538700     6.733704     0.860196       10        200

!! Write MITL single point entry for later read-in
!!      Keyword   N-segm         angle         R-cm         g-cm    length-cm  res-fac turn-kV/cm
!!  MITLA-pnt01       41   21.4832799    23.514200     0.974700     2.344040       10        200
!!  MITLA-pnt02       42   10.4834698    20.966200     1.216500     2.964330       10        200
!!  MITLB-pnt01       41   21.4832799    22.574436     1.186645     2.812600       10        200
!!  MITLB-pnt02       42   21.4832799    20.154680     1.316045     2.205080       10        200
!!  MITLC-pnt01       50   47.8832194    23.054200     1.287978     2.580200       10        200
!!  MITLC-pnt02       51   47.8832194    21.348200     1.269614     2.580250       10        200
!!  MITLC-pnt03       52   47.8832194    19.639900     1.240908     2.588040       10        200


TIME-STEP              9.1E-13
RESOLUTION-TIME        1.0E-10
END-TIME               5.0E-07
NUMBER-PRINTS                1
EXECUTE-CYCLES             ALL
ECHO                        NO
MAX-POINTS                2000

! ================================================================
!                 D   L E V E L   B L O C K S   S T A R T S   H E R E
! ================================================================
!
BRANCH

***** The full deck (8,031 lines) for the baseline all-levels Z model  *****
```

D.1.2. Individual Level MITL segment geometries

```
.....printing MITL geometry summary table, A-level (SHORT30_BASE_ONN.txt)

!  We divide the MITL space between Ra and Rb into 40 segments of equal length
!  and use segment middle point to calculate MITL block geometry.
!
!  Middle line outer boundaries (segm. 1 - 40) are:
!  Ra = 128.7487 cm, gapa = 4.8958 cm, Za = 2.2800 Ohms
!  Rb = 24.6048 cm, gapb = 0.9356 cm, Zb = 2.2800 Ohms
!
!  Middle line length (segm. 1 - 40) is 113.8923 cm (3.7990 ns)
!  Segment length is 2.8473 cm (0.0950 ns)
!  Middle line angle is 23.8784103 degrees
!
!  Total L (segm. 1 - 40) = sum of Zt = 8.6618 nH
!
!-------------------------------------------------------------------------------------------------------------
! Segm  midpoint-cm  circum-cm  area-cm2   gap-cm  height-cm  length-cm  length-ns  Zvac-Ohms  resol-ns  Eon-kV/cm
!-------------------------------------------------------------------------------------------------------------
!    1     127.447     800.77   2280.05    4.846      5.300      2.847      0.095     2.2800     0.0095     200
!    2     124.843     784.41   2233.47    4.747      5.192      2.847      0.095     2.2800     0.0095     200
!    3     122.240     768.05   2186.89    4.648      5.083      2.847      0.095     2.2800     0.0095     200
!    4     119.636     751.70   2140.31    4.549      4.975      2.847      0.095     2.2800     0.0095     200
!    5     117.033     735.34   2093.73    4.450      4.867      2.847      0.095     2.2800     0.0095     200
!    6     114.429     718.98   2047.15    4.351      4.759      2.847      0.095     2.2800     0.0095     200
!    7     111.825     702.62   2000.57    4.252      4.650      2.847      0.095     2.2800     0.0095     200
!    8     109.222     686.26   1953.99    4.153      4.542      2.847      0.095     2.2800     0.0095     200
!    9     106.618     669.90   1907.42    4.054      4.434      2.847      0.095     2.2800     0.0095     200
!   10     104.015     653.54   1860.84    3.955      4.326      2.847      0.095     2.2800     0.0095     200
!   11     101.411     637.18   1814.26    3.856      4.217      2.847      0.095     2.2800     0.0095     200
!   12      98.807     620.82   1767.68    3.757      4.109      2.847      0.095     2.2800     0.0095     200
!   13      96.204     604.47   1721.10    3.658      4.001      2.847      0.095     2.2800     0.0095     200
!   14      93.600     588.11   1674.52    3.559      3.892      2.847      0.095     2.2800     0.0095     200
!   15      90.997     571.75   1627.94    3.460      3.784      2.847      0.095     2.2800     0.0095     200
!   16      88.393     555.39   1581.36    3.361      3.676      2.847      0.095     2.2800     0.0095     200
!   17      85.789     539.03   1534.79    3.262      3.568      2.847      0.095     2.2800     0.0095     200
!   18      83.186     522.67   1488.21    3.163      3.459      2.847      0.095     2.2800     0.0095     200
!   19      80.582     506.31   1441.63    3.064      3.351      2.847      0.095     2.2800     0.0095     200
!   20      77.979     489.95   1395.05    2.965      3.243      2.847      0.095     2.2800     0.0095     200
!   21      75.375     473.59   1348.47    2.866      3.135      2.847      0.095     2.2800     0.0095     200
!   22      72.771     457.24   1301.89    2.767      3.026      2.847      0.095     2.2800     0.0095     200
!   23      70.168     440.88   1255.31    2.668      2.918      2.847      0.095     2.2800     0.0095     200
!   24      67.564     424.52   1208.73    2.569      2.810      2.847      0.095     2.2800     0.0095     200
!   25      64.961     408.16   1162.16    2.470      2.701      2.847      0.095     2.2800     0.0095     200
!   26      62.357     391.80   1115.58    2.371      2.593      2.847      0.095     2.2800     0.0095     200
!   27      59.753     375.44   1069.00    2.272      2.485      2.847      0.095     2.2800     0.0095     200
!   28      57.150     359.08   1022.42    2.173      2.377      2.847      0.095     2.2800     0.0095     200
!   29      54.546     342.72    975.84    2.074      2.268      2.847      0.095     2.2800     0.0095     200
!   30      51.943     326.36    929.26    1.975      2.160      2.847      0.095     2.2800     0.0095     200
!   31      49.339     310.01    882.68    1.876      2.052      2.847      0.095     2.2800     0.0095     200
!   32      46.735     293.65    836.10    1.777      1.944      2.847      0.095     2.2800     0.0095     200
!   33      44.132     277.29    789.52    1.678      1.835      2.847      0.095     2.2800     0.0095     200
!   34      41.528     260.93    742.95    1.579      1.727      2.847      0.095     2.2800     0.0095     200
!   35      38.925     244.57    696.37    1.480      1.619      2.847      0.095     2.2800     0.0095     200
!   36      36.321     228.21    649.79    1.381      1.510      2.847      0.095     2.2800     0.0095     200
!   37      33.717     211.85    603.21    1.282      1.402      2.847      0.095     2.2800     0.0095     200
!   38      31.114     195.49    556.63    1.183      1.294      2.847      0.095     2.2800     0.0095     200
!   39      28.510     179.13    510.05    1.084      1.186      2.847      0.095     2.2800     0.0095     200
!   40      25.907     162.78    463.47    0.985      1.077      2.847      0.095     2.2800     0.0095     200
!   41      23.514     147.74    346.32    0.975      1.047      2.344      0.078     2.4854     0.0078     200
!   42      20.966     131.73    390.50    1.216      1.237      2.964      0.099     3.4789     0.0099     200
!-------------------------------------------------------------------------------------------------------------
*** In MITL A: segments 41, 42 (above) are downstream transition segments required for the MITL to mate with the
convolute hardware. These are unchanged in all designs.


.....printing MITL geometry summary table, B-level (SHORT30_BASE_ONN.txt)

!  We divide the MITL space between Ra and Rb into 40 segments of equal length
!  and use segment middle point to calculate MITL block geometry.
!
!  Middle line outer boundaries (segm. 1 - 40) are:
!  Ra = 120.9057 cm, gapa = 4.7791 cm, Za = 2.3700 Ohms
!  Rb = 23.9216 cm, gapb = 0.9456 cm, Zb = 2.3700 Ohms
!
!  Middle line length (segm. 1 - 40) is 108.8771 cm (3.6318 ns)
!  Segment length is 2.7219 cm (0.0908 ns)
!  Middle line angle is 27.0302828 degrees
!
!  Total L (segm. 1 - 40) = sum of Zt = 8.6073 nH
!
!-------------------------------------------------------------------------------------------------------------
! Segm  midpoint-cm  circum-cm  area-cm2   gap-cm  height-cm  length-cm  length-ns  Zvac-Ohms  resol-ns  Eon-kV/cm
!-------------------------------------------------------------------------------------------------------------
!    1     119.693     752.06   2047.04    4.731      5.311      2.722      0.091     2.3700     0.0091     200
!    2     117.269     736.82   2005.58    4.635      5.204      2.722      0.091     2.3700     0.0091     200
!    3     114.844     721.59   1964.11    4.539      5.096      2.722      0.091     2.3700     0.0091     200
!    4     112.420     706.35   1922.64    4.444      4.989      2.722      0.091     2.3700     0.0091     200
!    5     109.995     691.12   1881.18    4.348      4.881      2.722      0.091     2.3700     0.0091     200
```

```
!    6     107.570     675.88   1839.71    4.252      4.773      2.722      0.091    2.3700     0.0091     200
!    7     105.146     660.65   1798.24    4.156      4.666      2.722      0.091    2.3700     0.0091     200
!    8     102.721     645.42   1756.78    4.060      4.558      2.722      0.091    2.3700     0.0091     200
!    9     100.297     630.18   1715.31    3.964      4.451      2.722      0.091    2.3700     0.0091     200
!   10      97.872     614.95   1673.84    3.869      4.343      2.722      0.091    2.3700     0.0091     200
!   11      95.447     599.71   1632.38    3.773      4.235      2.722      0.091    2.3700     0.0091     200
!   12      93.023     584.48   1590.91    3.677      4.128      2.722      0.091    2.3700     0.0091     200
!   13      90.598     569.25   1549.44    3.581      4.020      2.722      0.091    2.3700     0.0091     200
!   14      88.174     554.01   1507.98    3.485      3.913      2.722      0.091    2.3700     0.0091     200
!   15      85.749     538.78   1466.51    3.389      3.805      2.722      0.091    2.3700     0.0091     200
!   16      83.324     523.54   1425.04    3.294      3.697      2.722      0.091    2.3700     0.0091     200
!   17      80.900     508.31   1383.58    3.198      3.590      2.722      0.091    2.3700     0.0091     200
!   18      78.475     493.07   1342.11    3.102      3.482      2.722      0.091    2.3700     0.0091     200
!   19      76.051     477.84   1300.65    3.006      3.375      2.722      0.091    2.3700     0.0091     200
!   20      73.626     462.61   1259.18    2.910      3.267      2.722      0.091    2.3700     0.0091     200
!   21      71.201     447.37   1217.71    2.814      3.160      2.722      0.091    2.3700     0.0091     200
!   22      68.777     432.14   1176.25    2.719      3.052      2.722      0.091    2.3700     0.0091     200
!   23      66.352     416.90   1134.78    2.623      2.944      2.722      0.091    2.3700     0.0091     200
!   24      63.928     401.67   1093.31    2.527      2.837      2.722      0.091    2.3700     0.0091     200
!   25      61.503     386.43   1051.85    2.431      2.729      2.722      0.091    2.3700     0.0091     200
!   26      59.078     371.20   1010.38    2.335      2.622      2.722      0.091    2.3700     0.0091     200
!   27      56.654     355.97    968.91    2.239      2.514      2.722      0.091    2.3700     0.0091     200
!   28      54.229     340.73    927.45    2.144      2.406      2.722      0.091    2.3700     0.0091     200
!   29      51.805     325.50    885.98    2.048      2.299      2.722      0.091    2.3700     0.0091     200
!   30      49.380     310.26    844.51    1.952      2.191      2.722      0.091    2.3700     0.0091     200
!   31      46.955     295.03    803.05    1.856      2.084      2.722      0.091    2.3700     0.0091     200
!   32      44.531     279.79    761.58    1.760      1.976      2.722      0.091    2.3700     0.0091     200
!   33      42.106     264.56    720.11    1.664      1.868      2.722      0.091    2.3700     0.0091     200
!   34      39.682     249.33    678.65    1.569      1.761      2.722      0.091    2.3700     0.0091     200
!   35      37.257     234.09    637.18    1.473      1.653      2.722      0.091    2.3700     0.0091     200
!   36      34.832     218.86    595.72    1.377      1.546      2.722      0.091    2.3700     0.0091     200
!   37      32.408     203.62    554.25    1.281      1.438      2.722      0.091    2.3700     0.0091     200
!   38      29.983     188.39    512.78    1.185      1.330      2.722      0.091    2.3700     0.0091     200
!   39      27.559     173.16    471.32    1.089      1.223      2.722      0.091    2.3700     0.0091     200
!   40      25.134     157.92    429.85    0.993      1.115      2.722      0.091    2.3700     0.0091     200
!   41      22.574     141.84    398.94    1.187      1.275      2.813      0.094    3.1518     0.0094     200
!   42      20.155     126.64    279.24    1.316      1.414      2.205      0.074    3.9151     0.0074     200
!-------------------------------------------------------------------------------------------------------------
*** In MITL B: segments 41, 42 (above) are downstream transition segments required for the MITL to mate with the
convolute hardware. These are unchanged in all designs.


.....printing MITL geometry summary table, C-level (SHORT30_BASE_ONN.txt)

!  We divide the MITL space between Ra and Rb into 49 segments of equal length
!  and use segment middle point to calculate MITL block geometry.
!
!  Middle line outer boundaries (segm. 1 - 49) are:
!  Ra = 122.2593 cm, gapa = 6.6637 cm, Za = 3.2680 Ohms
!  Rb = 23.9073 cm, gapb = 1.3031 cm, Zb = 3.2680 Ohms
!
!  Middle line length (segm. 1 - 49) is 146.6531 cm (4.8918 ns)
!  Segment length is 2.9929 cm (0.0998 ns)
!  Middle line angle is 47.8832194 degrees
!
!  Total L (segm. 1 - 49) = sum of Zt = 15.9865 nH
!
!-------------------------------------------------------------------------------------------------------------
! Segm  midpoint-cm  circum-cm  area-cm2   gap-cm  height-cm  length-cm  length-ns  Zvac-Ohms  resol-ns  Eon-kV/cm
!-------------------------------------------------------------------------------------------------------------
!    1     121.256     761.87   2280.22    6.609      9.855      2.993      0.100    3.2680     0.0100     200
!    2     119.249     749.26   2242.48    6.500      9.692      2.993      0.100    3.2680     0.0100     200
!    3     117.241     736.65   2204.73    6.390      9.528      2.993      0.100    3.2680     0.0100     200
!    4     115.234     724.04   2166.99    6.281      9.365      2.993      0.100    3.2680     0.0100     200
!    5     113.227     711.43   2129.24    6.171      9.202      2.993      0.100    3.2680     0.0100     200
!    6     111.220     698.81   2091.50    6.062      9.039      2.993      0.100    3.2680     0.0100     200
!    7     109.213     686.20   2053.75    5.953      8.876      2.993      0.100    3.2680     0.0100     200
!    8     107.205     673.59   2016.01    5.843      8.713      2.993      0.100    3.2680     0.0100     200
!    9     105.198     660.98   1978.26    5.734      8.550      2.993      0.100    3.2680     0.0100     200
!   10     103.191     648.37   1940.52    5.624      8.387      2.993      0.100    3.2680     0.0100     200
!   11     101.184     635.76   1902.77    5.515      8.223      2.993      0.100    3.2680     0.0100     200
!   12      99.177     623.15   1865.02    5.406      8.060      2.993      0.100    3.2680     0.0100     200
!   13      97.170     610.53   1827.28    5.296      7.897      2.993      0.100    3.2680     0.0100     200
!   14      95.162     597.92   1789.53    5.187      7.734      2.993      0.100    3.2680     0.0100     200
!   15      93.155     585.31   1751.79    5.077      7.571      2.993      0.100    3.2680     0.0100     200
!   16      91.148     572.70   1714.04    4.968      7.408      2.993      0.100    3.2680     0.0100     200
!   17      89.141     560.09   1676.30    4.859      7.245      2.993      0.100    3.2680     0.0100     200
!   18      87.134     547.48   1638.55    4.749      7.081      2.993      0.100    3.2680     0.0100     200
!   19      85.126     534.86   1600.81    4.640      6.918      2.993      0.100    3.2680     0.0100     200
!   20      83.119     522.25   1563.06    4.530      6.755      2.993      0.100    3.2680     0.0100     200
!   21      81.112     509.64   1525.32    4.421      6.592      2.993      0.100    3.2680     0.0100     200
!   22      79.105     497.03   1487.57    4.312      6.429      2.993      0.100    3.2680     0.0100     200
!   23      77.098     484.42   1449.83    4.202      6.266      2.993      0.100    3.2680     0.0100     200
!   24      75.090     471.81   1412.08    4.093      6.103      2.993      0.100    3.2680     0.0100     200
!   25      73.083     459.20   1374.34    3.983      5.940      2.993      0.100    3.2680     0.0100     200
!   26      71.076     446.58   1336.59    3.874      5.776      2.993      0.100    3.2680     0.0100     200
!   27      69.069     433.97   1298.85    3.765      5.613      2.993      0.100    3.2680     0.0100     200
!   28      67.062     421.36   1261.10    3.655      5.450      2.993      0.100    3.2680     0.0100     200
!   29      65.055     408.75   1223.36    3.546      5.287      2.993      0.100    3.2680     0.0100     200
!   30      63.047     396.14   1185.61    3.436      5.124      2.993      0.100    3.2680     0.0100     200
!   31      61.040     383.53   1147.87    3.327      4.961      2.993      0.100    3.2680     0.0100     200
!   32      59.033     370.92   1110.12    3.218      4.798      2.993      0.100    3.2680     0.0100     200
```

```
!   33      57.026     358.30   1072.37    3.108      4.635      2.993      0.100    3.2680     0.0100     200
!   34      55.019     345.69   1034.63    2.999      4.471      2.993      0.100    3.2680     0.0100     200
!   35      53.011     333.08    996.88    2.889      4.308      2.993      0.100    3.2680     0.0100     200
!   36      51.004     320.47    959.14    2.780      4.145      2.993      0.100    3.2680     0.0100     200
!   37      48.997     307.86    921.39    2.671      3.982      2.993      0.100    3.2680     0.0100     200
!   38      46.990     295.25    883.65    2.561      3.819      2.993      0.100    3.2680     0.0100     200
!   39      44.983     282.63    845.90    2.452      3.656      2.993      0.100    3.2680     0.0100     200
!   40      42.976     270.02    808.16    2.342      3.493      2.993      0.100    3.2680     0.0100     200
!   41      40.968     257.41    770.41    2.233      3.330      2.993      0.100    3.2680     0.0100     200
!   42      38.961     244.80    732.67    2.124      3.166      2.993      0.100    3.2680     0.0100     200
!   43      36.954     232.19    694.92    2.014      3.003      2.993      0.100    3.2680     0.0100     200
!   44      34.947     219.58    657.18    1.905      2.840      2.993      0.100    3.2680     0.0100     200
!   45      32.940     206.97    619.43    1.795      2.677      2.993      0.100    3.2680     0.0100     200
!   46      30.932     194.35    581.69    1.686      2.514      2.993      0.100    3.2680     0.0100     200
!   47      28.925     181.74    543.94    1.577      2.351      2.993      0.100    3.2680     0.0100     200
!   48      26.918     169.13    506.20    1.467      2.188      2.993      0.100    3.2680     0.0100     200
!   49      24.911     156.52    468.45    1.358      2.025      2.993      0.100    3.2680     0.0100     200
!   50      23.054     144.85    373.75    1.288      1.921      2.580      0.086    3.3497     0.0086     200
!   51      21.348     134.13    346.10    1.270      1.893      2.580      0.086    3.5658     0.0086     200
!   52      19.640     123.40    319.37    1.241      1.850      2.588      0.086    3.7884     0.0086     200
!-------------------------------------------------------------------------------------------------------------
*** In MITL C: segments 50, 51, 52 (above) are downstream transition segments required for the MITL to mate with
the convolute hardware. These are unchanged in all designs.


.....printing MITL geometry summary table, D-level (SHORT30_BASE_ONN.txt)

!  We divide the MITL space between Ra and Rb into 57 segments of equal length
!  and use segment middle point to calculate MITL block geometry.
!
!  Middle line outer boundaries (segm. 1 - 57) are:
!  Ra = 122.1612 cm, gapa = 6.7337 cm, Za = 3.3050 Ohms
!  Rb = 15.5387 cm, gapb = 0.8602 cm, Zb = 3.3192 Ohms
!
!  Middle line length (segm. 1 - 57) is 168.1920 cm (5.6103 ns)
!  Segment length is 2.9507 cm (0.0984 ns)
!  Middle line angle is 50.6591000 degrees
!
!  Total L (segm. 1 - 57) = sum of Zt = 18.5578 nH
!
!-------------------------------------------------------------------------------------------------------------
! Segm  midpoint-cm  circum-cm  area-cm2   gap-cm  height-cm  length-cm  length-ns  Zvac-Ohms  resol-ns  Eon-kV/cm
!-------------------------------------------------------------------------------------------------------------
!    1     121.226     761.68   2247.53    6.682     10.541      2.951      0.098    3.3050     0.0098     200
!    2     119.355     749.93   2212.85    6.579     10.378      2.951      0.098    3.3050     0.0098     200
!    3     117.485     738.18   2178.17    6.476     10.216      2.951      0.098    3.3051     0.0098     200
!    4     115.614     726.43   2143.49    6.373     10.053      2.951      0.098    3.3051     0.0098     200
!    5     113.744     714.67   2108.81    6.270      9.891      2.951      0.098    3.3052     0.0098     200
!    6     111.873     702.92   2074.13    6.167      9.728      2.951      0.098    3.3052     0.0098     200
!    7     110.002     691.17   2039.45    6.064      9.566      2.951      0.098    3.3052     0.0098     200
!    8     108.132     679.41   2004.77    5.961      9.403      2.951      0.098    3.3053     0.0098     200
!    9     106.261     667.66   1970.09    5.858      9.240      2.951      0.098    3.3053     0.0098     200
!   10     104.391     655.91   1935.41    5.755      9.078      2.951      0.098    3.3054     0.0098     200
!   11     102.520     644.15   1900.73    5.652      8.915      2.951      0.098    3.3054     0.0098     200
!   12     100.650     632.40   1866.05    5.549      8.753      2.951      0.098    3.3054     0.0098     200
!   13      98.779     620.65   1831.37    5.446      8.590      2.951      0.098    3.3055     0.0098     200
!   14      96.909     608.89   1796.69    5.343      8.428      2.951      0.098    3.3055     0.0098     200
!   15      95.038     597.14   1762.01    5.240      8.265      2.951      0.098    3.3056     0.0098     200
!   16      93.167     585.39   1727.33    5.137      8.103      2.951      0.098    3.3056     0.0098     200
!   17      91.297     573.63   1692.65    5.033      7.940      2.951      0.098    3.3057     0.0098     200
!   18      89.426     561.88   1657.96    4.930      7.778      2.951      0.098    3.3058     0.0098     200
!   19      87.556     550.13   1623.28    4.827      7.615      2.951      0.098    3.3058     0.0098     200
!   20      85.685     538.38   1588.60    4.724      7.452      2.951      0.098    3.3059     0.0098     200
!   21      83.815     526.62   1553.92    4.621      7.290      2.951      0.098    3.3059     0.0098     200
!   22      81.944     514.87   1519.24    4.518      7.127      2.951      0.098    3.3060     0.0098     200
!   23      80.073     503.12   1484.56    4.415      6.965      2.951      0.098    3.3061     0.0098     200
!   24      78.203     491.36   1449.88    4.312      6.802      2.951      0.098    3.3062     0.0098     200
!   25      76.332     479.61   1415.20    4.209      6.640      2.951      0.098    3.3062     0.0098     200
!   26      74.462     467.86   1380.52    4.106      6.477      2.951      0.098    3.3063     0.0098     200
!   27      72.591     456.10   1345.84    4.003      6.315      2.951      0.098    3.3064     0.0098     200
!   28      70.721     444.35   1311.16    3.900      6.152      2.951      0.098    3.3065     0.0098     200
!   29      68.850     432.60   1276.48    3.797      5.990      2.951      0.098    3.3066     0.0098     200
!   30      66.979     420.84   1241.80    3.694      5.827      2.951      0.098    3.3067     0.0098     200
!   31      65.109     409.09   1207.12    3.591      5.664      2.951      0.098    3.3068     0.0098     200
!   32      63.238     397.34   1172.44    3.488      5.502      2.951      0.098    3.3069     0.0098     200
!   33      61.368     385.58   1137.76    3.385      5.339      2.951      0.098    3.3071     0.0098     200
!   34      59.497     373.83   1103.08    3.282      5.177      2.951      0.098    3.3072     0.0098     200
!   35      57.627     362.08   1068.40    3.179      5.014      2.951      0.098    3.3073     0.0098     200
!   36      55.756     350.33   1033.72    3.076      4.852      2.951      0.098    3.3075     0.0098     200
!   37      53.885     338.57    999.04    2.973      4.689      2.951      0.098    3.3076     0.0098     200
!   38      52.015     326.82    964.36    2.870      4.527      2.951      0.098    3.3078     0.0098     200
!   39      50.144     315.07    929.68    2.767      4.364      2.951      0.098    3.3080     0.0098     200
!   40      48.274     303.31    895.00    2.663      4.201      2.951      0.098    3.3082     0.0098     200
!   41      46.403     291.56    860.32    2.560      4.039      2.951      0.098    3.3084     0.0098     200
!   42      44.533     279.81    825.63    2.457      3.876      2.951      0.098    3.3086     0.0098     200
!   43      42.662     268.05    790.95    2.354      3.714      2.951      0.098    3.3089     0.0098     200
!   44      40.791     256.30    756.27    2.251      3.551      2.951      0.098    3.3091     0.0098     200
!   45      38.921     244.55    721.59    2.148      3.389      2.951      0.098    3.3094     0.0098     200
!   46      37.050     232.79    686.91    2.045      3.226      2.951      0.098    3.3098     0.0098     200
!   47      35.180     221.04    652.23    1.942      3.064      2.951      0.098    3.3101     0.0098     200
!   48      33.309     209.29    617.55    1.839      2.901      2.951      0.098    3.3105     0.0098     200
!   49      31.439     197.53    582.87    1.736      2.739      2.951      0.098    3.3110     0.0098     200
```

```
!   50      29.568     185.78    548.19    1.633      2.576      2.951      0.098    3.3115     0.0098     200
!   51      27.697     174.03    513.51    1.530      2.413      2.951      0.098    3.3121     0.0098     200
!   52      25.827     162.27    478.83    1.427      2.251      2.951      0.098    3.3127     0.0098     200
!   53      23.956     150.52    444.15    1.324      2.088      2.951      0.098    3.3135     0.0098     200
!   54      22.086     138.77    409.47    1.221      1.926      2.951      0.098    3.3144     0.0098     200
!   55      20.215     127.02    374.79    1.118      1.763      2.951      0.098    3.3154     0.0098     200
!   56      18.345     115.26    340.11    1.015      1.601      2.951      0.098    3.3167     0.0098     200
!   57      16.474     103.51    305.43    0.912      1.438      2.951      0.098    3.3183     0.0098     200
!-------------------------------------------------------------------------------------------------------------
```

D.2. Variable-Impedance MITLs

D.2.1. *input file stub*: `VAR3-VAR3-VAR3-VAR1` All-Levels Z Model

```
Z Variable LDRD  --  ALL LEVELS
! R. V. Shapovalov 02-Sep-2025 16:08:53
! This deck was created with MATLAB using the following inputs:
!!  Work folder = /Users/rsha/Documents/Work/LDRD-Power-Flow/ZRMITL-Variable-v60
!!  Sim. folder = Shots_all_levels/
!!  Matlab file = deck_all_levels.m
!!  top_branch = D-level
!!  vdrive = Empire
!!  fl_convolute = large
!!  fl_inner_MITL = large
!!  fl_load = SHORT30
!!  R_vsource = 0.712
!!  zflow = 0.800

!!  Level A MITL
!!  fl_MITLA_type = VAR3
!!  fl_MITLA_za = ZA1069
!!  fl_MITLA_emiss = ONN

!!  Level B MITL
!!  fl_MITLB_type = VAR3
!!  fl_MITLB_za = ZA1104
!!  fl_MITLB_emiss = ONN

!!  Level C MITL
!!  fl_MITLC_type = VAR3
!!  fl_MITLC_za = ZA1525
!!  fl_MITLC_emiss = ONN

!!  Level D MITL
!!  fl_MITLD_type = VAR1
!!  fl_MITLD_za = ZA2500
!!  fl_MITLD_emiss = ONN

!! Write main MITL boundaries for later read-in
!!      Keyword   N-segm        angle        Ra-cm        Rb-cm        ga-cm        gb-cm  res-fac turn-kV/cm
!!  MITLA-bound       40   23.8784103   128.748700    24.604800     2.295460     0.935630       10        200
!!  MITLB-bound       40   27.0302828   120.905700    23.921600     2.226205     0.945557       10        200
!!  MITLC-bound       49   47.8832194   122.259300    23.907300     3.109575     1.303052       10        200
!!  MITLD-bound       57   50.6591000   122.161200    15.538700     5.093573     0.860196       10        200

!! Write MITL single point entry for later read-in
!!      Keyword   N-segm        angle         R-cm         g-cm    length-cm  res-fac turn-kV/cm
!!  MITLA-pnt01       41   21.4832799    23.514200     0.974700     2.344040       10        200
!!  MITLA-pnt02       42   10.4834698    20.966200     1.216500     2.964330       10        200
!!  MITLB-pnt01       41   21.4832799    22.574436     1.186645     2.812600       10        200
!!  MITLB-pnt02       42   21.4832799    20.154680     1.316045     2.205080       10        200
!!  MITLC-pnt01       50   47.8832194    23.054200     1.287978     2.580200       10        200
!!  MITLC-pnt02       51   47.8832194    21.348200     1.269614     2.580250       10        200
!!  MITLC-pnt03       52   47.8832194    19.639900     1.240908     2.588040       10        200


TIME-STEP              9.1E-13
RESOLUTION-TIME        1.0E-10
END-TIME               5.0E-07
NUMBER-PRINTS                1
EXECUTE-CYCLES             ALL
ECHO                        NO
MAX-POINTS                2000

! ================================================================
!                D   L E V E L   B L O C K S   S T A R T S   H E R E
! ================================================================
!
BRANCH

***** The full deck (8,031 lines) for the variable-impedance all-levels Z model  *****
```

D.2.2. Individual Level MITL segment geometries

```
.....printing MITL geometry summary table, A-level (SHORT30_VAR3_VAR3_VAR3_VAR1_ONN.txt)

!  We divide the MITL space between Ra and Rb into 40 segments of equal length
!  and use segment middle point to calculate MITL block geometry.
!
!  Middle line outer boundaries (segm. 1 - 40) are:
!  Ra = 128.7487 cm, gapa = 2.2955 cm, Za = 1.0690 Ohms <- reduced gap
!  Rb = 24.6048 cm, gapb = 0.9356 cm, Zb = 2.2800 Ohms
!
!  Middle line length (segm. 1 - 40) is 113.8923 cm (3.7990 ns)
!  Segment length is 2.8473 cm (0.0950 ns)
!  Middle line angle is 23.8784103 degrees
!
!  Total L (segm. 1 - 40) = sum of Zt = 5.1974 nH <- exactly 40% reduction
!
!-------------------------------------------------------------------------------------------------------------
! Segm  midpoint-cm  circum-cm  area-cm2   gap-cm  height-cm  length-cm  length-ns  Zvac-Ohms  resol-ns  Eon-kV/cm
!-------------------------------------------------------------------------------------------------------------
!    1     127.447     800.77   2280.05    2.278      2.492      2.847      0.095     1.0719     0.0095     200
!    2     124.843     784.41   2233.47    2.244      2.455      2.847      0.095     1.0779     0.0095     200
!    3     122.240     768.05   2186.89    2.210      2.417      2.847      0.095     1.0842     0.0095     200
!    4     119.636     751.70   2140.31    2.176      2.380      2.847      0.095     1.0908     0.0095     200
!    5     117.033     735.34   2093.73    2.142      2.343      2.847      0.095     1.0976     0.0095     200
!    6     114.429     718.98   2047.15    2.108      2.306      2.847      0.095     1.1048     0.0095     200
!    7     111.825     702.62   2000.57    2.074      2.269      2.847      0.095     1.1123     0.0095     200
!    8     109.222     686.26   1953.99    2.040      2.231      2.847      0.095     1.1202     0.0095     200
!    9     106.618     669.90   1907.42    2.006      2.194      2.847      0.095     1.1284     0.0095     200
!   10     104.015     653.54   1860.84    1.973      2.157      2.847      0.095     1.1370     0.0095     200
!   11     101.411     637.18   1814.26    1.939      2.120      2.847      0.095     1.1461     0.0095     200
!   12      98.807     620.82   1767.68    1.905      2.083      2.847      0.095     1.1557     0.0095     200
!   13      96.204     604.47   1721.10    1.871      2.046      2.847      0.095     1.1658     0.0095     200
!   14      93.600     588.11   1674.52    1.837      2.008      2.847      0.095     1.1764     0.0095     200
!   15      90.997     571.75   1627.94    1.803      1.971      2.847      0.095     1.1877     0.0095     200
!   16      88.393     555.39   1581.36    1.769      1.934      2.847      0.095     1.1996     0.0095     200
!   17      85.789     539.03   1534.79    1.735      1.897      2.847      0.095     1.2123     0.0095     200
!   18      83.186     522.67   1488.21    1.701      1.860      2.847      0.095     1.2257     0.0095     200
!   19      80.582     506.31   1441.63    1.667      1.823      2.847      0.095     1.2400     0.0095     200
!   20      77.979     489.95   1395.05    1.633      1.785      2.847      0.095     1.2553     0.0095     200
!   21      75.375     473.59   1348.47    1.599      1.748      2.847      0.095     1.2716     0.0095     200
!   22      72.771     457.24   1301.89    1.565      1.711      2.847      0.095     1.2891     0.0095     200
!   23      70.168     440.88   1255.31    1.531      1.674      2.847      0.095     1.3079     0.0095     200
!   24      67.564     424.52   1208.73    1.497      1.637      2.847      0.095     1.3281     0.0095     200
!   25      64.961     408.16   1162.16    1.463      1.599      2.847      0.095     1.3499     0.0095     200
!   26      62.357     391.80   1115.58    1.429      1.562      2.847      0.095     1.3736     0.0095     200
!   27      59.753     375.44   1069.00    1.395      1.525      2.847      0.095     1.3994     0.0095     200
!   28      57.150     359.08   1022.42    1.361      1.488      2.847      0.095     1.4274     0.0095     200
!   29      54.546     342.72    975.84    1.327      1.451      2.847      0.095     1.4582     0.0095     200
!   30      51.943     326.36    929.26    1.293      1.414      2.847      0.095     1.4921     0.0095     200
!   31      49.339     310.01    882.68    1.259      1.376      2.847      0.095     1.5295     0.0095     200
!   32      46.735     293.65    836.10    1.225      1.339      2.847      0.095     1.5711     0.0095     200
!   33      44.132     277.29    789.52    1.191      1.302      2.847      0.095     1.6176     0.0095     200
!   34      41.528     260.93    742.95    1.157      1.265      2.847      0.095     1.6699     0.0095     200
!   35      38.925     244.57    696.37    1.123      1.228      2.847      0.095     1.7292     0.0095     200
!   36      36.321     228.21    649.79    1.089      1.191      2.847      0.095     1.7971     0.0095     200
!   37      33.717     211.85    603.21    1.055      1.153      2.847      0.095     1.8754     0.0095     200
!   38      31.114     195.49    556.63    1.021      1.116      2.847      0.095     1.9668     0.0095     200
!   39      28.510     179.13    510.05    0.987      1.079      2.847      0.095     2.0749     0.0095     200
!   40      25.907     162.78    463.47    0.953      1.042      2.847      0.095     2.2048     0.0095     200
!   41      23.514     147.74    346.32    0.975      1.047      2.344      0.078     2.4854     0.0078     200
!   42      20.966     131.73    390.50    1.216      1.237      2.964      0.099     3.4789     0.0099     200
!-------------------------------------------------------------------------------------------------------------
*** In MITL A: segments 41, 42 (above) are downstream transition segments required for the MITL to mate with the
convolute hardware. These are unchanged in all designs.


.....printing MITL geometry summary table, B-level (SHORT30_VAR3_VAR3_VAR3_VAR1_ONN.txt)

!  We divide the MITL space between Ra and Rb into 40 segments of equal length
!  and use segment middle point to calculate MITL block geometry.
!
!  Middle line outer boundaries (segm. 1 - 40) are:
!  Ra = 120.9057 cm, gapa = 2.2262 cm, Za = 1.1040 Ohms <- reduced gap
!  Rb = 23.9216 cm, gapb = 0.9456 cm, Zb = 2.3700 Ohms
!
!  Middle line length (segm. 1 - 40) is 108.8771 cm (3.6318 ns)
!  Segment length is 2.7219 cm (0.0908 ns)
!  Middle line angle is 27.0302828 degrees
!
!  Total L (segm. 1 - 40) = sum of Zt = 5.1655 nH <- exactly 40% reduction
!
!-------------------------------------------------------------------------------------------------------------
! Segm  midpoint-cm  circum-cm  area-cm2   gap-cm  height-cm  length-cm  length-ns  Zvac-Ohms  resol-ns  Eon-kV/cm
!-------------------------------------------------------------------------------------------------------------
!    1     119.693     752.06   2047.04    2.210      2.481      2.722      0.091     1.1072     0.0091     200
!    2     117.269     736.82   2005.58    2.178      2.445      2.722      0.091     1.1137     0.0091     200
!    3     114.844     721.59   1964.11    2.146      2.409      2.722      0.091     1.1205     0.0091     200
!    4     112.420     706.35   1922.64    2.114      2.373      2.722      0.091     1.1276     0.0091     200
!    5     109.995     691.12   1881.18    2.082      2.337      2.722      0.091     1.1350     0.0091     200
!    6     107.570     675.88   1839.71    2.050      2.302      2.722      0.091     1.1427     0.0091     200
```

```
!    7     105.146     660.65   1798.24    2.018      2.266      2.722      0.091    1.1508     0.0091     200
!    8     102.721     645.42   1756.78    1.986      2.230      2.722      0.091    1.1593     0.0091     200
!    9     100.297     630.18   1715.31    1.954      2.194      2.722      0.091    1.1682     0.0091     200
!   10      97.872     614.95   1673.84    1.922      2.158      2.722      0.091    1.1775     0.0091     200
!   11      95.447     599.71   1632.38    1.890      2.122      2.722      0.091    1.1873     0.0091     200
!   12      93.023     584.48   1590.91    1.858      2.086      2.722      0.091    1.1976     0.0091     200
!   13      90.598     569.25   1549.44    1.826      2.050      2.722      0.091    1.2085     0.0091     200
!   14      88.174     554.01   1507.98    1.794      2.014      2.722      0.091    1.2199     0.0091     200
!   15      85.749     538.78   1466.51    1.762      1.978      2.722      0.091    1.2320     0.0091     200
!   16      83.324     523.54   1425.04    1.730      1.942      2.722      0.091    1.2448     0.0091     200
!   17      80.900     508.31   1383.58    1.698      1.906      2.722      0.091    1.2584     0.0091     200
!   18      78.475     493.07   1342.11    1.666      1.870      2.722      0.091    1.2728     0.0091     200
!   19      76.051     477.84   1300.65    1.634      1.834      2.722      0.091    1.2882     0.0091     200
!   20      73.626     462.61   1259.18    1.602      1.798      2.722      0.091    1.3045     0.0091     200
!   21      71.201     447.37   1217.71    1.570      1.762      2.722      0.091    1.3220     0.0091     200
!   22      68.777     432.14   1176.25    1.538      1.726      2.722      0.091    1.3407     0.0091     200
!   23      66.352     416.90   1134.78    1.506      1.690      2.722      0.091    1.3607     0.0091     200
!   24      63.928     401.67   1093.31    1.474      1.655      2.722      0.091    1.3823     0.0091     200
!   25      61.503     386.43   1051.85    1.442      1.619      2.722      0.091    1.4056     0.0091     200
!   26      59.078     371.20   1010.38    1.410      1.583      2.722      0.091    1.4308     0.0091     200
!   27      56.654     355.97    968.91    1.378      1.547      2.722      0.091    1.4581     0.0091     200
!   28      54.229     340.73    927.45    1.346      1.511      2.722      0.091    1.4879     0.0091     200
!   29      51.805     325.50    885.98    1.314      1.475      2.722      0.091    1.5205     0.0091     200
!   30      49.380     310.26    844.51    1.282      1.439      2.722      0.091    1.5563     0.0091     200
!   31      46.955     295.03    803.05    1.250      1.403      2.722      0.091    1.5958     0.0091     200
!   32      44.531     279.79    761.58    1.218      1.367      2.722      0.091    1.6396     0.0091     200
!   33      42.106     264.56    720.11    1.186      1.331      2.722      0.091    1.6884     0.0091     200
!   34      39.682     249.33    678.65    1.154      1.295      2.722      0.091    1.7432     0.0091     200
!   35      37.257     234.09    637.18    1.122      1.259      2.722      0.091    1.8051     0.0091     200
!   36      34.832     218.86    595.72    1.090      1.223      2.722      0.091    1.8756     0.0091     200
!   37      32.408     203.62    554.25    1.058      1.187      2.722      0.091    1.9567     0.0091     200
!   38      29.983     188.39    512.78    1.026      1.151      2.722      0.091    2.0509     0.0091     200
!   39      27.559     173.16    471.32    0.994      1.115      2.722      0.091    2.1617     0.0091     200
!   40      25.134     157.92    429.85    0.962      1.079      2.722      0.091    2.2939     0.0091     200
!   41      22.574     141.84    398.94    1.187      1.275      2.813      0.094    3.1518     0.0094     200
!   42      20.155     126.64    279.24    1.316      1.414      2.205      0.074    3.9151     0.0074     200
!-------------------------------------------------------------------------------------------------------------
*** In MITL B: segments 41, 42 (above) are downstream transition segments required for the MITL to mate with the
convolute hardware. These are unchanged in all designs.


.....printing MITL geometry summary table, C-level (SHORT30_VAR3_VAR3_VAR3_VAR1_ONN.txt)

!  We divide the MITL space between Ra and Rb into 49 segments of equal length
!  and use segment middle point to calculate MITL block geometry.
!
!  Middle line outer boundaries (segm. 1 - 49) are:
!  Ra = 122.2593 cm, gapa = 3.1096 cm, Za = 1.5250 Ohms <- reduced gap
!  Rb = 23.9073 cm, gapb = 1.3031 cm, Zb = 3.2680 Ohms
!
!  Middle line length (segm. 1 - 49) is 146.6531 cm (4.8918 ns)
!  Segment length is 2.9929 cm (0.0998 ns)
!  Middle line angle is 47.8832194 degrees
!
!  Total L (segm. 1 - 49) = sum of Zt = 9.5913 nH <- exactly 40% reduction
!
!-------------------------------------------------------------------------------------------------------------
! Segm  midpoint-cm  circum-cm  area-cm2   gap-cm  height-cm  length-cm  length-ns  Zvac-Ohms  resol-ns  Eon-kV/cm
!-------------------------------------------------------------------------------------------------------------
!    1     121.256     761.87   2280.22    3.091      4.609      2.993      0.100    1.5285     0.0100     200
!    2     119.249     749.26   2242.48    3.054      4.554      2.993      0.100    1.5357     0.0100     200
!    3     117.241     736.65   2204.73    3.017      4.499      2.993      0.100    1.5431     0.0100     200
!    4     115.234     724.04   2166.99    2.981      4.444      2.993      0.100    1.5508     0.0100     200
!    5     113.227     711.43   2129.24    2.944      4.389      2.993      0.100    1.5588     0.0100     200
!    6     111.220     698.81   2091.50    2.907      4.334      2.993      0.100    1.5671     0.0100     200
!    7     109.213     686.20   2053.75    2.870      4.279      2.993      0.100    1.5756     0.0100     200
!    8     107.205     673.59   2016.01    2.833      4.224      2.993      0.100    1.5845     0.0100     200
!    9     105.198     660.98   1978.26    2.796      4.169      2.993      0.100    1.5937     0.0100     200
!   10     103.191     648.37   1940.52    2.759      4.114      2.993      0.100    1.6033     0.0100     200
!   11     101.184     635.76   1902.77    2.722      4.059      2.993      0.100    1.6132     0.0100     200
!   12      99.177     623.15   1865.02    2.686      4.005      2.993      0.100    1.6236     0.0100     200
!   13      97.170     610.53   1827.28    2.649      3.950      2.993      0.100    1.6344     0.0100     200
!   14      95.162     597.92   1789.53    2.612      3.895      2.993      0.100    1.6456     0.0100     200
!   15      93.155     585.31   1751.79    2.575      3.840      2.993      0.100    1.6574     0.0100     200
!   16      91.148     572.70   1714.04    2.538      3.785      2.993      0.100    1.6696     0.0100     200
!   17      89.141     560.09   1676.30    2.501      3.730      2.993      0.100    1.6824     0.0100     200
!   18      87.134     547.48   1638.55    2.464      3.675      2.993      0.100    1.6958     0.0100     200
!   19      85.126     534.86   1600.81    2.428      3.620      2.993      0.100    1.7098     0.0100     200
!   20      83.119     522.25   1563.06    2.391      3.565      2.993      0.100    1.7245     0.0100     200
!   21      81.112     509.64   1525.32    2.354      3.510      2.993      0.100    1.7399     0.0100     200
!   22      79.105     497.03   1487.57    2.317      3.455      2.993      0.100    1.7561     0.0100     200
!   23      77.098     484.42   1449.83    2.280      3.400      2.993      0.100    1.7732     0.0100     200
!   24      75.090     471.81   1412.08    2.243      3.345      2.993      0.100    1.7911     0.0100     200
!   25      73.083     459.20   1374.34    2.206      3.290      2.993      0.100    1.8101     0.0100     200
!   26      71.076     446.58   1336.59    2.169      3.235      2.993      0.100    1.8301     0.0100     200
!   27      69.069     433.97   1298.85    2.133      3.180      2.993      0.100    1.8513     0.0100     200
!   28      67.062     421.36   1261.10    2.096      3.125      2.993      0.100    1.8737     0.0100     200
!   29      65.055     408.75   1223.36    2.059      3.070      2.993      0.100    1.8976     0.0100     200
!   30      63.047     396.14   1185.61    2.022      3.015      2.993      0.100    1.9229     0.0100     200
!   31      61.040     383.53   1147.87    1.985      2.960      2.993      0.100    1.9499     0.0100     200
!   32      59.033     370.92   1110.12    1.948      2.905      2.993      0.100    1.9788     0.0100     200
!   33      57.026     358.30   1072.37    1.911      2.850      2.993      0.100    2.0097     0.0100     200
```

```
!   34      55.019     345.69   1034.63    1.875      2.795      2.993      0.100    2.0428     0.0100     200
!   35      53.011     333.08    996.88    1.838      2.740      2.993      0.100    2.0785     0.0100     200
!   36      51.004     320.47    959.14    1.801      2.685      2.993      0.100    2.1169     0.0100     200
!   37      48.997     307.86    921.39    1.764      2.630      2.993      0.100    2.1585     0.0100     200
!   38      46.990     295.25    883.65    1.727      2.575      2.993      0.100    2.2037     0.0100     200
!   39      44.983     282.63    845.90    1.690      2.520      2.993      0.100    2.2529     0.0100     200
!   40      42.976     270.02    808.16    1.653      2.465      2.993      0.100    2.3066     0.0100     200
!   41      40.968     257.41    770.41    1.616      2.410      2.993      0.100    2.3657     0.0100     200
!   42      38.961     244.80    732.67    1.580      2.355      2.993      0.100    2.4308     0.0100     200
!   43      36.954     232.19    694.92    1.543      2.300      2.993      0.100    2.5030     0.0100     200
!   44      34.947     219.58    657.18    1.506      2.245      2.993      0.100    2.5836     0.0100     200
!   45      32.940     206.97    619.43    1.469      2.190      2.993      0.100    2.6739     0.0100     200
!   46      30.932     194.35    581.69    1.432      2.135      2.993      0.100    2.7759     0.0100     200
!   47      28.925     181.74    543.94    1.395      2.080      2.993      0.100    2.8921     0.0100     200
!   48      26.918     169.13    506.20    1.358      2.025      2.993      0.100    3.0257     0.0100     200
!   49      24.911     156.52    468.45    1.321      1.970      2.993      0.100    3.1807     0.0100     200
!   50      23.054     144.85    373.75    1.288      1.921      2.580      0.086    3.3497     0.0086     200
!   51      21.348     134.13    346.10    1.270      1.893      2.580      0.086    3.5658     0.0086     200
!   52      19.640     123.40    319.37    1.241      1.850      2.588      0.086    3.7884     0.0086     200
!-------------------------------------------------------------------------------------------------------------
*** In MITL C: segments 50, 51, 52 (above) are downstream transition segments required for the MITL to mate with
the convolute hardware. These are unchanged in all designs.


.....printing MITL geometry summary table, D-level (SHORT30_VAR3_VAR3_VAR3_VAR1_ONN.txt)

!  We divide the MITL space between Ra and Rb into 57 segments of equal length
!  and use segment middle point to calculate MITL block geometry.
!
!  Middle line outer boundaries (segm. 1 - 57) are:
!  Ra = 122.1612 cm, gapa = 5.0936 cm, Za = 2.5000 Ohms <- reduced gap
!  Rb = 15.5387 cm, gapb = 0.8602 cm, Zb = 3.3192 Ohms
!
!  Middle line length (segm. 1 - 57) is 168.1920 cm (5.6103 ns)
!  Segment length is 2.9507 cm (0.0984 ns)
!  Middle line angle is 50.6591000 degrees
!
!  Total L (segm. 1 - 57) = sum of Zt = 14.9379 nH <- approx. 20% reduction
!
!-------------------------------------------------------------------------------------------------------------
! Segm  midpoint-cm  circum-cm  area-cm2   gap-cm  height-cm  length-cm  length-ns  Zvac-Ohms  resol-ns  Eon-kV/cm
!-------------------------------------------------------------------------------------------------------------
!    1     121.226     761.68   2247.53    5.056      7.976      2.951      0.098    2.5009     0.0098     200
!    2     119.355     749.93   2212.85    4.982      7.859      2.951      0.098    2.5028     0.0098     200
!    3     117.485     738.18   2178.17    4.908      7.742      2.951      0.098    2.5048     0.0098     200
!    4     115.614     726.43   2143.49    4.834      7.625      2.951      0.098    2.5068     0.0098     200
!    5     113.744     714.67   2108.81    4.759      7.508      2.951      0.098    2.5088     0.0098     200
!    6     111.873     702.92   2074.13    4.685      7.391      2.951      0.098    2.5110     0.0098     200
!    7     110.002     691.17   2039.45    4.611      7.273      2.951      0.098    2.5132     0.0098     200
!    8     108.132     679.41   2004.77    4.537      7.156      2.951      0.098    2.5155     0.0098     200
!    9     106.261     667.66   1970.09    4.462      7.039      2.951      0.098    2.5179     0.0098     200
!   10     104.391     655.91   1935.41    4.388      6.922      2.951      0.098    2.5203     0.0098     200
!   11     102.520     644.15   1900.73    4.314      6.805      2.951      0.098    2.5229     0.0098     200
!   12     100.650     632.40   1866.05    4.239      6.688      2.951      0.098    2.5255     0.0098     200
!   13      98.779     620.65   1831.37    4.165      6.570      2.951      0.098    2.5283     0.0098     200
!   14      96.909     608.89   1796.69    4.091      6.453      2.951      0.098    2.5311     0.0098     200
!   15      95.038     597.14   1762.01    4.017      6.336      2.951      0.098    2.5341     0.0098     200
!   16      93.167     585.39   1727.33    3.942      6.219      2.951      0.098    2.5372     0.0098     200
!   17      91.297     573.63   1692.65    3.868      6.102      2.951      0.098    2.5404     0.0098     200
!   18      89.426     561.88   1657.96    3.794      5.985      2.951      0.098    2.5437     0.0098     200
!   19      87.556     550.13   1623.28    3.720      5.867      2.951      0.098    2.5472     0.0098     200
!   20      85.685     538.38   1588.60    3.645      5.750      2.951      0.098    2.5508     0.0098     200
!   21      83.815     526.62   1553.92    3.571      5.633      2.951      0.098    2.5546     0.0098     200
!   22      81.944     514.87   1519.24    3.497      5.516      2.951      0.098    2.5586     0.0098     200
!   23      80.073     503.12   1484.56    3.423      5.399      2.951      0.098    2.5628     0.0098     200
!   24      78.203     491.36   1449.88    3.348      5.282      2.951      0.098    2.5671     0.0098     200
!   25      76.332     479.61   1415.20    3.274      5.165      2.951      0.098    2.5717     0.0098     200
!   26      74.462     467.86   1380.52    3.200      5.047      2.951      0.098    2.5765     0.0098     200
!   27      72.591     456.10   1345.84    3.125      4.930      2.951      0.098    2.5815     0.0098     200
!   28      70.721     444.35   1311.16    3.051      4.813      2.951      0.098    2.5868     0.0098     200
!   29      68.850     432.60   1276.48    2.977      4.696      2.951      0.098    2.5924     0.0098     200
!   30      66.979     420.84   1241.80    2.903      4.579      2.951      0.098    2.5984     0.0098     200
!   31      65.109     409.09   1207.12    2.828      4.462      2.951      0.098    2.6046     0.0098     200
!   32      63.238     397.34   1172.44    2.754      4.344      2.951      0.098    2.6112     0.0098     200
!   33      61.368     385.58   1137.76    2.680      4.227      2.951      0.098    2.6183     0.0098     200
!   34      59.497     373.83   1103.08    2.606      4.110      2.951      0.098    2.6257     0.0098     200
!   35      57.627     362.08   1068.40    2.531      3.993      2.951      0.098    2.6337     0.0098     200
!   36      55.756     350.33   1033.72    2.457      3.876      2.951      0.098    2.6422     0.0098     200
!   37      53.885     338.57    999.04    2.383      3.759      2.951      0.098    2.6513     0.0098     200
!   38      52.015     326.82    964.36    2.308      3.641      2.951      0.098    2.6610     0.0098     200
!   39      50.144     315.07    929.68    2.234      3.524      2.951      0.098    2.6715     0.0098     200
!   40      48.274     303.31    895.00    2.160      3.407      2.951      0.098    2.6827     0.0098     200
!   41      46.403     291.56    860.32    2.086      3.290      2.951      0.098    2.6949     0.0098     200
!   42      44.533     279.81    825.63    2.011      3.173      2.951      0.098    2.7081     0.0098     200
!   43      42.662     268.05    790.95    1.937      3.056      2.951      0.098    2.7225     0.0098     200
!   44      40.791     256.30    756.27    1.863      2.939      2.951      0.098    2.7382     0.0098     200
!   45      38.921     244.55    721.59    1.789      2.821      2.951      0.098    2.7553     0.0098     200
!   46      37.050     232.79    686.91    1.714      2.704      2.951      0.098    2.7743     0.0098     200
!   47      35.180     221.04    652.23    1.640      2.587      2.951      0.098    2.7952     0.0098     200
!   48      33.309     209.29    617.55    1.566      2.470      2.951      0.098    2.8185     0.0098     200
!   49      31.439     197.53    582.87    1.491      2.353      2.951      0.098    2.8445     0.0098     200
!   50      29.568     185.78    548.19    1.417      2.236      2.951      0.098    2.8739     0.0098     200
```

```
!   51      27.697     174.03     513.51     1.343      2.118      2.951      0.098     2.9072     0.0098     200
!   52      25.827     162.27     478.83     1.269      2.001      2.951      0.098     2.9453     0.0098     200
!   53      23.956     150.52     444.15     1.194      1.884      2.951      0.098     2.9894     0.0098     200
!   54      22.086     138.77     409.47     1.120      1.767      2.951      0.098     3.0410     0.0098     200
!   55      20.215     127.02     374.79     1.046      1.650      2.951      0.098     3.1021     0.0098     200
!   56      18.345     115.26     340.11     0.972      1.533      2.951      0.098     3.1756     0.0098     200
!   57      16.474     103.51     305.43     0.897      1.415      2.951      0.098     3.2659     0.0098     200
!-------------------------------------------------------------------------------------------------------------------
```

DISTRIBUTION

Hardcopy—External

Number of Copies	Name(s)	Company Name and Company Mailing Address

Hardcopy—Internal

Number of Copies	Name	Org.	Mailstop
1	Greg Frye	1330	1152
1	Joshua Leckbee	1651	1195
1	Kate Suzanne Bell	1685	1186
1	Michael E. Cuneo	1650	1195
1	Keith Matzen	1000	0110
1	Kyle John Peterson	1680	1186
1	Richard Michael Jack Kramer	1323	1152
1	D. Chavez, LDRD Office	1911	0359

Email—Internal

Name	Org.	Sandia Email Address
Technical Library	01177	libref@sandia.gov

Sandia National Laboratories is a multimission laboratory managed and operated by National Technology & Engineering Solutions of Sandia LLC, a wholly owned subsidiary of Honeywell International Inc., for the U.S. Department of Energy's National Nuclear Security Administration under contract DE-NA0003525.